Master's Thesis

**Master in Neuroengineering and Rehabilitation**

# Design of a new approach to register biomechanical gait data, when combining lower limb powered exoskeletons controlled by neural machine interfaces and transcutaneous spinal current stimulation.

**MEMORY**


**Author:** Laura Blanco Coloma
**Director:** Diana Sofía Herrera Valenzuela
Josep Maria Font-Llagunes

**Convocation:** April 2023



Escola Tècnica Superior
d'Enginyeria Industrial de Barcelona


**Abstract**

To analyze the effect of robotic-aided gait rehabilitation controlled with brain-machine interfaces, it is necessary to ensure a strategy to assess gait biomechanics recording data that is not disturbed by the rehabilitation technologies. To this end, a protocol to measure the kinematics of the lower extremities on the three planes based on Inertial Measurement Units (IMUs) is developed. To evaluate the IMUs system accuracy and reliability, it is validated with a high-precision reference device, an optoelectronic system. The validation of the protocol is performed in one healthy subject in two steps: 1) testing four different configurations of the IMUs to identify the optimal gait data registration model, including the number and location of sensors, since these affect the system's output, and 2) validation of IMUs with Vicon through synchronously walking records (Condition 1) and exoskeleton-assisted walking (Condition 2). The within-day multiple correlation coefficients ($CMC_w$) from Kadaba and its reformulation, the inter-protocol CMC ($CMC_p$), are used respectively for Part 1 and Part 2 to assess the waveform similarity of each lower limb joint angle, removing the between-gait-cycle variability. In addition, other parameters are studied to assess the technological error and the differences between the biomechanical models, such as Pearson's correlation, range of motion, offset, and the Root Mean Square Error. For Part 1, it is concluded that the optimal configuration for the rest of the project is Model 2, showing good $CMC_w$ values for every joint angle ($CMC_w \geq 0.8$). During the walking test (Part 2, Condition 1) the $CMC_p$ shows that gait kinematics measured by both systems for the right limb are equivalent, demonstrating IMUs accuracy, for the hip and the knee flexion/extension ($CMC_p = 1$), and for the knee adduction/abduction ($CMC_p = 0.91$). For exoskeleton-assisted walking (Part 2, Condition 2), after adjusting the position of the IMUs located at the ankles, the gait kinematics for the right limb are equivalent for every joint in the sagittal plane ($CMC_p \geq 0.9$), for the knee and the ankle in frontal plane ($CMC_p \geq 0.95$), and for the hip in transversal plane ($CMC_p = 0.99$).

**Resumen**

Para analizar el efecto de la rehabilitación de la marcha asistida por robots controlada con interfaces cerebro-máquina, es necesario garantizar una estrategia para evaluar los datos de registro de la biomecánica de la marcha de forma que no estén alterados por las tecnologías de rehabilitación. Para ello, se desarrolla un protocolo para medir la cinemática de las extremidades inferiores en los tres planos basado en Unidades de Medición Inercial (IMUs). Para evaluar la precisión y fiabilidad del sistema de IMUs, se valida con un dispositivo de referencia de alta precisión, un sistema optoelectrónico. La validación del protocolo se realiza en un sujeto sano en dos pasos: 1) prueba de cuatro configuraciones diferentes de las IMUs para identificar el modelo óptimo de registro de datos de la marcha, incluyendo el número y la ubicación de los sensores, ya que estos afectan a la salida del sistema, y 2) validación de las IMUs con Vicon a través de registros sincronizados de marcha (Condición 1) y marcha asistida por exoesqueleto (Condición 2). Los coeficientes de correlación múltiple dentro del día ($CMC_w$) de Kadaba y su reformulación, el CMC interprotocolo ($CMC_p$), se utilizan respectivamente en la Parte 1 y la Parte 2 para evaluar la similitud de la forma de onda de cada ángulo articular de la extremidad inferior, eliminando la variabilidad entre ciclos de la marcha. Además, se estudian otros parámetros para evaluar el error tecnológico y las diferencias entre los modelos biomecánicos, como la correlación de Pearson, el rango de movimiento, el desplazamiento y el error cuadrático medio. Para la Parte 1, se concluye que la configuración óptima para el resto del proyecto es el Modelo 2, mostrando buenos valores de $CMC_w$ para cada ángulo articular ($CMC_w \geq 0.8$). Durante la prueba de marcha (Parte 2, Condición 1), el $CMC_p$ muestra que la cinemática de la marcha medida por ambos sistemas para la extremidad derecha es equivalente, demostrando la precisión de las IMUs, para la flexo-extensión de la cadera y la rodilla ($CMC_p = 1$), y para la aducción/abducción de la rodilla ($CMC_p = 0.91$). Para la marcha asistida por exoesqueleto (Parte 2, Condición 2), tras ajustar la posición de las IMUs situadas en los tobillos, la cinemática de la marcha para la extremidad derecha es equivalente para cada articulación en el plano sagital ($CMC_p \geq 0.9$), para la rodilla y el tobillo en el plano frontal ($CMC_p \geq 0.95$), y para la cadera en el plano transversal ($CMC_p = 0.99$).

**Resum**

Per analitzar l'efecte de la rehabilitació de la marxa assistida per robòtica controlada amb interfícies cervell-màquina, cal garantir una estratègia per avaluar la biomecànica de la marxa registrant dades que no es vegi alterada per les tecnologies de rehabilitació. Amb aquesta finalitat, es desenvolupa un protocol per mesurar la cinemàtica de les extremitats inferiors en els tres plans basat en Unitats de Mesurament Inercial (IMU). Per avaluar la precisió i la fiabilitat del sistema IMU, es valida amb un dispositiu de referència d'alta precisió, un sistema optoelectrònic. La validació del protocol es realitza en un subjecte sa en dos passos: 1) provant quatre configuracions diferents de les IMU per identificar el model òptim de registre de dades de la marxa, inclòs el nombre i la ubicació dels sensors, ja que aquests afecten la sortida del sistema, i 2 ) validació de les IMU amb Vicon mitjançant registres de marxa sincrònica (Condició 1) i caminada assistida per exoesquelet (Condició 2). Els coeficients de correlació múltiple d'un dia ($CMC_w$) de Kadaba i la seva reformulació, el CMC interprotocol ($CMC_p$), s'utilitzen respectivament per a la part 1 i la part 2 per avaluar la similitud de la forma d'ona de cada angle d'articulació de l'extremitat inferior, eliminant l'entre- variabilitat del cicle de la marxa. A més, s'estudien altres paràmetres per avaluar l'error tecnològic i les diferències entre els models biomecànics, com ara la correlació de Pearson, el rang de moviment, l'offset i l'error quadràtic mitjà. Per a la part 1, es conclou que la configuració òptima per a la resta del projecte és el model 2, que mostra bons valors de $CMC_w$ per a cada angle d'articulació ($CMC_w \geq 0,8$). Durant la prova de marxa (part 2, condició 1), el $CMC_p$ mostra que la cinemàtica de la marxa mesurada pels dos sistemes per a l'extremitat dreta és equivalent, demostrant la precisió de les IMU, per al maluc i la flexió/extensió del genoll ($CMC_p = 1$) i per a la adducció/abducció del genoll ($CMC_p = 0,91$). Per a la marxa assistida per exoesquelet (Part 2, Condició 2), després d'ajustar la posició de les IMU situades als turmells, la cinemàtica de la marxa de l'extremitat dreta és equivalent per a cada articulació del pla sagital ($CMC_p \geq 0,9$), per al genoll. i el turmell en pla frontal ($CMC_p \geq 0,95$), i per al maluc en pla transversal ($CMC_p = 0,99$).

# INDEX

# FIGURE INDEX

# TABLE INDEX

# Glossary

**SCI**: Spinal Cord Injury.

**tSCS**: Transcutaneous Spinal Cord Stimulation.

**IG**: Institutt Guttman.

**UMH**: Miguel Hernández University of Elche.

**HNP:** National Hospital for Paraplegics.

**NMI**: Neural-Machine Interface.

**BCI**: Brain-Computer Interface.

**IMUs**: Inertial Measurements Units.

**CPGs**: Central Pattern Generators.

**MEMS**: Micro Electro Mechanical Systems.

**DCM**: Directing Cosine Matrix.

**sEMG**: Surface Electromyography.

**Mocap**: Motion Capture.

**3D**: Three Dimensional.

**3D Acc**: 3D Accelerometer.

**3D Mag**: 3D Magnetometer.

**3D Gyro**: 3D Gyroscope.

**EKF**: Extended Kalman Filter.

**CMC**: Coefficient of Multiple Correlation.

**$CMC_w$**: Within-day Coefficient of Multiple Correlation.

**$CMC_p$**: Inter-protocol Coefficient of Multiple Correlation.

**ROM**: Range of Motion.

**STD**: Standard Deviation.

**CV**: Coefficient of Variation.

**UW**: Upper Whisker.

**LW**: Lower Whisker.

# 1. Preface

## 1.1. Project Origin

This thesis stems from the national project entitled ReGAIT: A new rehabilitation approach of locomotion for incomplete spinal cord injury patients by integrating neural interfaces, lower-limb powered robotic systems and transcutaneous spinal current stimulation strategies (PID2021-124111OB-C31 funded by MCIN/AEI/ 10.13039/501100011033 and by "ERDF A way of making Europe"). In this way, ReGAIT proposes a new strategy to enhance neuroplasticity changes during locomotion rehabilitation in incomplete thoracic spinal cord injury (SCI) patients by associating and synchronizing the use of lower limb powered robotic systems with neural activity voluntarily generated by patients and transcutaneous spinal cord stimulation (tSCS) strategies. Thus, this project combines the knowledge of experts in neural engineering, biomechanics, machine learning and biomedical signals processing from basic and translational research with neurologists and rehabilitation physicians with extensive experience in the functional and clinical evaluation of patients using robotics-based rehabilitation technologies.

ReGAIT encompasses three subprojects and institutions based on the multidisciplinary expertise needed to meet its ambitious objectives and ensure adequate exploitation of the results, the Institut Guttmann (IG), the Miguel Hernández University of Elche (UMH) and the National Hospital for Paraplegics of Toledo (HNP). Within this project, the HNP performs the third subproject, which aims to develop a strategy to analyze the effect on gait biomechanics when combining motorized lower limb exoskeletons controlled by neural-machine interfaces (NMIs) and tSCS in patients with incomplete SCI. To carry out this work, the aim of this thesis is to design a new approach to register biomechanical gait data that will lead to the design of new metrics to measure the effect of these combined technologies on gait biomechanics.

## 1.2. Motivation

The main motivation of ReGAIT is to develop a new therapy, arising from the combination of the previously mentioned systems, for the rehabilitation of locomotion in patients with incomplete SCI to promote neural plasticity and the improvement of functional outcomes, optimizing their quality of life.

Therefore, in this thesis the main motivation is to provide a new model for recording biomechanical gait data that allows, through new and existing metrics, to evaluate the effect of the technologies in the gait kinematics of the patients during the new proposed therapy. In this way, it is meant to obtain objective information to improve the therapy and provide the population with SCI with the best opportunities for recovery of functional motor control and autonomy.

## 1.3. Requirements

First, it has been needed to deepen the knowledge about the human gait and how it is affected by SCI. In addition, a review of the protocols used in biomechanical data recording and three-dimensional (3D) motion analysis has been carried out.

The literature has also been consulted to acquire knowledge about different methods that could be used to validate and compare the biomechanical measurements acquired by different protocols and systems. The research performed focuses on similarity assessments to quantify the similarity between waveforms measured synchronously among different protocols.

Focusing on the task assigned for this thesis, it has been necessary to adapt the use of biomechanical data acquisition equipment, such as inertial measurement sensors (IMUs) or photogrammetry systems, as well as the design and reconstruction of system-specific models. Previous knowledge in biomedical signal processing and analysis has also been employed.

Finally, it was also required to know the systems involved during therapy, the Exo-H3 exoskeleton, Brain Computer Interfaces (BCI) and tSCS, since the biomechanical model must be able to record the data of interest without interference and without disturbing the combined action of these devices during the therapy session.

# 2. Introduction

## 2.1. Objectives

Loss of motor function is one of the most common consequences of neurological injuries such as SCI, with a worldwide incidence of 12.1 to 57.8 cases per million population [1]. Some of the main rehabilitation objectives for these patients are to improve the level of functional independence, increase social participation and enhance quality of life [2]. Among all these targets, patients and the clinical professionals involved identify walking ability as a priority [3]. The evolution of robotic technologies has led to the use of portable exoskeletons, which offer a wider variety of training and therapy contexts that combine different rehabilitation techniques than traditional robotic technologies [4, 5].

Biomechanics is considered an important tool to assess gait during rehabilitation therapies, since it allows the quantitative analysis of human walking and its use for diagnosis and treatment planning purposes [6, 7]. However, in complex rehabilitation therapies that combine several systems, evaluating the biomechanical outcomes becomes a challenge. ReGAIT suggests a new TOP-DOWN and BOTTOM-UP approach to enhance neuroplasticity changes during locomotion rehabilitation in patients with incomplete thoracic SCI by combining motorized lower limb exoskeletons controlled by NMIs and tSCS strategies.

There are multiple devices that allow assessing biomechanics such as optoelectronic systems based on 3D photogrammetry and IMUs to evaluate kinematics, or force platforms in the case of kinetic analysis. Currently, photogrammetry systems are the most widely used for in-depth analysis of gait kinematics due to their high accuracy. However, in this case, due to the numerous obstacles that will appear between the patient and the cameras (exoskeleton, auxiliary trolley behind the patient to transport the material needed for NMI and tSCS and physiotherapist holding the exoskeleton from behind), optoelectronic devices are not an alternative due to occlusion. Therefore, as an alternative, the IMUs system Tech-MCS V3 (Technaid S.L., Spain) is used to evaluate gait kinematics [8].

The use of gait analysis as a diagnostic device requires an accurate, reproducible, and precise measurement system. Reliability (repeatability) of gait parameters with minimal measurement error is an outstanding consideration in the clinical use of quantitative gait analysis outcomes [7]. It is important to investigate whether a variation between measurements is a therapy effect or is solely due to variation in measurements [9]. Significant information will be lost if measurement errors mask important gait deviations. Therefore, before using IMUs directly, it is important to validate the technology with a

reference. Common approaches are to use an optoelectronic system as a reference due to its proven precision [10, 11, 12, 13]. In this work, the Vicon system plays the role of the reference [14].

For all these reasons, the aim of this study is to present a validation protocol designed to evaluate the accuracy and reliability of gait kinematic assessment with IMUs, consisting of two parts: 1) exploring four different configurations offered by the IMUs to record gait data, and 2) validation of IMUs with Vicon through synchronously walking records and exoskeleton-assisted walking.

# 3. State of art and theoretical framework

## 3.1. Biomechanics of human gait

Human gait is the process of locomotion in an upright position, characterized by the alternating activity of the lower limbs, which perform the functions of body weight support and progression, allowing forward movement while maintaining stability [15, 16]. Gait is therefore the successive repetition of a series of events in each limb, leading to the gait cycle.

### 3.1.1. Gait neurophysiology

To understand the complexity of human gait, a brief description of gait generation and the basic signal flows involved in gait control are described.

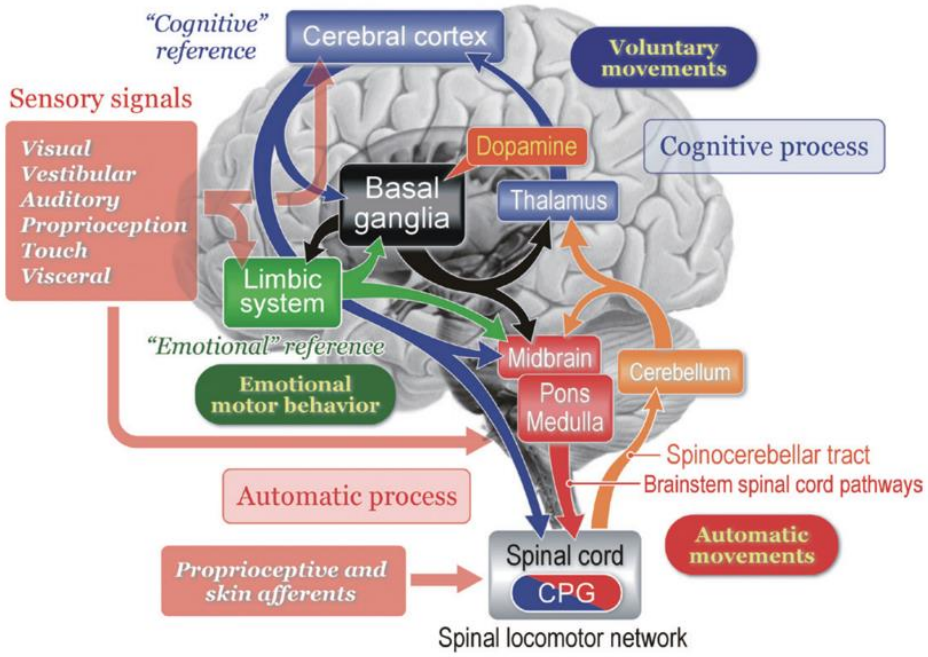


*Figure 1. Cognitive, emotional, and automatic human gait processing (From* [17]*).*

Motor control of gait is organized through automatic, emotional, and voluntary processing (Figure 1). The afferences that behave as basic signals that activate the gait pattern are sensory, external, and visceral. Depending on their origin and the type of stimuli, the gait pattern can be triggered by volitional (cognitive) processing or by emotional processing. Volitional gait movements come from motor commands generated in the neural circuits of the cerebral cortex, which are projected to the brainstem and spinal cord. On the other hand, an emotional reference can contribute to motor behavior, which is

guided by projections from the limbic system and the hypothalamus to the brainstem. This occurs, for example, in escape or fight reactions [17, 18, 19].

The generated motor behaviors, regardless of the voluntary or emotional onset of gait, are always accompanied by automatic processing of postural control, such as tone regulation, postural adjustment of movements and rhythmic limb movements. This processing is evoked by the activation of neurons in the brainstem and spinal cord sequentially. Basic locomotor patterns are generated by spinal neural networks such as the central pattern generators (CPGs), located in the lumbar area of the spinal cord, that generate rhythmic outputs without the requirement of rhythmic inputs from sensory afferents. The basic rhythm is generated by the flexor and extensor half-centers. Myotatic, autogenic inhibition and flexion reflexes are related to these CPGs [17, 18, 19].

In both volitional and automatic processes, the cerebellum and basal ganglia are involved in controlling the excitability of neurons in the cerebral cortex, via ascending projections, and in the brainstem, via descending projections. Ascending projections contribute to the planning and initiation of gait, and descending projections can modulate pattern generators and muscle tone during locomotion [18, 20].

### 3.1.2. Phases of gait cycle

The gait cycle is defined as the sequence of events that happen between two successive contacts of the same foot with the ground [21]. In unaffected subjects, contact is usually made with the heel. To facilitate the analysis and study of gait, it is described in terms of time periods and phases (Figure 2)[15, 22].

The gait cycle is divided into two periods: stance, when the foot is in contact with the ground, allowing the transfer of weight from one limb to the other; and swing, the time during which the foot is suspended in the air, promoting its progression [15]. For each limb, three intervals can be distinguished during the stance period in the gait cycle, taking the contralateral foot as a reference. Initial bipodal support or double support, in which both feet are in contact with the ground after initial contact; a monopodal support or single support, which begins with the toe-off of the contralateral foot; and a final bipodal support, which begins with the initial contact of the contralateral foot and ends with the toe-off of the homolateral foot. The stance period constitutes a total of 60% of the gait cycle, with each double support occupying 10% and the single support 40% (which coincides with the swing period of the contralateral leg), and the swing period the remaining 40% [16, 23].

Due to various affections, there may be variations in the critical events of each phase, altering the gait pattern. For this reason, and to facilitate identification, the functional phases of gait are described generically, dividing the gait cycle into 8 phases, which present a functional goal and a specific movement pattern [16, 23, 24, 25]. In other words, the stance and swing periods are themselves subdivided into 8 phases according to a specific functional objective [15, 16].

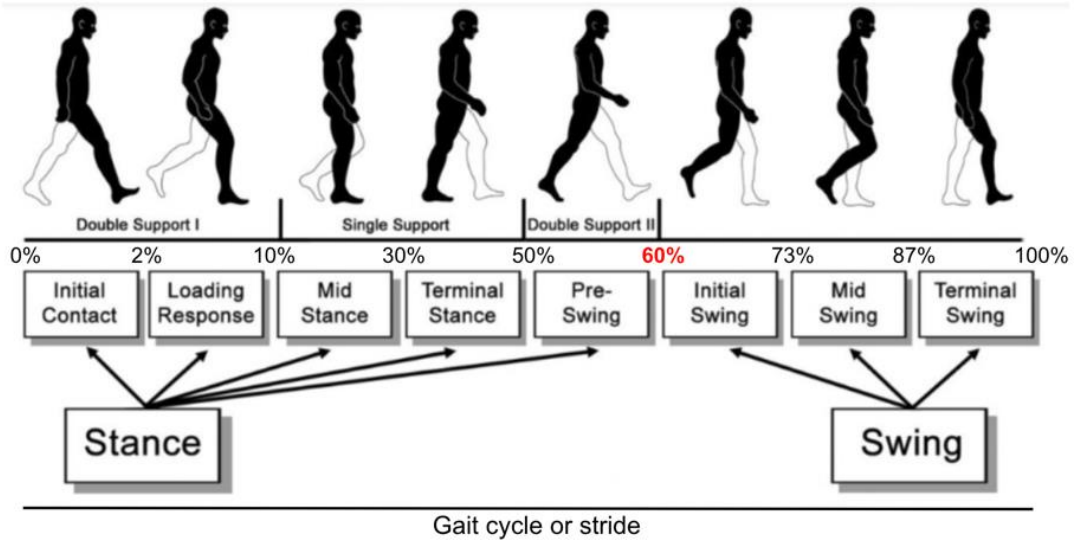


*Figure 2. Phases of gait cycle. (Adapted from* [22]*).*

Load reception is the task with the highest functional demand and includes three critical functional patterns: heel shock absorption, initial stability of the limb and preservation of progression. This includes [15]:

- Phase 1 or initial contact (0-2%): when the foot contacts the ground through heel strike.
- Phase 2 or loading response (2-10%): the initial phase of the bipodal support period in which full contact of the foot with the ground and weight transfer from one leg to the other occurs, it ends when the contralateral foot initiates swing.

During monopodal or single support, while the contralateral limb initiates the swing, the reference limb assumes body weight support as the progression continues. This functional task demands good trunk and limb stability. It consists of two phases [15]:

- Phase 3 or mid stance (10-30%): first half of the monopodal support period. Starts with the toe-off of the contralateral foot and continues until the body weight is aligned with the forefoot of the reference foot.
- Phase 4 or terminal stance (30-50%): completes the period of single support. In this phase, the body weight overcomes the forefoot. Starts with heel strike and ends with heel strike of the contralateral foot.

In the functional task of moving the lower limb forward, the lower limb takes off from the ground, in order to carry out its own progression and that of the trunk forward. Two components are differentiated: an acceleration component, which includes the pre-oscillation and initial oscillation phases, and a deacceleration component, which includes the final oscillation phase. This function consists of four phases [15]:

- Phase 5 or pre-swing (50-60%): begins with heel strike of the contralateral foot and ends with toe-off of the homolateral foot. It coincides with a bipodal support in which there is a transfer of body weight from the limb that is going to start swinging to the contralateral limb.
- Phase 6 or initial swing (60-73%): first third of oscillation. It begins with the foot leaving the ground and ends when the swinging foot reaches the position of the contralateral foot, which is supported.
- Phase 7 or mid-swing (73-87%): second third of oscillation. It ends when the tibia of the swinging limb reaches a vertical position, overtaking the supported limb.
- Phase 8 or terminal swing phase (87-100%): represents the last third of oscillation. It starts with a vertical position of the tibia and ends when the foot encounters the ground.

All this information is schematized in Figure 2 and Figure 3.

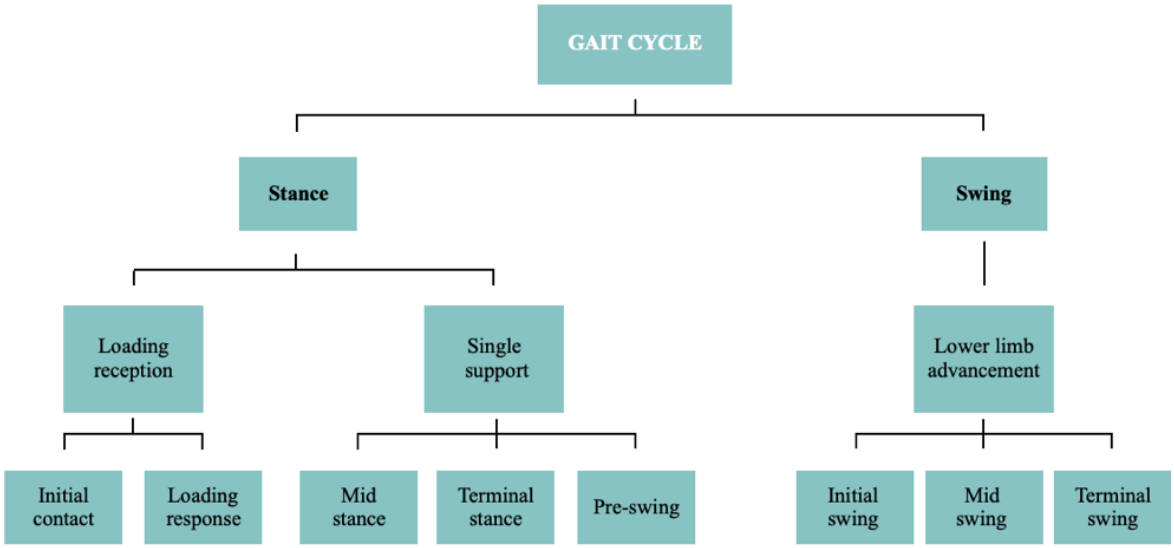


*Figure 3. Outline of the periods and phases of the gait cycle.*

Finally, the spatiotemporal parameters of gait are related both to the functional conditions of the subject and to the fear and risk of falling or to situations of cognitive deterioration. They are therefore fundamental in the analysis of gait, to evaluate the progress of a pathological process and/or to assess the effectiveness of a therapeutic intervention [26].

The main spatiotemporal parameters most often described in the literature are cadence, step length and time, stride length and time, step width and speed [16].

### 3.1.3. Kinematic pattern of the hip, knee, and ankle during gait.

Kinematics focuses on the mobility of the main joints involved in human gait, regardless of the forces that cause it, limiting itself to the study of trajectories in function of time and allowing to know the ranges of mobility [15]. The knowledge of the ranges of mobility considered common to the human population

facilitates the detection of any alteration in gait.

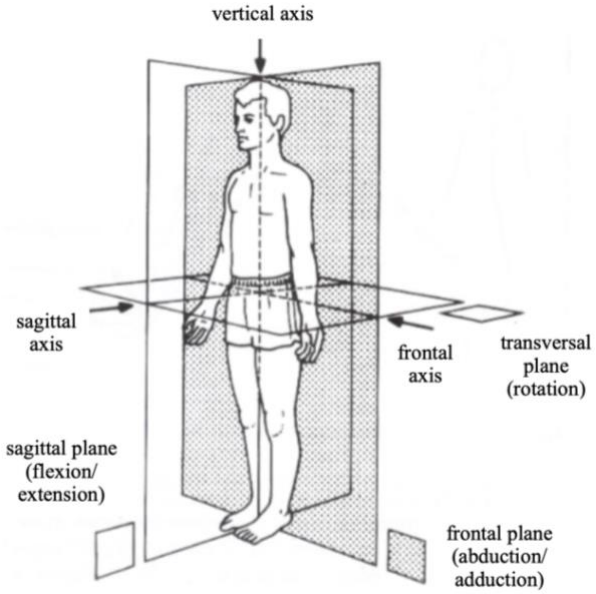


*Figure 4. Planes and axes of motion.*

To study the angular relationships between the various segments of the lower extremity, the body segments of the hip, knee and ankle-foot complex must be considered in the three planes of space. It is true that, during movement, the greatest arcs occur in the sagittal plane, but one must consider movements in the frontal and transverse planes as well, since they are associated with balance and metabolic cost related to gait. Figure 4 shows an illustration of the axes of motion and the planes with the movements observed in each of them.

Each degree of freedom is defined in terms of its joint amplitude (degrees). The main degrees of freedom of the lower limb joints during a gait cycle are summarized in Table 1.

The hip joint, by its direct direction with the pelvis, is involved in the stability and advancement of the lower limb (locomotor unit) and in the weight support and stable transport of the subject unit (trunk, head, and upper limbs). Regarding the hip kinematic pattern during the gait cycle, in the sagittal plane, flexion-extension takes place (Figure 5). From the initial contact, in which the hip is flexed about 30º, its function is to bring the subject closer to the vertical, to ensure stability in single support. The hip is extended throughout the stance period, reaching its maximum value (10º) around 50% of the cycle, coinciding with the end of the mid stance and the beginning pre-swing phases [15, 27]. Then begins a flexion that increases during the pre-swing, initial swing, and mid swing phases. This flexion reaches its maximum value (30º) in the transition to the terminal swing phase. In this final phase the hip prepares for the contact of the limb with the ground, the beginning of the next cycle, for this it loses acceleration and begins its change towards the extension movement [15, 28].

*Table 1. Joint amplitude for hip, knee, and ankle during gait cycle. (Adapted from [15, 16]).*

| Joint | Sagittal plane | Frontal plane | Transversal plane |
|---|---|---|---|
| **Hip** | 30º of flexion (IC)<br>10º of extension (PS)<br>30º of flexion (MS) | 0-5º of adduction (IC)<br>8-10º of adduction (LR-MSt)<br>8º of abduction (IS)<br>0º of adduction (TS) | Max. internal rotation (LR)<br>Max. external rotation (PS-IS) |
| **Knee** | 0-5º of flexion (IC)<br>15-20º of flexion (LR)<br>0-5º of flexion (TSt)<br>60º of flexion (IS)<br>0-5º of flexion (TS) | 4º of valgus (IC)<br>4º of varus (IS-MS)<br>4º of valgus (TS) | External rotation during all the gait cycle<br>External rotation (IC)<br>Tendency to internal rotation (LR)<br>External rotation (MSt-TSt)<br>Tendency to internal rotation (PS)<br>External rotation (IS-MS-TS) |
| **Ankle** | 0º of neutral flexion (IC)<br>5º of plantar flexion (LR)<br>10-12º of dorsal flexion (MSt-TSt)<br>20º of plantar flexion (PS)<br>0º of neutral flexion (IS-MS-TS) | Supination and adduction (IC)<br>Pronation and abduction (LR)<br>Supination and adduction (MSt-TSt-PS)<br>Neutral position (IS-MS)<br>Supination and adduction (TS) | |
| **IC: initial contact; LR: loading response; MSt: mid stance; TSt: terminal stance; PS: pre-swing; MS: mid swing; IS: initial swing; TS: terminal swing** | | | |

In the frontal plane, the hip covers a small amplitude. During the initial contact the limb, that comes from the swing period, is in a neutral position or slight adduction. It is in the following phases, that of loading response and initial mid stance, that it reaches maximum adduction (8-10º). From this point on, adduction moderates as the support period progresses [29]. This happens because of pelvic obliquity, which causes the contralateral hemipelvis to descend and decreases the articular amplitude of the homolateral hip in the frontal plane. After the response to the load, the hip goes into abduction and reaches during initial swing the maximum value of about 8°. In the last phases of the swing, a neutral posture or slight adduction is regained [15].

Finally, in the transversal plane during the gait cycle, the joint range is about 10-15°. In the loading response phase, the hip performs a maximum internal rotation, and during the pre-swing and initial swing phases, it performs a maximum external rotation. In the mid and terminal swing phases, a neutral position is restored [15, 29, 30].

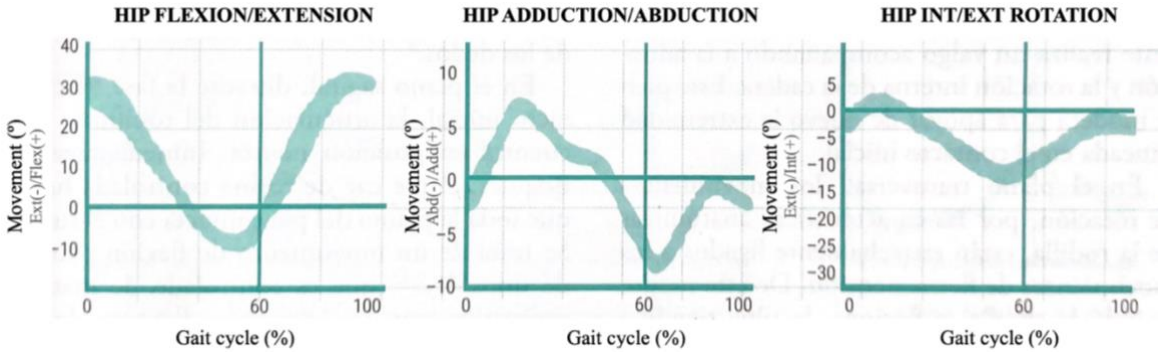


*Figure 5. Hip kinematics. The vertical line represents the toe-off. (Adapted from* [16] *and* [29]*).*

During the gait cycle, the fundamental function of the knee is the absorption of body weight, as it must ensure stability in the mid and end stance phases. In the sagittal plane, in the initial contact, the knee is in a neutral position or very little flexion (5°) [15]. Throughout the loading response, the knee flexes by 15-20º, which promotes cushioning and the reception of the weight. Then, the knee begins an extension movement until it reaches a neutral position, allowing the body to move forward. Over the final stance and pre-swing phases, the knee begins to flex as the heel comes off the ground and the trunk moves forward. The maximum peak of flexion (60°) is reached during the swing period, around 70% of the cycle [15][30]. In the mid and final swing phases, the knee extends again to promote the forward movement of the foot and prepares it for the initial contact phase. For this, the knee returns to the neutral or slightly flexed position (Figure 6).

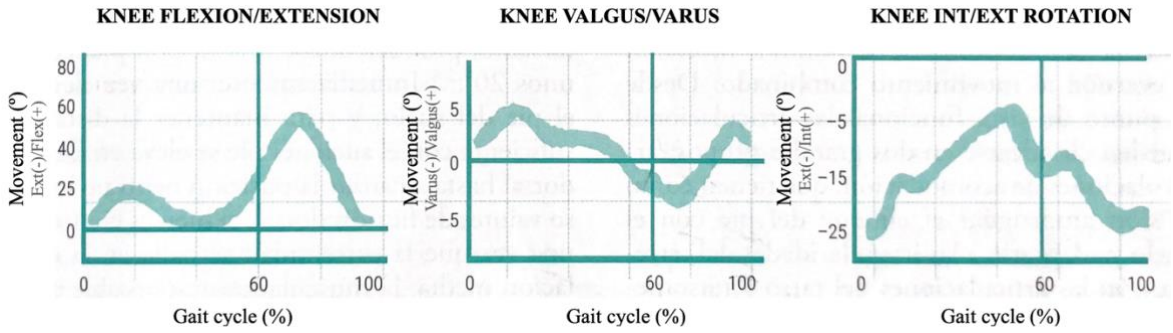


*Figure 6. Knee kinematics. The vertical line represents the toe-off. (Adapted from [16] and* [29]*).*

In the frontal plane, the knee describes a movement similar to that of the hip in this same plane, the valgus and varus movement has an amplitude of barely 8° [30]. When the femur abducts during stance, knee valgus is slightly increased, up to 4° in the loading response. During the mid and terminal swing, the movement is reversed, and the maximum abduction value is reached [15]. Subsequently, in the last swing phase, when the supporting leg is overstepped, the swinging knee performs a valgus accompanying adduction and internal rotation of the hip. This peak is then adjusted to have the limb aligned for the first stance phase, at the initial contact [16].

In the transversal plane, rotations are linked to the flexion-extension movement due to the anatomical characteristics of the knee. Thus, the tibia tends to rotate inward when the knee is flexed, and outward when the knee is extended [16, 30]. Under normal conditions, the tibia is in external rotation throughout the cycle. Therefore, the rotational movements are described as follows: on initial contact the knee is in external rotation and during the loading response it rotates about 4-8° inwards. During monopodal stance in mid and terminal stance, the knee begins to extend, and an external rotation is initiated which, in conjunction with extension, locks the joint to stabilize the limb. The highest peak of internal rotation is reached in pre-swing during knee flexion, then it returns to the external rotation required for the start of the next cycle [15, 30].

Finally, the kinematic pattern of the ankle during gait is described (Figure 7). The ankle-foot complex has multiple joints that allow it to move in all three planes of space: flexion-extension, pronation-supination, and adduction (internal rotation) - abduction (external rotation). The combined movements are eversion (pronation, abduction, and dorsal flexion) and inversion (supination, adduction, and plantar flexion) [31]. From the functional point of view, there are the accommodation joints (tarsal and metatarsal), which absorb the impact of the foot against the ground and adapt it to land irregularities, and the movement joints (ankle and toes), whose function is dynamic, and which are essential for walking [16, 32].

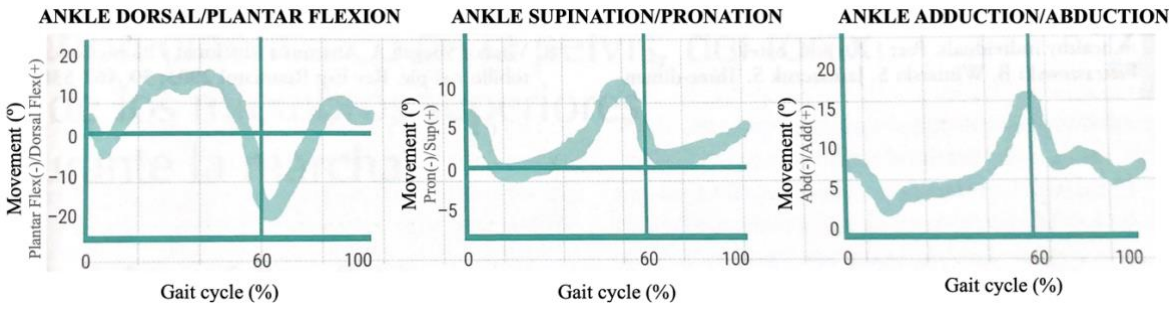


*Figure 7. Ankle kinematics. The vertical line represents the toe-off. (Adapted from [16] and* [29]*).*

In the initial contact in the sagittal plane, the ankle is in neutral position. The foot then immediately drops in a controlled manner until the sole of the foot contacts the ground, this is a plantar flexion of about 5º. This movement of foot fall with the heel landing is called *heel rocker*. This 10% of the gait cycle is a body weight absorption mechanism. Then, with the foot on the ground, about 10-12º of dorsal flexion is achieved due to the anterior displacement of the tibia, this occurs during the mid and terminal stance phases [15, 27, 30]. This displacement helps to ensure the progression of the body during the cycle.

The dorsal flexion movement corresponds to the term *ankle rocker*, that is because the tibia 'rolls' over the talus. Then, thanks to the forward displacement of the body and the oscillation of the contralateral limb, and to the concentric contraction of the plantar flexors, the heel of the foot separates from the ground and pre-swing begins. At this point, the displacement of the limb is performed on the forefoot (*forefoot rocker)*, decreasing the support surface up to the first metatarsal as the body moves forward,

resulting in a plantar flexion of 20º [15, 16, 30]. The foot is then off the ground and lifted in dorsiflexion until it reaches neutral position or slight dorsiflexion values. When the limb is in mid swing there is a subtle foot drop caused by the relaxation of the musculature responsible for dorsal flexion. However, it recovers quickly in the terminal swing to prepare the foot for the initial contact of the new cycle [16].

Concerning the frontal and transverse planes, the movements of foot orientation and plantar adaptation to irregularities are essential, which contribute to the absorption of the impact of the foot with the ground and the transfer of weight from one leg to the other. On the initial contact, the foot, which comes accompanied by tibial external rotation, is in supination and adduction. Until the end of the loading response, this is progressively turned into pronation and abduction. From this point onwards, supination and adduction movements begin again, which reaches its highest peak at the pre-swing phase. Throughout the swing period the foot tends to a neutral position, returning in the terminal phase to prepare in supination and adduction for the next initial contact [15, 16, 29].

For the appropriate analysis of the kinematic gait pattern, it is crucial not only to record the magnitude of the peak angles (maximum and minimum), but also to consider the chronology of the action and to represent the movement in each phase of the cycle.

## 3.2. Lower limb exoskeletons for gait rehabilitation and biomechanical assessment

Currently, rehabilitation based on reinforcing the neuroplasticity of the central nervous system has been encouraged to promote motor relearning, through the implementation of functional, immersive, and intensive therapies that provide neurosensory feedback [33]. Robotics is interesting for this type of therapies since it allows to generate repetitive and controlled movements along with monitoring and evaluation alternatives for motor function. In fact, there is evidence that robotic-assisted rehabilitation has similar outcomes than traditional rehabilitation interventions [34]. One of the major advantages is that they allow repetitive task-focused training on the ground, challenging the patient in terms of balance and muscle exercise while providing visual and functional feedback, which generates an opportunity to increase the results of the rehabilitation process [5].

The evolution of robotic technologies has led to the use of portable exoskeletons, and some of the most used for neurorehabilitation are shown in Figure 8. However, only 6 of them have FDA approval or CE mark, these are: Ekso, HAL, Indego, REX, ReWalk and SMA. Among them, Ekso, HAL and ReWalk are the ones with more clinical studies and, in conjunction with Indego, they are the most tested with patients [35]. Currently, in fact, there are studies demonstrating the reliability of the effect of lower extremity exoskeletons in improving lower extremity function in patients with SCI [36].


*Figure 8. Exoskeletons used for gait rehabilitation. (From* [35]*).*

There are multiple ways of assessing exoskeleton performance and its impact on subject health. Some of the measurements on which the evaluation is based on are surface electromyography (sEMG), physiological parameters, such as cardiovascular and respiratory variables, biomechanics, subjective data, and clinical evaluation tests, such as the 10 meter walk test, the 6 minutes walking test or the 1 minute sit-to-stand test [36 – 40].

EMG-based protocols assess the assistive performance of exoskeletons focusing on the muscle response

of the muscle groups of interest [41]. These sEMG techniques not only quantify the intensity of muscle activations, using parameters such as activation percentage or fiber recruitment, but also quantify and compare activation times in different gait training environments [42]. This also allows to monitor the patient's progress and to identify muscle impairments, such as fatigue or incoordination of muscle synergy. In addition, it is often feasible to use EMG as a simultaneous biofeedback during the rehabilitation session [43].

Biomechanics assessment is a crucial tool for validating the effectiveness of exoskeleton-assisted gait rehabilitation. Kinetics describes the relationship between forces and movement in the joints. To assess this in gait analysis, systems such as force platforms, also known as force plates, are used to measure the ground reaction force and displacements of center of mass when a subject walks on the ground [44]. However, there are also some recent studies that propose protocols for kinetic analysis based on muscle activation, using EMG systems [45].

Currently, the gold standard for assessing kinematics during motion are optoelectronic systems based on photogrammetry, either with active or passive markers, as they allow in-depth analysis of the kinematics and are characterized by their high accuracy. However, the quality of the capture depends on whether the markers are captured by the cameras, which is a huge drawback on certain occasions where there are too many obstacles in the recording area. Vicon is nowadays a widely used system [46].

Other alternatives used in kinematic analysis, although less precise, are potentiometers, digital direction finders or IMUs. IMUs are used to track joint angles, velocities, and accelerations during different movements. Many studies evaluate the impact and performance of the exoskeleton with IMUs due to their light weight and portability, and to avoid the visualization problems that optoelectronic systems present [47 – 49]. The problem here is that there are multiple measurement protocols, including differences in sensor placement.

Depending on the type of evaluation to be carried out, a specific protocol is executed, and data are recorded with a particular system. It is therefore required to verify that, for the same measurement, kinematics recorded with different protocols and devices are sufficiently similar to be considered interchangeable. There are multiple studies that evaluate the accuracy of IMUs with photogrammetry systems by means of waveform similarity assessment of synchronous signals [10, 12, 13, 50].

## 3.3. Conclusions

When assessing gait with exoskeletons, it is necessary to deepen the elements of biomechanical analysis to detect small changes and to understand the mechanisms of recovery of function. For this, it is considered indispensable to evaluate muscular activity, kinematics, and kinetics.

However, for this rehabilitation therapy combining exoskeleton, with BCI and tSCS, assessing kinetics with force platforms is not an option, and a specific signal processing protocol needs to be developed to

recover the voluntary contraction of the EMG signal (which will be composed of volitional and involuntary contraction elicited by stimulation).

Regarding the kinematic analysis, it is not feasible to perform it with an optoelectronic system because wearing an exoskeleton and the other devices leads to occlusion of the markers. Therefore, a biomechanical analysis protocol based on IMUs is to be developed, but for this purpose, in this study, the accuracy of these sensors is tested with the Vicon motion capture (mocap) system.

# 4. Materials and methods

This chapter describes the tools used to carry out the validation designed to evaluate the accuracy and reliability of the kinematic gait assessment with IMUs, and thus achieve a biomechanical assessment model as adapted as possible to the therapy, so that the recorded data are valid for further analysis without being corrupted by interferences caused by the assistive technologies. The methodology used in the project is also detailed, relating the theory explained above with the proposed methods to develop each step.

## 4.1. Materials

### 4.1.1. Tech-MCS V3 motion capture system

The Tech-MCS V3 is a complete motion capture system based on inertial technology, which incorporates 3D inertial sensors, called "Tech-IMUs" (connected to each other and to the HUB by cables), a concentrator device called "Tech-HUB V3" to organize and send the information obtained by the Tech-IMUs to the PC (USB cable, wireless via Bluetooth or recording to Micro SD memory), its own software to manage and display the motion captures made, textile and plastic fastening adapters for Tech-IMUs and cables specially designed to place the Tech-IMUs on the different parts or segments of the human body [8] (Figure 9).


*Figure 9. Tech-MCS components.*

The Tech-HUB V3 is the data concentrator of the Tech-MCS V3 motion capture system. It receives and manages the information coming from the Tech-IMUs connected to it and forward it to the PC via USB cable, wirelessly via Bluetooth or by recording on a Micro SD memory. The Tech-IMUs are connected to the Tech-HUB V3 in groups of four sensors. For this purpose, the Tech-HUB V3 has four specific ports for Tech-IMUs, resulting in a maximum of 16 sensors that can be connected simultaneously. Ports 1 and 3 belong to channel 1, and ports 2 and 4 to channel 2. Each group of Tech-IMUs are connected in series via cables to the corresponding port (Figure 10).

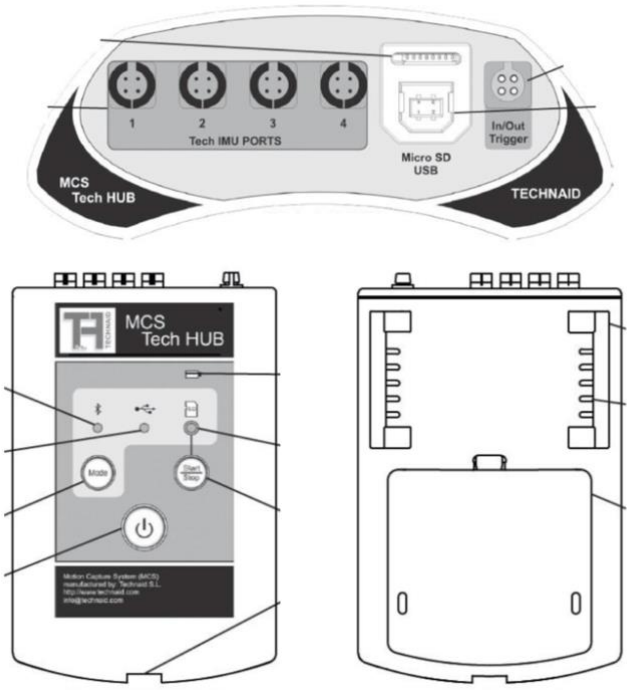


*Figure 10. Tech-HUB V3: connection panel and control panel.*

Tech-IMUs are small motion sensor devices, based on MEMS (Micro Electro Mechanical Systems) technology. These electronic measuring devices make it possible to estimate the orientation of a body, attached to it, from the inertial forces experienced by that body. Their principle of functioning is based on the measurement of the forces of acceleration and angular velocity exerted independently on small masses located inside them. They incorporate an accelerometer, a gyroscope, and a magnetometer, all of them orthogonal three-dimensional, a temperature sensor and a powerful microprocessor.

The signals obtained from the accelerometer, gyroscope and magnetometer are merged to obtain the IMU orientation, represented by the Directing Cosine Matrix (DCM), also called the rotation matrix. The DCM expresses the orientation of the IMU with respect to a fixed coordinate system in which the X-axis direction points toward magnetic north, and the Z-axis direction points in the same direction as the Earth's gravitational force. The process by which the IMU orientation is estimated can be divided into two main steps. The first consists of the estimation of the initial orientation through the measurements of the 3D accelerometer (3D Acc) and the 3D magnetometer (3D Mag), see (Eq. 1. This

process is performed only once, when the IMU is stationary and before the user is allowed to start its movement.

$$3D\ Acc = \vec{W} \approx [0\ 0\ 9.8]$$
$$3DMag = \vec{M} = [M_X\ M_Y\ M_Z]$$

$$\overrightarrow{U_{(X)}} = \left| \overrightarrow{W_{(Z)}}\ X\ \vec{M} \right|$$

$$\overrightarrow{V_{(Y)}} = |\overrightarrow{W_{(Z)}}\ X\ \overrightarrow{U_{(X)}}|$$

$$DCM = \left[\overrightarrow{U_{(X)}}\ \overrightarrow{V_{(Y)}}\ \overrightarrow{W_{(Z)}}\right] = \begin{Bmatrix} \hat{u}_x & \hat{v}_x & \hat{w}_x \\ \hat{u}_y & \hat{v}_y & \hat{w}_y \\ \hat{u}_z & \hat{v}_z & \hat{w}_z \end{Bmatrix}$$

*(Eq. 1)*

The second step is the estimation of the orientation of the IMU when it starts its movement. The 3D gyroscope (3D Gyro) is the sensor involved in this process. From the integration of the angular velocity signals obtained from the 3D Gyro, it is possible to know the angle of rotation of each axis of the IMU. The previous DCM (*DCM(t-1)*) is updated by adding the newly calculated rotation (Eq. 2). These two steps are used in a sensory fusion process to obtain the orientation estimation from the inertial information by means of an extended Kalman filter (EKF) running on the IMU. This process is summarized in Figure 11.

$$3DGyro = \vec{w} = [\omega_X \omega_Y \omega_Z]$$
$$DCM(t) = DCM(t-1) + \int \overrightarrow{w(t)}$$

*(Eq. 2)*

In this way, an IMU can measure the orientation of the body to which it is attached whenever and wherever it is needed without the need for cameras or specially equipped laboratories, as long as the magnetic field is not distorted [51].

Regarding the sensor model, regardless of the type of physical variable (*f*) to be measured with the Tech-IMU sensor device (acceleration, angular velocity, or magnetic field), the output value (*S*) obtained at the sensor can be represented by the following (Eq. *3*.

$$S = gf + Rf + Nf + bf + c(t)f + \epsilon(f)$$

*(Eq. 3)*

Where,

- *g*: Sensor axis gains.
- *R*: Rotation matrix of the sensor with respect to the coordinate axis of the sensor case.
- *N*: Orthogonality matrix of the sensor axes.
- *bf*: Bias of the sensor axes.
- *c*: Temperature coefficient of the sensor axes.
- *t*: Temperature at the sensor.
- $\epsilon$: Random noise at the sensor.

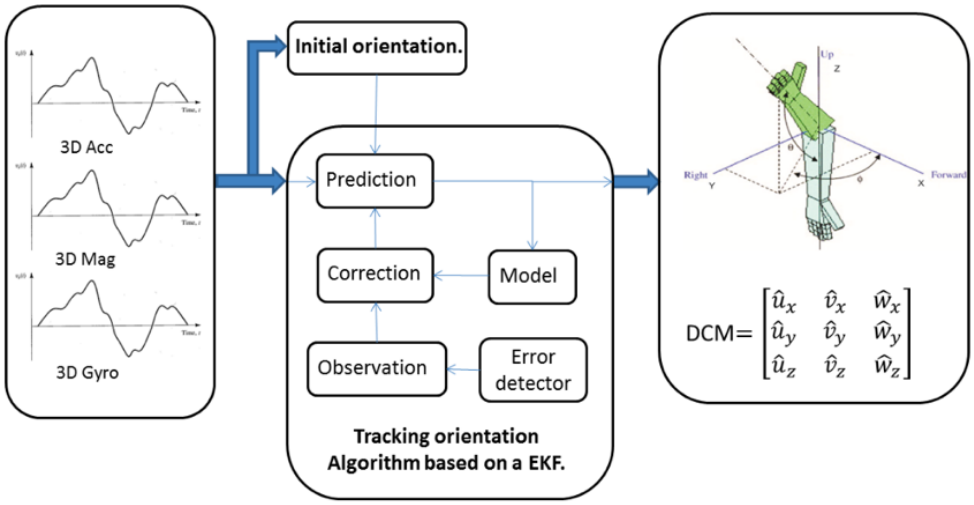


*Figure 11. Diagram of the IMU's internal process for obtaining 3D orientation.*

Before starting the movement, it is necessary to perform a calibration process which consists of determining each of the model values and correcting the sensor output so that it accurately represents the physical variable to be measured. The internal sampling rate of each sensor is 1kHz.

According to the user's requirements, the Tech-IMU V3 can deliver movement data in four types of formats: digital, physical, DCM orientation and quaternion orientation. The one that is relevant to this project is quaternion orientation, which allows to obtain the orientation of the Tech-IMU with only four *float32* values (IEEE-747). The four values delivered correspond to the quaternion representing the rotation of the sensor axes with respect to the reference coordinate system. The data is presented in the format *[qw qx qy qz]*, where *qw* is the real part of the quaternion and *qx*, *qy*, and *qz* are the imaginary parts. The range of values in quaternions is between -1.0 and +1.0. In addition, this format offers the possibility of obtaining quaternion data transformed into joint angles, thus reducing the need for subsequent processing.

Depending on the format selected, the size of the data transmitted changes and therefore the connection

used, PC connection via USB cable, wireless PC connection via Bluetooth or recording to Micro SD memory, which limits the amount of Tech-IMUs that can be connected to the system. In turn, each transmission channel has a different bandwidth, which limits the acquisition frequency of the captures. The configuration proposed for quaternion orientation data format for wireless PC connection via Bluetooth, which is the optimal capture condition for this work, is shown in Figure 12.

| MODO BLUETOOTH | | | | | | | | | | | | | | | | |
|---|---|---|---|---|---|---|---|---|---|---|---|---|---|---|---|---|
| **# Tech-IMUs** | 1 | 2 | 3 | 4 | 5 | 6 | 7 | 8 | 9 | 10 | 11 | 12 | 13 | 14 | 15 | 16 |
| **25 Hz** | OK | OK | OK | OK | OK | OK | OK | OK | OK | OK | OK | OK | OK | OK | OK | OK |
| **30 Hz** | OK | OK | OK | OK | OK | OK | OK | OK | OK | OK | OK | OK | OK | OK | OK | No |
| **35 Hz** | OK | OK | OK | OK | OK | OK | OK | OK | OK | OK | OK | OK | OK | OK | OK | No |
| **40 Hz** | OK | OK | OK | OK | OK | OK | OK | OK | OK | OK | OK | OK | OK | OK | OK | No |
| **45 Hz** | OK | OK | OK | OK | OK | OK | OK | OK | OK | OK | OK | No | No | No | No | No |
| **50 Hz** | OK | OK | OK | OK | OK | OK | OK | OK | OK | OK | No | No | No | No | No | No |

*Figure 12. Configuration of data acquisition rate and number of sensors for quaternion orientation data format.*

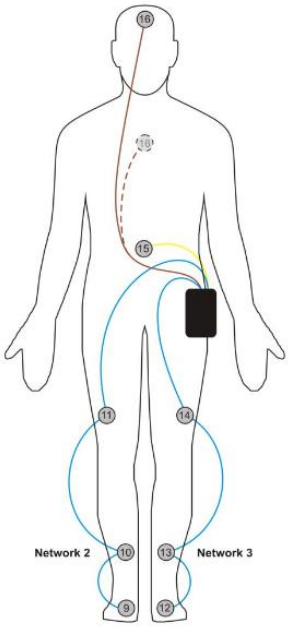


*Figure 13. Lower limb Tech-IMUs configuration, network for port 2 and 3.*

Moreover, the manual offers a series of recommendations for the amount, connection and positioning of cables and sensors to create the network to be placed on the human body. For example, the configuration proposed for the lower limb can be seen in Figure 13.

Before starting to record a capture, after having placed and connected the IMUs, their correct detection can be checked in the right sidebar of the software, shown in Figure 14.

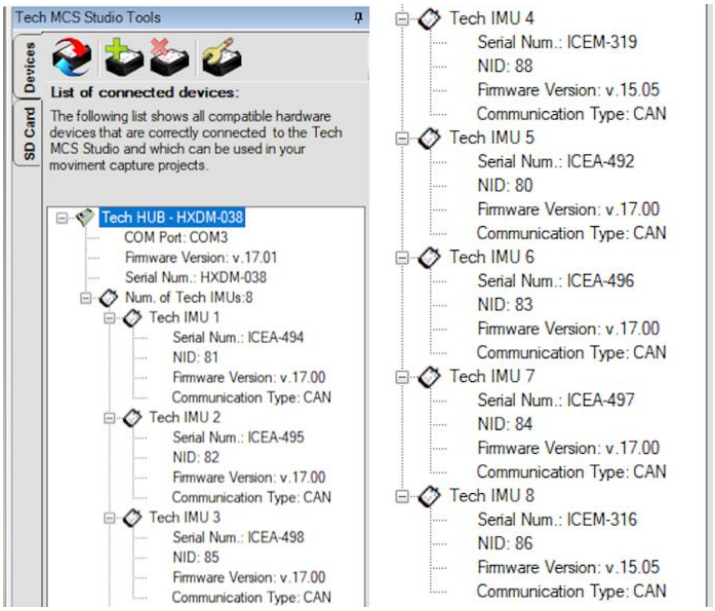


*Figure 14. Tech-MCS: list of connected devices.*

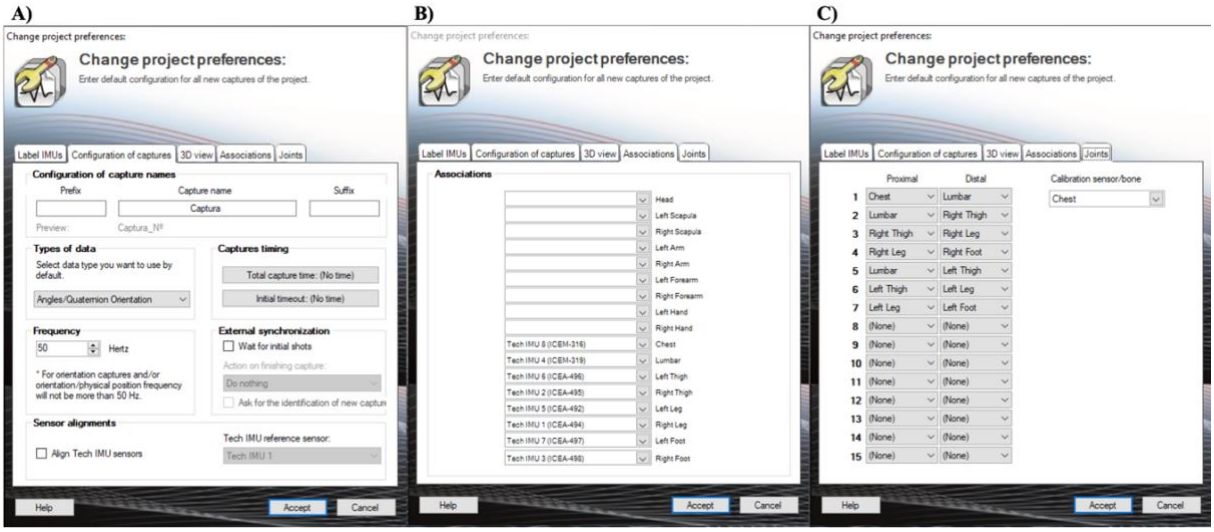


*Figure 15. A) Configuration of captures: format and frequency settings. B) Associations for segment definition. C) Joints creation and calibration reference setting.*

Once detected, a new project is created, and its characteristics are set. The output frequency of interest is selected, the type of data format to be obtained is chosen, and the body segments are defined by relating each IMU to the part of the body where it is located (Figure 15A-B). In this way each joint will be delimited by two segments, defined from proximal to distal, for example, the 'Right thigh' and 'Right Leg' segments make up the right knee. Finally, the reference sensor for calibration is established (Figure 15C).

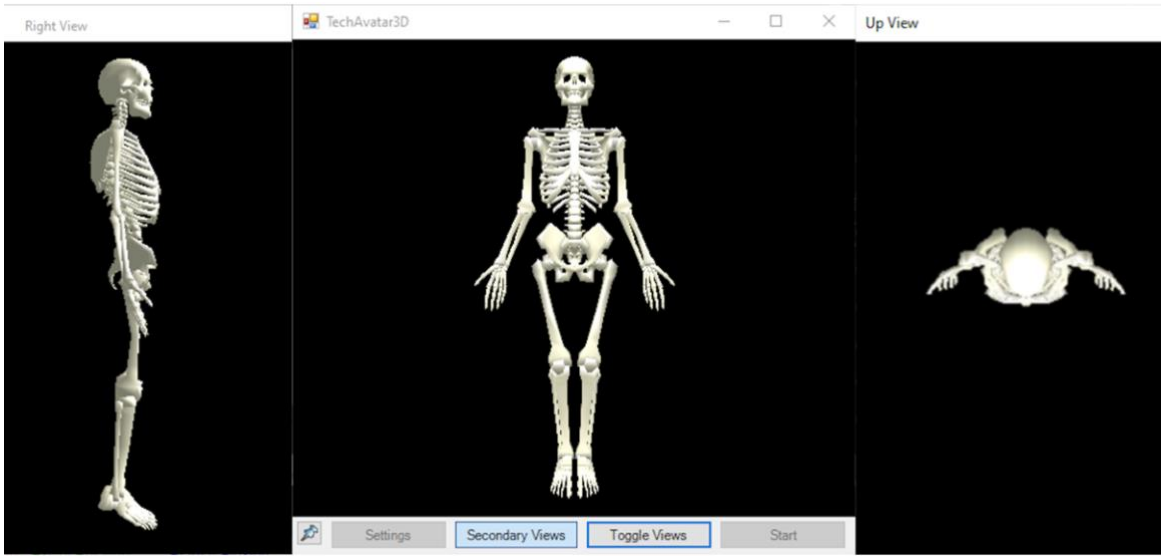


*Figure 16. Tech-MCS: real-time skeleton avatar.*

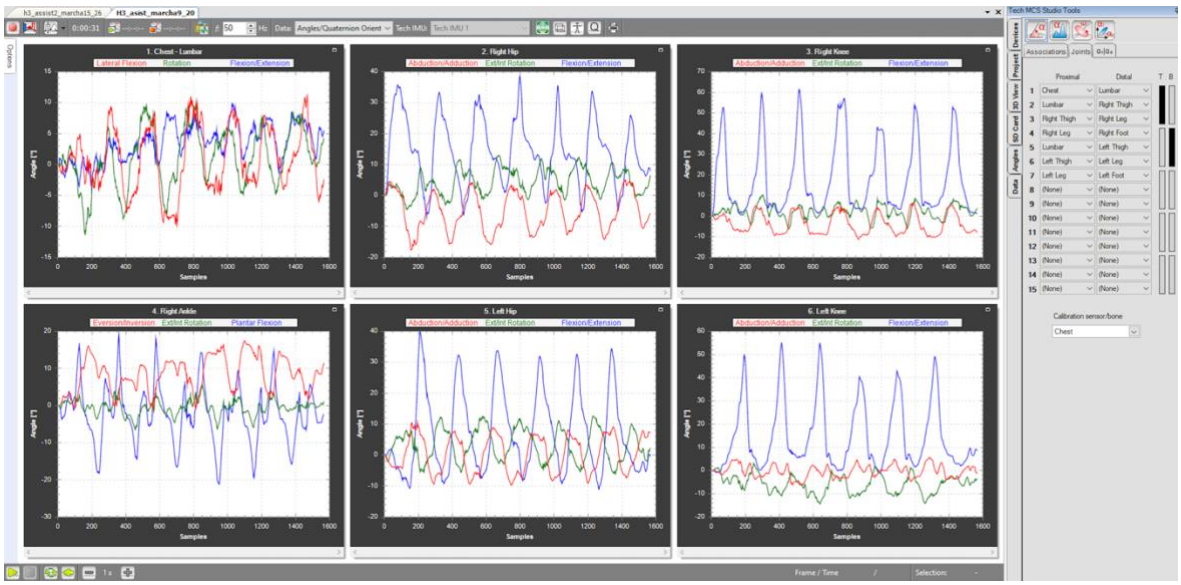

*Figure 17. Tech-MCS: recorded data.*

When all these parameters have been set, the recording can begin. The first step in recording is to perform the calibration, for which the user is asked to stand in a T-position, with legs spread shoulder-width apart, trunk straight and arms stretched perpendicular to the trunk. This process takes about 5 seconds. Then the subject can start the asked movement, walking in this case. The Bluetooth mode enables real-time visual monitoring of the data recorded by the IMUs and allows to ensure the good calibration of the sensors through the real-time skeleton avatar (Figure 16).

After the test is completed, the recorded data can be displayed and new parameters, such as angular velocity or gait cycle, can be calculated from them (Figure 17). Lastly, the recorded data can be exported

for further analysis.

### 4.1.2. VICON Photogrammetry system

Mocap systems are a powerful tool for biomechanics, robotics, and gait analysis. Vicon is an optical-passive optoelectronic mocap system. Optical-passive mocap technique uses retro-reflective markers that are tracked by infrared cameras [46]. Currently, it is the most accurate method used in the industry. This Vicon system consists of 8 Vicon Vero digital infrared cameras with adjustable lenses and focus, and a software for data processing and visualization, Vicon Nexus 2.10.3 (Vicon Motion Systems, Oxford, UK).

The setup of the cameras and, therefore, the recording space can be seen in Figure 18, where the definition of the global coordinates of the system is also observed. The global Z-axis (blue) defines the vertical, that is, perpendicular to the laboratory floor. The global X (red) and Y (green) axes are in the plane of the laboratory floor, with X defining the direction of normal motion along the laboratory walkway (RGB = XYZ).

Before starting to record it is necessary to set up the system, this includes reducing the noise and brightness detected by the camera and calibrating the recording area.

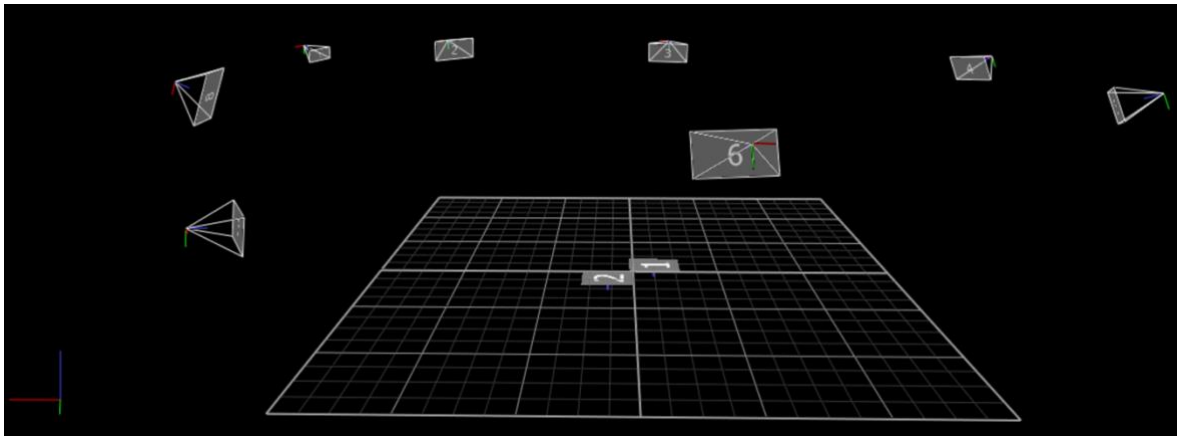

*Figure 18. Laboratory recording space and Vicon Vera cameras disposition.*

Next, a new project is created and the configuration for patient or control subject is selected, a subject is created from a marker template. The mandatory anthropometric measurements must be filled in. Once the profile is created, the system is ready and all markers are visible, the recording starts. The first step is to perform a short trial corresponding to a Static Calibration, placing the subject in the center in a T-shape. If this test is valid and the markers are visible, the markers are labelled, saved, and the dynamic gait trials can begin.

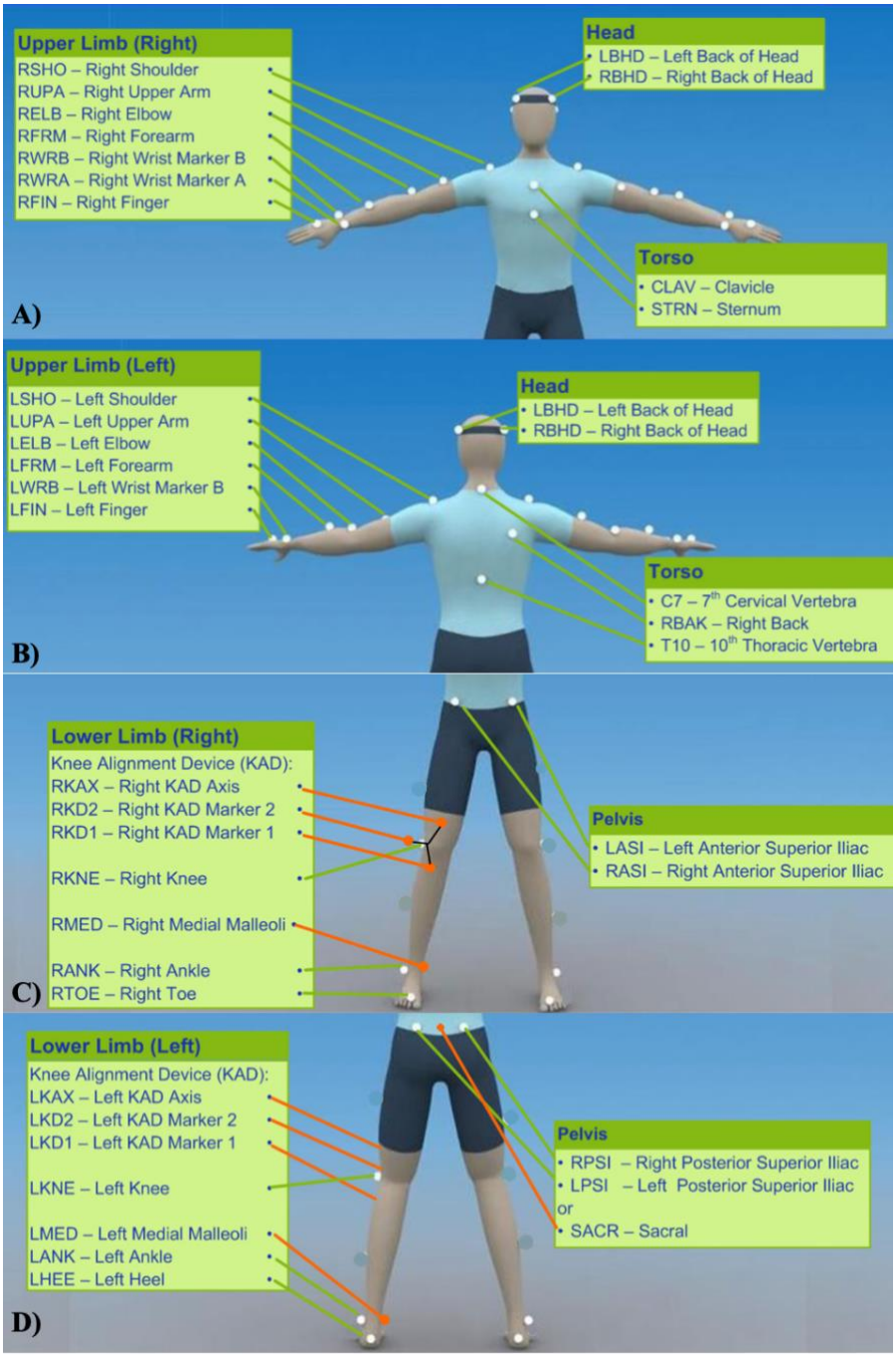


*Figure 19. Plug-in Gait marker set for upper and lower body. A) Upper body, front view. B) Upper body, back view. C) Lower body, front view. D) Lower body, back view.*

Vicon reconstructs the motion kinematics and kinetics of the user walking through the recording scenario by detecting the passive markers attached to the body surface. For the proper reconstruction of each segment and the optimal calculation of joint angles, it is necessary to place the markers in appropriate positions guided by different proposed models. The Plug-in Gait model is Vicon's implementation of the Conventional Gait Model, which provides broadly used and reliable full-body kinematic and kinetic

modelling without the need for additional customization [52]. It is built on the Newington-Helen Hayes gait model and has been validated through its extensive citations in peer-reviewed publications [53][54]. Vicon Nexus also includes the pre-defined Plug-in Gait marker set and the necessary pipelines to enable the calculation of joint kinematics and kinetics outputs for gait analysis patients [55]. The marker set proposed for lower limb Plug-in Gait is shown in Figure 19**Error! Reference source not found.**.

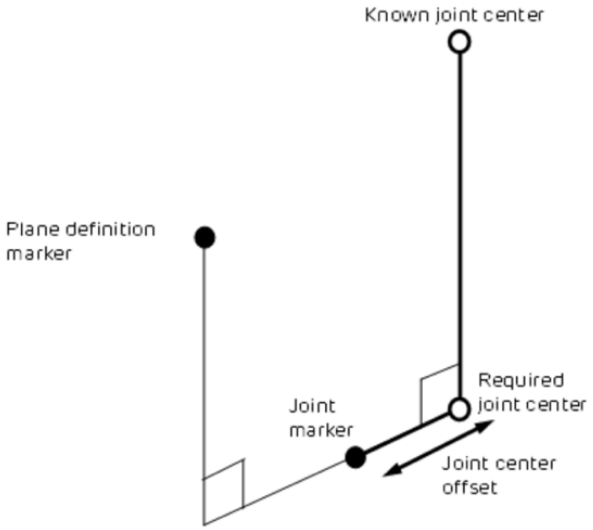


*Figure 20. Chord function for joint center calculation.*

The Plug-in Gait biomechanical model calculates joint kinematics and kinetics from XYZ marker positions and subject-specific anthropometric measurements. To obtain the kinematics, it is necessary to define the rigid body segments and calculate the joint angles between them. For this, the center of each joint must be calculated [56]. In the case of the lower limb, the Newington-Gage model is used to define the positions of the hip joint centers in the pelvis segment. The Chord function is used to define the other joint centers (knees and ankles). As a general explanation, three points are used to describe a plane: one of these points is meant to be a pre-calculated center of articulation, the second is a real marker at a known perpendicular distance from the requested center of articulation (the offset of the center of articulation), and the third point is the required joint center. The offsets are calculated from the anthropometric measurements of the subject entered in the system and the position of the actual markers. This is represented in Figure 20.

A modified version of the function estimates the required position of the joint center when the plane definition marker is rotated out of this plane by a known angle around the suggested joint center axis. The function is adapted to static and dynamic processing.

Once the joint centers have been calculated and the segments have been defined, the departure angles of all the joints are calculated from the YXZ Cardan angles obtained by comparing the relative orientations of the two segments that make up each joint. For more information on the calculation of kinematics and kinetics see the links referenced throughout this section.

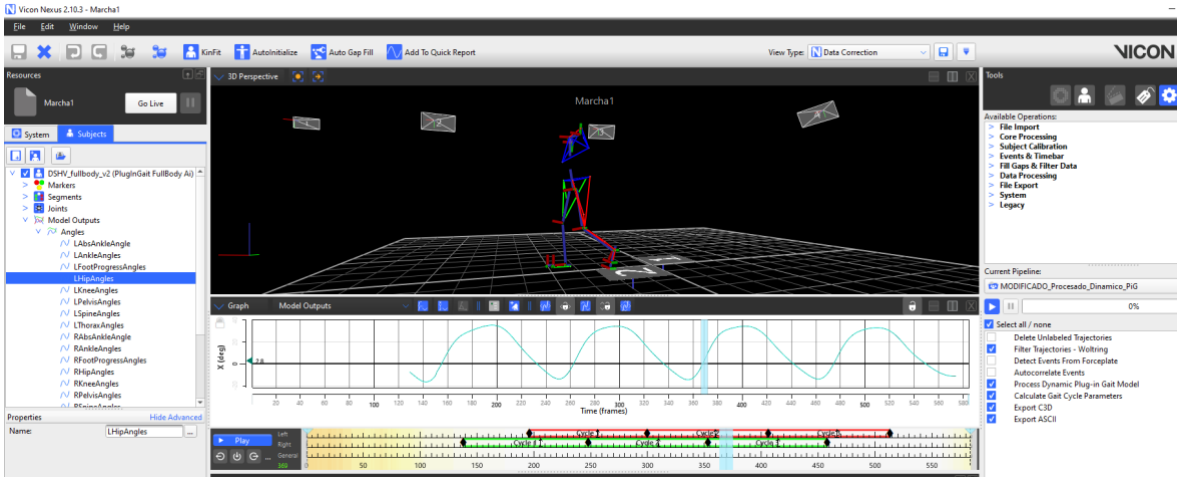


*Figure 21. Vicon Nexus processed trials visualization.*

The kinematic outputs obtained during processing in Vicon Nexus software (Figure 21) can be exported to a CSV file and analyzed on other platforms.

### 4.1.3. Exo-H3 lower limb exoskeleton

The Exo-H3 is the third version of Technaid's lower limb exoskeleton designed specifically for research [57]. It can emulate human gait, replicating gait patterns that have been previously introduced, through its six motorized joints in the sagittal plane. Thus, it has six degrees of freedom in the sagittal plane, one for hip, one for knee and one for ankle in right and left legs (Figure 22).

It also has position control, torque control and real-time admittance control, for this purpose it is equipped with six joint position sensors, six torque sensors and four toe and heel pressure sensors. The device is designed to be used by subjects between 110 and 210 cm in height, and between 40 and 100 kg in weight. The exoskeleton weights 17 kg (battery included).

The Exo-H3 also has an app for Android systems designed to operate the basic functions of the device such as standing up, sitting down, walking speed, or walking assistance (Figure 23). The application allows to determine independent step patterns and different percentage of assistance for each leg, from 10% to 100%, increasing (+) or decreasing (-) in steps of 10%. Furthermore, it permits regulation of the level of resistance through three modes: the 'Passive' mode, which allows free movement of the motors with resistance; the 'Complain' mode, which enables the same but with very little resistance; and the 'Free' mode, which does not impose any resistance. Once the end user and the user controlling the exoskeleton are ready to use the device, ‘Walk’ bottom allows starting the operation with a pre-loaded gait pattern. Using the ‘Up’ and ‘Down’ arrows it is possible to increase or decrease the walking speed, for which there are ten levels.

*Figure 22. Exo-H3.*

In this way, the exoskeleton can be adjusted to the needs of the end user, helping people who have partially lost the ability to walk after a partial SCI, thus contributing to the development of neurorehabilitation research.

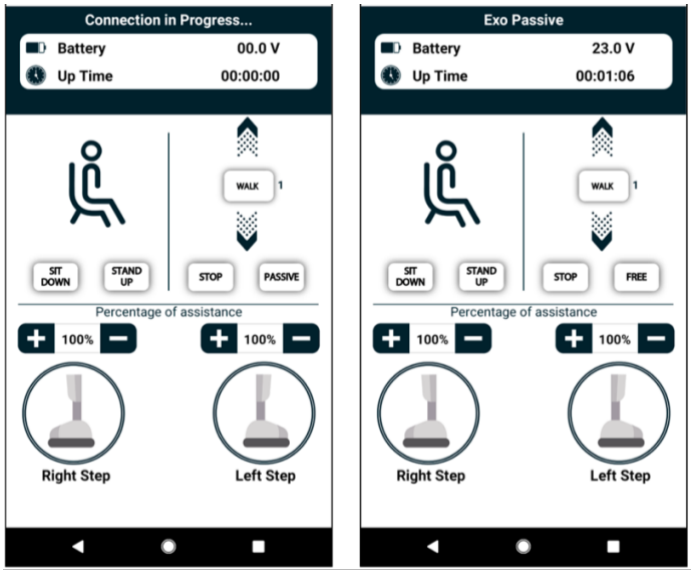


*Figure 23. Exo-H3 control app.*

## 4.2. Methodology

The study of gait kinematics involves a 3D analysis of the movement of the hip, knee, and ankle. However, in rehabilitation processes with lower limb exoskeletons, the analysis focuses on the sagittal plane, as this is the only one in which the exoskeleton acts, the others being limited. Consequently, in this validation, despite having studied joint movements in all planes, only the data obtained for the sagittal plane are decisive. The three tests explained beneath have been carried out on a healthy 27-year-old subject.

### 4.2.1. Part I. Exploring the different configurations offered by the IMUs

#### 4.2.1.1. Data acquisition

To record the angles of the lower extremity joints, it is first necessary to learn how to use the Tech-MCS system, its IMUs and software, as well as to design a model with the optimal positioning so that the recordings are as accurate as possible.

According to the literature reviewed and explained above in section 3.2, many of the models used consist of at least 7 IMUs: three IMUs for each leg, arranged at the thigh and lower leg segments and at the ankle joint, and one IMU in proximal position that acts as a reference for calibration, almost always placed in the lumbar region. However, on the other hand, according to the models suggested by the Technaid guide (Figure 13), 8 IMUs are used, the eighth being an extra IMU for calibration reference, which can be placed on the chest or on the subject's head.

Furthermore, although the system recalculates the orientation of each IMU according to the position of the adjacent IMUs and this is not a mentioned problem in any study, it is considered essential to evaluate whether the placement and orientation of the axes of each IMU sensor affects or has a decisive impact on the measurement.

Therefore, in the first phase, four models of IMUs configurations are proposed, whose differences lie in the number of sensors employed, their placement on the human body surface, and, consequently, their axes orientation (Figure 24). For every configuration, the IMUs network placed on the right limb (1, 2 and 3) are connected to the Tech-HUB port 2, the ones for left limb (4, 5 and 6) and the one on the chest (8) are connected to port 3. The lumbar one (7) is connected to port 4.

Models 1 (M1) and 2 (M2) propose the same positioning for the thighs, legs, and ankles, this is based on the sensor and strap placement recommendations provided in the Tech-MCS guide (Figure 13). From a front view, the IMUs of the thighs are slightly positioned on the outside, those of the lower legs are slightly positioned on the inside, and the ankles ones are positioned on the external part of the joint (over the subject's sneakers, below the lateral malleolus). They differ from each other in that the reference proximal IMU for calibration in Model 1 is number 7, positioned in the lumbar area, while in Model 2,

an eighth sensor (8) is added, positioned on the chest (over the sternum), becoming the calibration sensor.

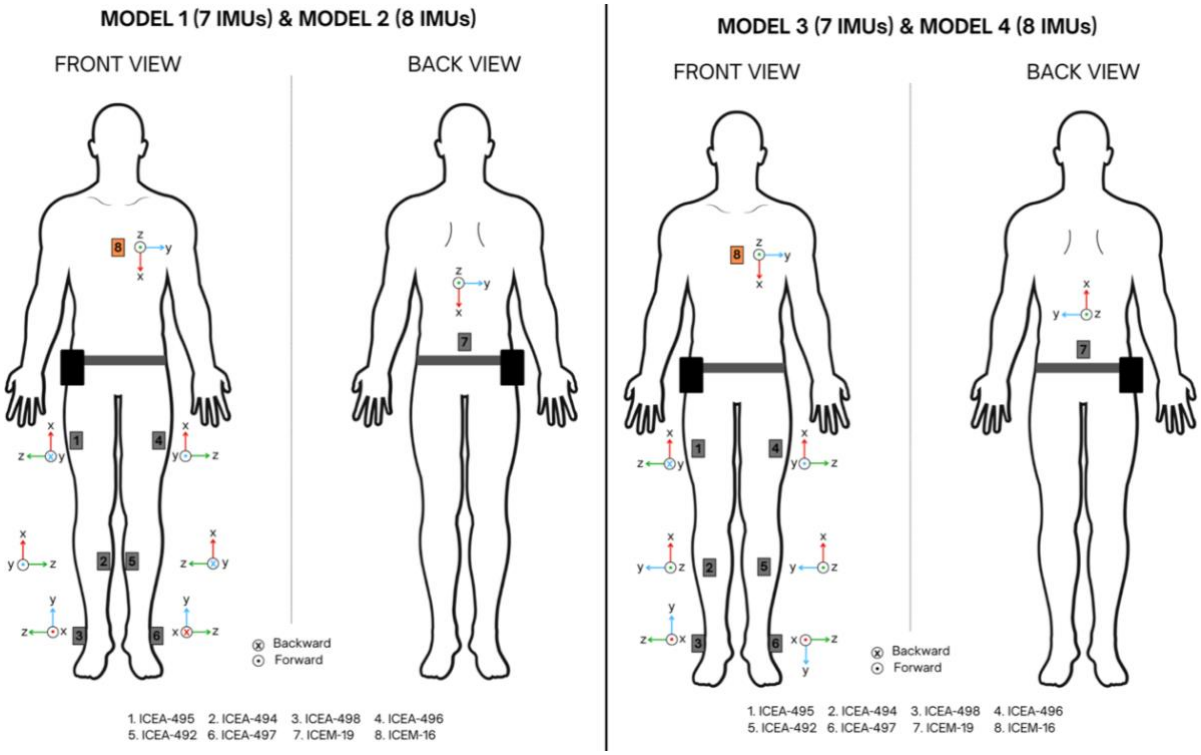


*Figure 24. Proposed IMUs configurations.*

For Models 3 (M3) and 4 (M4), another IMU arrangement is proposed. The thigh sensors are kept slightly external and with the same axes orientation, while the leg sensors are placed centered and reoriented. In addition, the ankle sensors remain positioned on the outer area of the joint, but the left one is reoriented, changing the axes arrangement. The reference for Model 3 is the IMU 7, positioned in the lumbar area but with a change in orientation with respect to the previous models. And for Model 4, the reference sensor for calibration is number 8, positioned on the chest.

Two captures are recorded with each model configuration during bare-legged walking at a sampling rate of 50 Hz (Figure 12) and with the quaternion and angle type format, to obtain the gait kinematics without post-processing (Figure 15). These tests are recorded in the Biomechanics and Technical Aids Unit of the HNP, in a walkway of 10 m, shown in Figure 18.

#### 4.2.1.2. Data analysis

Once the signals are recorded and exported to CSV, the signal processing is done in MATLAB_R2021b (The MathWorks, Inc., Natick, Massachusetts, USA). Smoothing is performed with the Saviztky-Golay filter of order 3 and with frame length of 21 samples, and the gait cycles are extracted manually.

Repeatability of gait variables is an important consideration in the clinical use of quantitative gait

analysis results. To validate the robustness and consistency of each configuration, the similarity and variability of the waveforms of the gait cycles extracted for each proposed model is studied.

To perform the waveform similarity assessment for each model and for each joint angle, the statistical measure called the within-day Coefficient of Multiple Correlation ($CMC_w$) of Kadaba is calculated to assess the repeatability of kinematics removing the between-gait-cycle variability. The $CMC_w$ is computed as follows, e.g. when for a subject and a joint-angle, *W* waveforms are acquired in each of *S* different sessions and for each waveform *F* frames are available [58, 59]:

$$CMC_w = \sqrt{1 - \frac{\sum_{s=1}^{S}\sum_{w=1}^{W}\sum_{f=1}^{F}\left(Y_{swf} - \bar{Y}_{sf}\right)^2 / SF(W-1)}{\sum_{s=1}^{S}\sum_{w=1}^{W}\sum_{f=1}^{F}\left(Y_{swf} - \bar{Y}_{s}\right)^2 / S(WF-1)}}$$

*(Eq. 4)*

Where,

- $Y_{swf}$ is the ordinate at frame *f* of the waveform *w* of session *s*.
- $\overrightarrow{Y_{sf}}$ is the ordinate at frame *f* of the average waveform among the *W* waveforms of the session *s*.
- $\overrightarrow{Y_s}$ is the grand mean of the $\overrightarrow{Y_{sf}}$ of session *s*.

Thus, the closer the $CMC_w$ is to 1, the more similar and repeatable the measurements are and the more consistent the configuration is.

Also, for each model and each joint angle, the average range of motion (ROM) of the extracted gait cycles is calculated, as well as the standard deviation (std), and its dispersion is measured with the coefficient of variation (CV). Although this value does not exclude variability between gait cycles, within a single trial and immediately successive trials registered in the same session the difference between gait cycles is considered to be minimal for a healthy user. In this way, given a gait cycle signal *g*:

$$ROM_g = max(g) - min(g)$$

$$CV = std\left(ROM_g\right)/mean\left(ROM_g\right) * 100\ (\%)$$

*(Eq. 5)*

Despite not being synchronous records, as Model 1 and 2 records are taken in immediate succession, and Model 3 and 4 records too, the Root Mean Square Error (RMSE) between the means of each pair is computed to see if the eighth IMU introduces changes.

Finally, the mean gait cycle for each model and each joint is calculated and plotted against the normality (mean and std) of the subject recorded with Vicon.

### 4.2.2. Part II. Validation of IMUs with Vicon: similarity assessment

#### 4.2.2.1. Data acquisition

- Condition 1: walking test

The aim of this test is to evaluate if IMUs and Vicon are interchangeable by assessing their outcomes waveform similarity. For this purpose, the subject is instrumented with the optimal IMUs configuration chosen from Part I (Model 2) and, in turn, with the Vicon markers following the Plug-in Gait marker set model. The marker set used in these captures consists of the 23 markers: RASI, LASI, RPSI, LPSI, LTHI, LKNE, LTIB, LANK, LHEE, LTOE, RTHI, RKNE, RTIB, RANK, RHEE and RTOE for the lower body; and the markers RSHO, LSHO, RBAK, STRN, CLAV, T10 and C7 for upper body. Their arrangement is shown in Figure 19. The complete instrumentation for this test is shown in Figure 25.

Four gait captures are recorded synchronously with both systems. To make these captures, both systems are set up. The IMUs maintain the same characteristics as in Part 1, sampling frequency of 50 Hz and data format type of quaternions and angles. The Vicon system, has a sampling frequency of 100 Hz, and it is configured and prepared for recording following the instructions explained in section 4.1.2.


*Figure 25. Part II, condition 1: walking test, IMUs and Vicon instrumentation A) Lateral view. B) Frontal view. C) Back view.*

The anthropometric measurements entered in Nexus to create the subject and used for the subsequent reconstruction are body mass (kg), height (mm) and distance between anterior iliac spines (mm); and for each limb, leg length (mm), knee width (mm) and ankle width (mm).

- Condition 2: exoskeleton-assisted walking test with Exo-H3

In this last test, the aim is to evaluate the similarity between IMUs and Vicon outcomes when the subject is wearing the Exo-H3 exoskeleton providing 10% assistance. It has been necessary to readjust the positioning of some IMUs and Vicon markers.

Regarding the IMUs model, the ankle sensors must be readapted because, due to the structure of the exoskeleton, it is no longer possible to place them on the outer side. Furthermore, according to the results obtained in the previous test, which will be explained in the results section, it is considered necessary to reposition these sensors to improve the kinematic registration accuracy. Starting from Model 2, the ankle IMUs (3 and 6) are repositioned and placed frontally in the upper instep area (Figure 26).

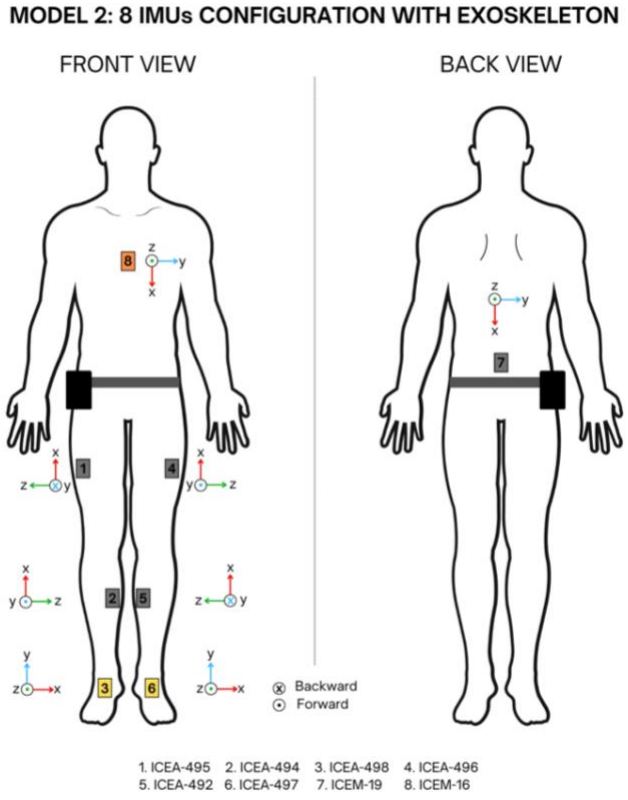


*Figure 26. Model 2 IMUs configuration with exoskeleton.*

As for Vicon, because of the trunk corset of the exoskeleton, the trunk markers used in the previous test have been omitted, leaving a set of 16 markers, the ones belonging to the lower limb Plug-in Gait (Figure 19C-D). In addition, this model has been readapted, positioning some of the markers on components of the exoskeleton.

The thigh markers, RTHI and LTHI, and the tibia markers, RTIB, LTIB, are placed on the metal bars of the exoskeleton. On the other hand, since the motors of the exoskeleton must always be well aligned with the joints on which they exert movement (hips, knees, and ankles) for their correct action, the RKNE, LKNE, RANK and LANK markers are placed in the center of their associated motors. The foot markers, RHEE, LHEE, RTOE and LTOE are placed in the same positions but on the exoskeleton foot grip straps. And finally, the pelvic markers, RASI, LASI, RPSI and LPSI are placed in position on the human body, as they are not occluded by the device components. All these changes can be seen in Figure 27, where the complete instrumentation of this test is shown.

In this test, due to changes in marker placement, some anthropometric data entered in Vicon varies. As explained in section 4.1.2, the kinematics are calculated from the joint centers that are estimated with the Chord function from the actual markers and their offsets to the center of the articulation. Like some of the markers are no longer placed on the surface of the human body, the distances (offsets) between joint centers and markers change.

In bare leg tests, the knee and ankle offset are calculated as follows (Eq. 6):

$$Knee\ or\ Ankle\ offset\ = \frac{(Knee\ or\ Ankle\ width\ +\ marker\ diameter)}{2}$$

*(Eq. 6)*

Where the knee and ankle width are known anthropometric measurements of the subject.

When the marker is placed on the exoskeleton, the width of the knee or ankle is no longer the same as the bare body width, but also includes the space from the lateral epicondillum or malleolus to the base of the marker. Even if this measurement is modified, the above equation would erroneously calculate the joint center, placing it in the center of this new 'width'. For optimal reconstruction, the anthropometric data determining the offsets are recalculated as follows:

$$Knee\ or\ Ankle\ width = actual\ knee\ or\ ankle\ width + 2\ x\ d_m$$

$$d_m\text{: } distance\ from\ lateral\ epicondillum/malleolus\ to\ marker\ base$$

*(Eq. 7)*

For the rest of the anthropometric parameters the measurement remains unchanged.

These gait captures are recorded synchronously with both systems, maintaining the same settings for IMUs (50Hz and quaternion-angle data type). It is also synchronized with the start-up of the exoskeleton, which is configurated on ‘Free’ mode providing a 10% of assistance for both legs.

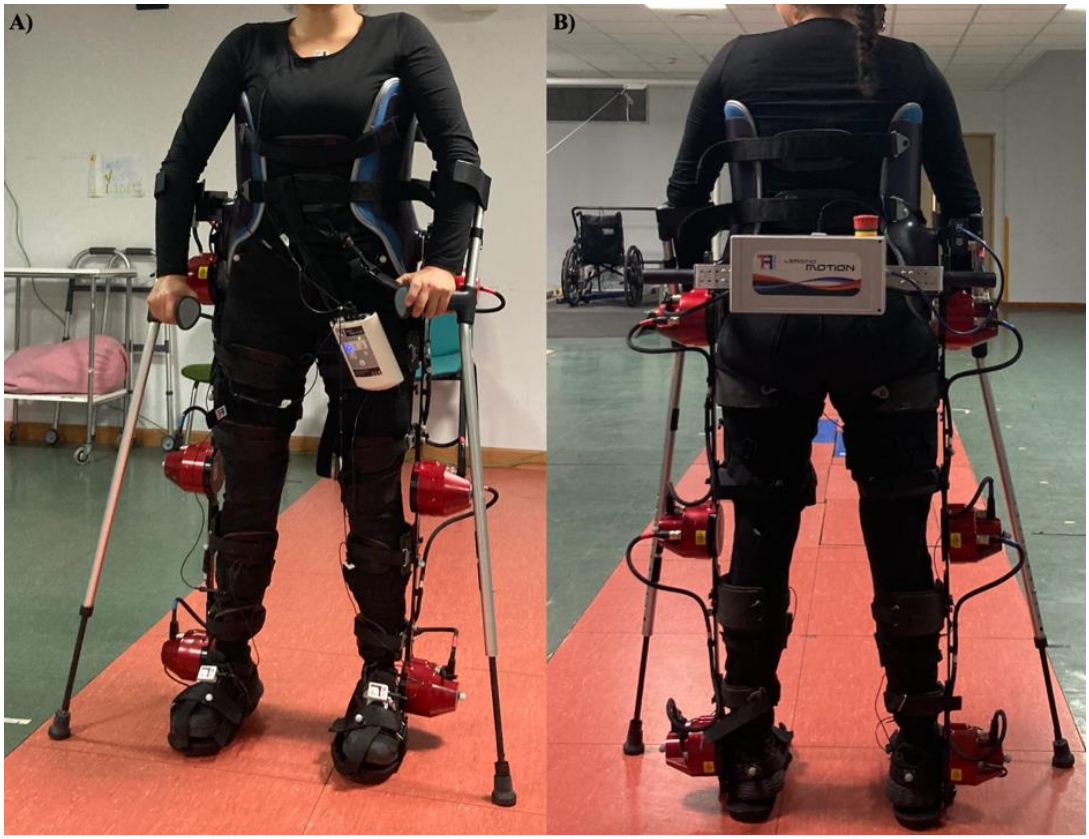


*Figure 27. Part II, condition 2: exoskeleton-assisted walking test with Exo-H3, IMUs and Vicon instrumentation. A) Frontal view. B) Back view.*

#### 4.2.2.2. Data analysis

- Vicon processing for condition 1: walking test

To process and obtain the kinematic outputs of each capture recorded with Vicon, the Nexus software offers pipelines with predefined tools and functions to process the Plug-in Gait model.

The first step is to process the static capture, which consists of the reconstruction and positioning of the markers in the 3D space, labeling the markers, and skeleton calibration. The Plug-in Gait Static Pipeline calculates the subject-specific offsets that are used as inputs to the Plug-in Gait Dynamic Pipeline (Figure 28A).

Next, the dynamic trials are processed. For this, the reconstruction and labelling of the markers is computed again. And, once the gaps in the trajectories caused by occluded markers during the capture are filled, the Plug-in Gait Dynamic Pipeline is executed to obtain the kinematic model outputs. Besides, the processes of deleting unlabeled trajectories is applied in this protocol, filtering data using the Woltring filter to ensure smooth trajectories and the calculation of gait parameters to obtain the model outputs (Figure 21 and Figure 28B).

Once all captures are processed with the dynamic model, they are exported to CSV file.

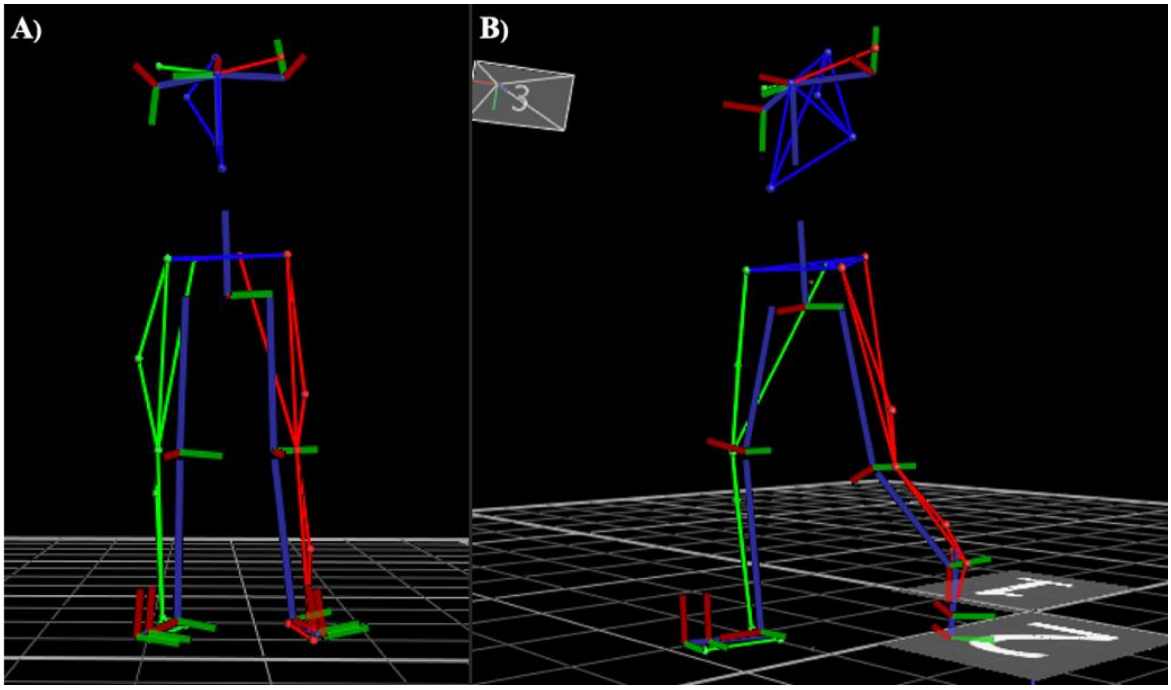


*Figure 28. Part I, condition 1: A) Plug-in Gait Static processing. B) Plug-in Gait Dynamic processing. Right limb in green and left in red.*

- Vicon processing for condition 2: exoskeleton-assisted walking test with Exo-H3

The adaptation of the anthropometric measurements introduced to calculate the offsets used in the estimation of the joint centers is carried out so that, once the captures have been recorded, the same Plug-in Gait processing protocol described above can be performed. However, when processing the static capture data, although the markers are recognized and the segments are generated correctly, the rotation axes, which are established automatically by Nexus, are erroneous (Figure 29). The definition of these axes of rotation is indispensable to obtain the kinematics correctly.

To solve this problem and to be able to use the recorded data, virtual markers are created with BodyLanguage to replace, at the knees and ankles, the real markers, thus simulating that they are placed on the subject's body surface correcting the calculation of the joint centers and consequently the rotation axes.

First, to generate these markers in the static trial, the real markers RKNE, LKNE, RANK and LANK are renamed as RKNE1, LKNE1, RANK1 and LANK1, so that the real names can be used and labeled in the creation of the virtual markers.

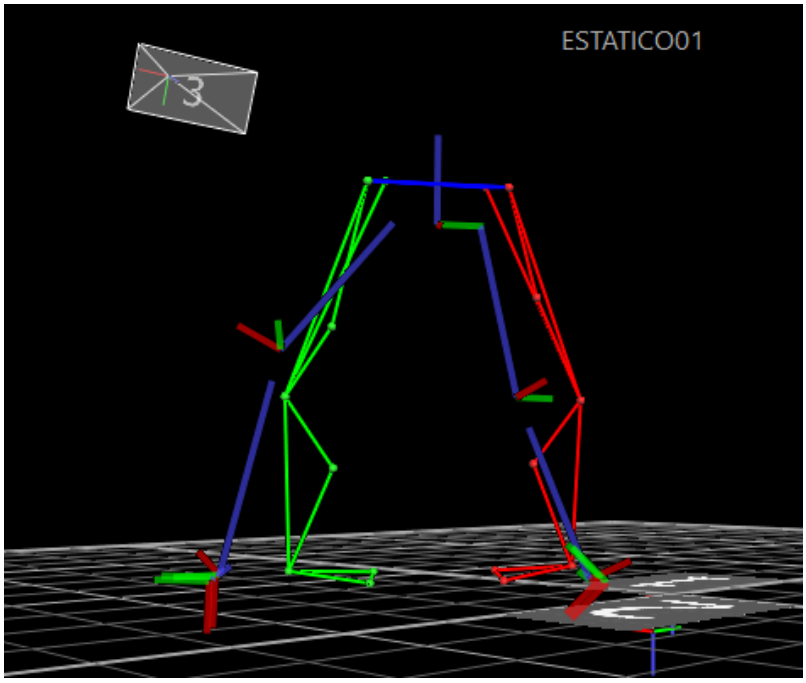


*Figure 29. Part II, condition 2: incorrect reconstruction of the axes of rotation.*

Next, in the MP file containing the subject information, the local XYZ coordinates are entered to locate the new markers in space (Figure 30). These coordinates are estimated from the actual markers used during the recordings, placed on the exoskeleton and body surface, and the subject's real anthropometric measurements, and they are manually adjusted to locate the markers at the points of interest.

```
$RKNELOCALX = 30
$RKNELOCALY = 65
$RKNELOCALZ = 100.195
$LKNELOCALX = 35
$LKNELOCALY = -100
$LKNELOCALZ = 60.1954
$RANKLOCALX = 80
$RANKLOCALY = -70.183
$RANKLOCALZ = 40
$LANKLOCALX = 80
$LANKLOCALY = 70
$LANKLOCALZ = 40
```

*Figure 30. Part II, condition II: local coordinates XYZ in the MP file for the generation of virtual markers.*

In Nexus, the subject's anthropometric measurements are then replaced by the actual values, this means, the true knee and ankle width. Later, four MOD files are created, one for each virtual marker (RKNE, LKNE, RANK, LANK), containing the functions that generate them. For example, to construct the virtual right knee marker (RKNE), a new femur segment (femur1) is first estimated from the real markers in the following order: origin, main direction, secondary direction, and axes of rotation. In the case of the right femur, the origin is the real knee marker placed on the exoskeleton motor (RKNE1), the main

direction is determined by this origin marker and the right anterior iliac spine marker (RASI), and the secondary direction by the origin and the right tibia marker placed on the exoskeleton (RTHI), and the XYZ axes of rotation. Finally, to create the new virtual marker RKNE, the local coordinates are multiplied by the newly estimated femur1 segment. This process is done for the generation of the other three markers, adapting the function to each one (Figure 31).

**A)**

```
femur1 = [RKNE1,(RASI-RKNE1),(RTHI-RKNE1),XYZ]

RKNE = $RKNELOCAL*femur1

OUTPUT(RKNE)
```

**B)**

```
pie1 = [RHEE,(RTOE-RHEE),(RTIB-RHEE),XYZ]

RANK = $RANKLOCAL*pie1

OUTPUT(RANK)
```

**C)**

```
femur2 = [LKNE1,(LASI-LKNE1),(LTHI-LKNE1),XYZ]

LKNE = $LKNELOCAL*femur2

OUTPUT(LKNE)
```

**D)**

```
pie2 = [LHEE,(LTOE-LHEE),(LTIB-LHEE),XYZ]

LANK = $LANKLOCAL*pie2

OUTPUT(LANK)
```

*Figure 31. Part II, condition 2: virtual markers functions. A) RKNE virtual marker computation. B) RANK virtual marker computation. C) LKNE virtual marker computation. D)LANK virtual marker computation.*

When these files are created, the Plug-in Gait Static model processing is executed and the new markers are generated, which allows the recalibration of the subject properly. The reconstruction obtained with the corrected rotation axes is shown in Figure 32.

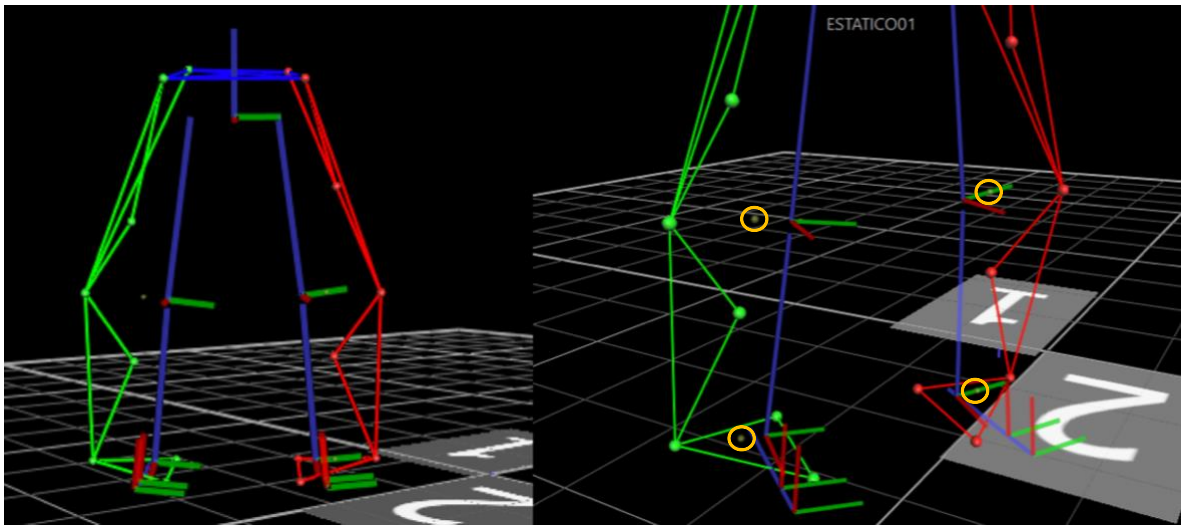


*Figure 32. Part II, condition 2: Plug-in Gait Static processing with BodyLanguage and virtual markers.*

Once the results achieved in the static reconstruction are checked, the Gait Plug-in Gait Dynamic model processing protocol is run in the same way to obtain the model outputs. In this way it is possible to calculate gait kinematics with a set of markers positioned on the exoskeleton. After checking the

kinematic results in Nexus, they are exported to a CSV file.

- MATLAB analysis

From this point on, the following analysis is repeated for each condition separately in MATLAB.

First, once the trials recorded by each system are exported, they are pre-processed. The signals from the IMUs are smoothed with the Saviztky-Golay filter in the same way as in Part I (section 4.2.1.2). The Vicon signals are taken with a sampling frequency of 100 Hz, therefore, these are resampled to 50 Hz and aligned with the corresponding IMUs signals, see diagram in **Error! Reference source not found.**.

Thus, the signals recorded by the IMUs are referred to as I(t) and those recorded by Vicon V(t). Then, for each pair of trials, the gait cycles are extracted, obtaining a pair of waveforms for each gait cycle, [I(t), V(t)]. For Condition 1, 11 pairs of gait cycles [I(t), V(t)] are detected for each limb and are analyzed in the three planes of the space. For Condition 2, four pairs of gait cycles [I(t), V(t)] are recovered for each limb. This decrease in the number of available cycles is due to reconstruction problems caused by Vicon and visibility limitations imposed by the exoskeleton, in addition to the fact that the number of available cycles in IMUs records is usually higher than in Vicon records, because with the photogrammetry system the visibility of the markers is constrained within part of the 10 m walkway, as can be seen in the last step of Figure 18**Error! Reference source not found.**. Therefore, not all synchronized captures are correct for both systems. So, out of 9 captures with the exoskeleton assisting at 10%, only two are usable, and within each of these, two gait cycles are extracted for each limb.

To determine whether these two devices are interchangeable (equivalents) for measuring kinematics, the evaluation of similar waveforms is performed. To assess the similarity between I(t) and V(t) in terms of displacement, correlation, and gain, four parameters are calculated for each [I(t), V(t)] and each joint-angle: the offset between I(t) and V(t) (off), their Pearson correlation coefficient (r), the difference between their range of motion (ΔROM) and the RMSE [12]. All these formulas are shown in (Eq. 8).

$$off = mean[I(t)] - mean[V(t)]$$

$$r = \frac{n(\sum xy) - (\sum x)(\sum y)}{\sqrt{[n\sum x^2 - (\sum x)^2][n\sum y^2 - (\sum y)^2]}}$$

$$\Delta ROM = ROM[I(t)] - ROM[V(t)]$$

*(Eq. 8)*

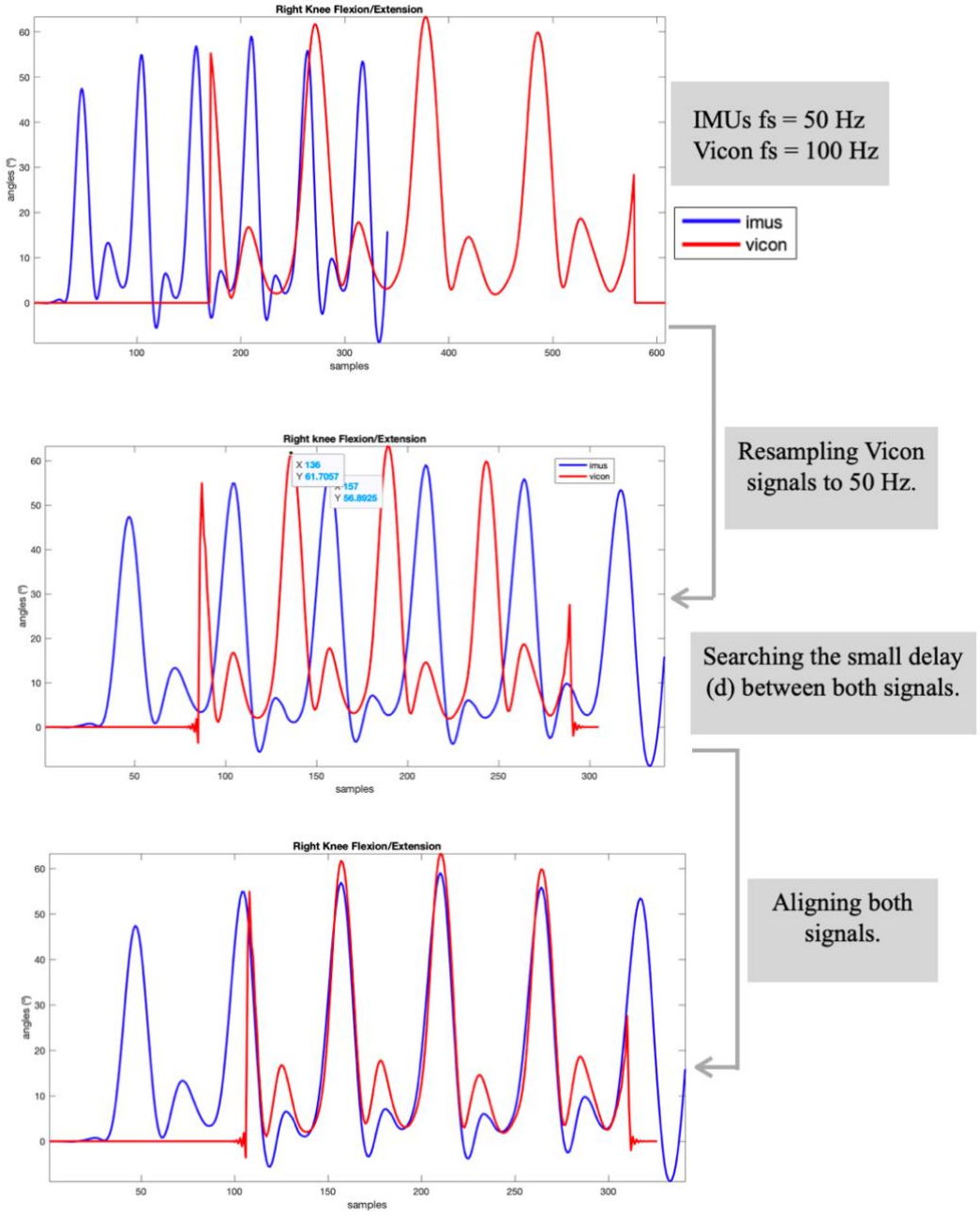


*Figure 33. Signal pre-processing diagram. E.g., right knee flexion/extension.*

In addition, the adjusted variation of the within-day CMC of Kadaba, the inter-protocol CMC ($CMC_p$) is calculated, which removes all other sources of 'gait-cycle-to-gait-cycle' variability: 1) the biological variability of the subject's lower limb kinematics, 2) the variability in the spread of soft tissue artefact in the lower limb kinematics and 3) the variability in the performance of the measurement system [12, 59, 60]. Given that each I(t) can be compared only with its synchronous V(t), the aim of this new CMC statistic formulation is to assess the similarity of waveforms (joint angles) acquired synchronously across different media (different protocols and different measurement systems), within each of the many

movement cycles (gait cycle), when the effect of the media on waveform similarity is the only one of interest. It considers the magnitude of the waveform data and provides a value between 0 and 1, with a value of 1 indicating perfect similarity between the two waveforms, [I(t), V(t)].

To evaluate the inter-protocol similarity, the reinterpreted formulation of the $CMC_w$ (Eq. 4) is shown in (Eq. 9. Suppose that for a subject and a joint angle, the kinematics are measured synchronously through *P* protocols, in *G* gait cycles. Consequently, *P* waveforms are available for each $g^{th}$ gait cycle, one per protocol, each of $F_g$ frames [59].

$$CMC_p = \sqrt{1 - \frac{\sum_{g=1}^{G}\left[\sum_{p=1}^{P}\sum_{f=1}^{F}\left(Y_{gpf} - \bar{Y}_{gf}\right)^2 / GF_g(P-1)\right]}{\sum_{g=1}^{G}\left[\sum_{p=1}^{P}\sum_{f=1}^{F}\left(Y_{gpf} - \bar{Y}_{g}\right)^2 / G\left(PF_g - 1\right)\right]}}$$

*(Eq. 9)*

Where,

- $Y_{gpf}$ *is the* ordinate at frame *f* of the waveform provided by protocol *p* at gait cycle *g*.
- $\overrightarrow{Y_{gf}}$ is the ordinate at frame *f* of the average waveform among the *P* waveforms for the gait cycle *g*.
- $\overrightarrow{Y_g}$ is the grand mean for the gait-cycle *g* among its *P* waveforms.

This first computation is referred to as $CMC1_p$. If within each gait cycle, the variability of the P-waveforms around their mean waveform is less than the variance around their overall mean, the $CMC1_p$ approaches 1. Otherwise, the $CMC_p$ tends to zero or even turns into a complex number. This happens, for instance, when the ROM of the P-waveforms is comparable to the phase difference (offset) among them [58, 59].

Besides, the $CMC_p$ after zeroing the offset for each couple [I(t), V(t)] is recomputed to measure the effect this displacement on the similarity ($CMC2_p$). It is zeroed by subtracting from each gait cycle I(t) the offset (Eq. 8) between it and its partner V(t) [58].

The values of the six parameters are given with box-and-whisker plots as well as in terms of median and whisker range for each limb and each joint angle. Median and whiskers are used because all the parameters do not have normal distributions for all joint angles; normality is tested with the Shapiro-Wilk test.

To interpret the $CMC1_p$ and r values obtained, the following ranges are established based on previous publications [7][12]: moderate (0.65-0.75), good (0.75-0.85), very good (0.85-0.95) and excellent (0.95-1). However, since $CMC1_p$ considers the overall effect of the offset, r and gain between waveforms, this project sets out the following conditions for considering the two devices to be interchangeable regarding

the walking test of Condition 1:

- Cond. 1.1: In the sagittal plane, the median and whiskers values of $CMC1_p$ must belong to the excellent range.
- Cond. 1.2: In the frontal and transverse planes the $CMC1_p$ median values must belong at least to the very good range, and the whiskers to the very good or excellent ranges.

And for Condition 2, walking test with exoskeleton, since the kinematics are affected by the problems of reconstruction and by the exoskeleton itself, the conditions that must be met to at least consider that the data provided by the IMUs may contain information worth analyzing are:

- Cond. 2.1: In the sagittal plane, the $CMC1_p$ median value must belong to the very good or excellent range, and the whiskers from good to excellent range.
- Cond. 2.2: In the frontal and transverse planes, for r and $CMC1_p$, the median values must belong at least to the good range, and the whiskers from good to excellent ranges.

When these conditions are only met by $CMC2_p$, the similarity is confirmed exclusively if the offset is not a concern. At last, a visualization of the kinematics recorded is given and, as well, $CMC1_p$ and $CMC2_p$ are calculated for all pairs of gait cycles. These parameters are referred to as $CMC1_T$ and $CMC2_T$.

# 5. Results

This section presents the results obtained from the methodology explained above.

## 5.1. Part I. Exploring different configurations offered by the IMUs

Depending on the model used, the number of extracted gait cycles varies because of drift accumulation. This number is fewer for Models 1 and 3, consisting of 7 IMUs. For these models, sometimes the trunk is not correctly calibrated, which introduces a bias in the other joint angles. In these cases, the captures are repeated until at least three analyzable gait cycles are obtained for each limb.

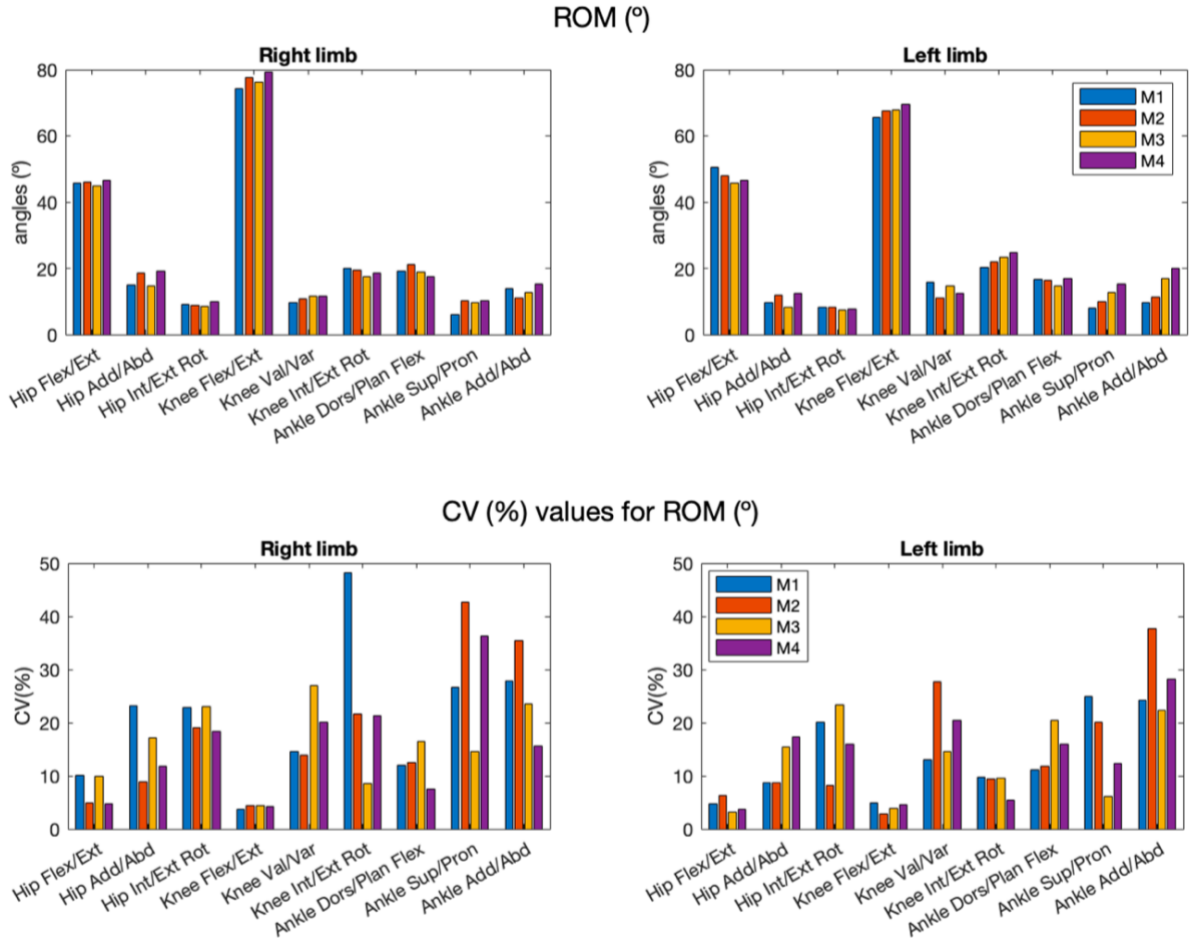


*Figure 34. ROM (º) and CV (%) results for each joint angle for each IMUs configuration.*

The average ROM extracted from the gait cycles registered by each model and its dispersion (CV) are results shown in the Figure 34**Error! Reference source not found.**. Considering that these recordings are not synchronous, if all the configurations were valid, the ROM results would not necessarily be the

same, but they would be similar for a healthy subject in successive captures. In general, all the configurations measure around similar ranges, not exceeding differences higher than 5º between them, except for the left ankle on frontal and transversal planes, where the mean ROM values vary more (> 7º between Models 1 and 4). The maximum variation is obtained for the left ankle adduction/abduction between Models 1 and 4 (10º).

Regarding the variability of these ROMs, the higher the value of the CV percentage, the more variable and, therefore, less consistent the measurements is. Greater dispersion is observed in all models in the frontal and transverse planes, especially for the ankles, which even exceed a 30%. However, the maximum dispersion is reached by Model 1 in right knee rotation (48.22%). Whereas for the hip and knee on the sagittal plane the CV does not exceed the 10% of dispersion for any configuration.

The analysis of the waveform's similarity, evaluated with the $CMC_w$ statistical measure, shows the following values for the gait cycles registered with each of the proposed configurations for every joint angle (M1, M2, M3 and M4):

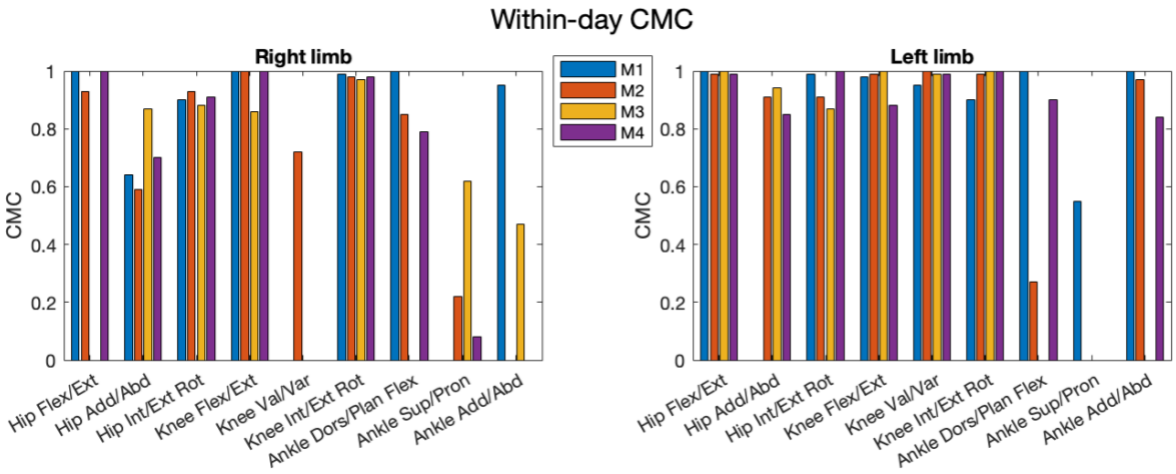


*Figure 35. Within-day CMC values for each joint angle for each IMUs configuration.*

The nearer to 1, the more similar the waveform of the recorded cycles is, and therefore the more repeatable the measurement is. This provides information on the measurement consistency of each configuration. However, for the same configuration, $CMC_w$ values vary greatly between joints and planes, being complex number for some of them. For example, for both limbs, the similarity concerning the ankles is very uncertain for every model (Figure 35). The bars that are not represented in the graph correspond to complex $CMC_w$ values. These complex values are frequent when computing the $CMC_w$ over joint angles with limited ROM and great dispersion, as happens in the ankles. This affects the formula ((Eq. 4) in such a way that, if the variability of the waves studied for the same session around their mean waveform ($Y_{swf} - \bar{Y}_{sf}$) is greater than the variance around their overall mean ($Y_{swf} - \bar{Y}_{s}$), the $CMC_w$ tends to zero or becomes a complex number [59, 62].

For Model 1, the $CMC_w$ values are 1 for sagittal plane and > 0.8 for the transversal plane. However, for

frontal plane, where ROMs are smaller, the values are lower (< 0.7) or even complex numbers (i.e., right knee, right ankle, and left hip), except for the left knee valgus/varus ($CMC_w$ = 0.95). Observing Model 2 results, $CMC_w$ values for hips and knees in sagittal plane are > 0.9, but for the ankle dorsi/plantar flexion decreases, being 0.85 for the right limb and 0.27 for the left one. On the frontal and transversal planes, this value is higher for the left hip and knee than for the right ones (right: $CMC_w$ > 0.6; left: $CMC_w$ > 0.85), and much lower for both ankles, being complex values for the right ankle adduction/abduction and the left ankle supination/pronation.

Regarding Model 3, on the sagittal plane, for right hip and both ankles the $CMC_w$ is a complex number. For the frontal plane, hip and knee adduction and abduction are higher for left limb (> 0.8), but for the ankles these values are complex or < 0.7. And for Model 4, hip and knee flexion/extension for both legs are ≥ 0.9, and for the ankles ≥ 0.8. The transversal plane obtains values > 0.8 except for the right ankle adduction/abduction, whereas the frontal plane, only presents good similarity for the adduction/abduction movement of the left hip and knee (≥ 0.85).

*Table 2. RMSE(º) between IMUs configurations.*

| | **RMSE (º)** | | | |
|---|---|---|---|---|
| | **Model 1 & 2** | | **Model 3 & 4** | |
| | Right limb | Left limb | Right limb | Left limb |
| **Hip Flexion/Extension** | 2.44 º | 3.58 º | 13.45 º | 2.48 º |
| **Hip Adduction/Abduction** | 2.17 º | 2.06 º | 3.73 º | 3.44 º |
| **Hip Int/Ext Rotation** | 1.30 º | 2.99 º | 5.00 º | 2.03 º |
| **Knee Flexion/Extension** | 5.88 º | 5.07 º | 22.46 º | 3.60 º |
| **Knee Valgus/Varus** | 1.82 º | 3.21 º | 1.98 º | 2.58 º |
| **Knee Int/Ext Rotation** | 2.30 º | 2.59 º | 3.93 º | 1.53 º |
| **Ankle Dorsi/Plantar Flexion** | 4.66 º | 1.69 º | 3.09 º | 1.37 º |
| **Ankle Supination/Pronation** | 1.33 º | 1.80 º | 0.98 º | 0.78 º |
| **Ankle Adduction/Abduction** | 1.42 º | 1.28 º | 3.14 º | 2.61 º |

Concerning the RMSE between Models 1 (7 IMUs) and 2 (8 IMUs), the error values do not exceed 3º on frontal and transversal planes nor 6º on sagittal plane, being the knee flexion/extension and the ankle dorsi/plantar flexion errors the highest ones, around 5º. For Models 3 (7 IMUs) and 4 (8 IMUs), the error values are greater on sagittal plane, exceeding 13º and 22º for right hip and knee flexion/extension. While the errors for frontal and transversal planes do not exceed 5º (Table 2).

The last results generated for Part I, are the graphs containing the mean gait cycle for each model and each joint angle plotted against the normality recorded on other captures with Vicon to this subject (Figure 36 and Figure 37). These graphs allow a visual assessment of whether the kinematics obtained are consistent with the $CMC_w$, ROM and CV values obtained. Besides, they provide a primary visual description for the next steps.

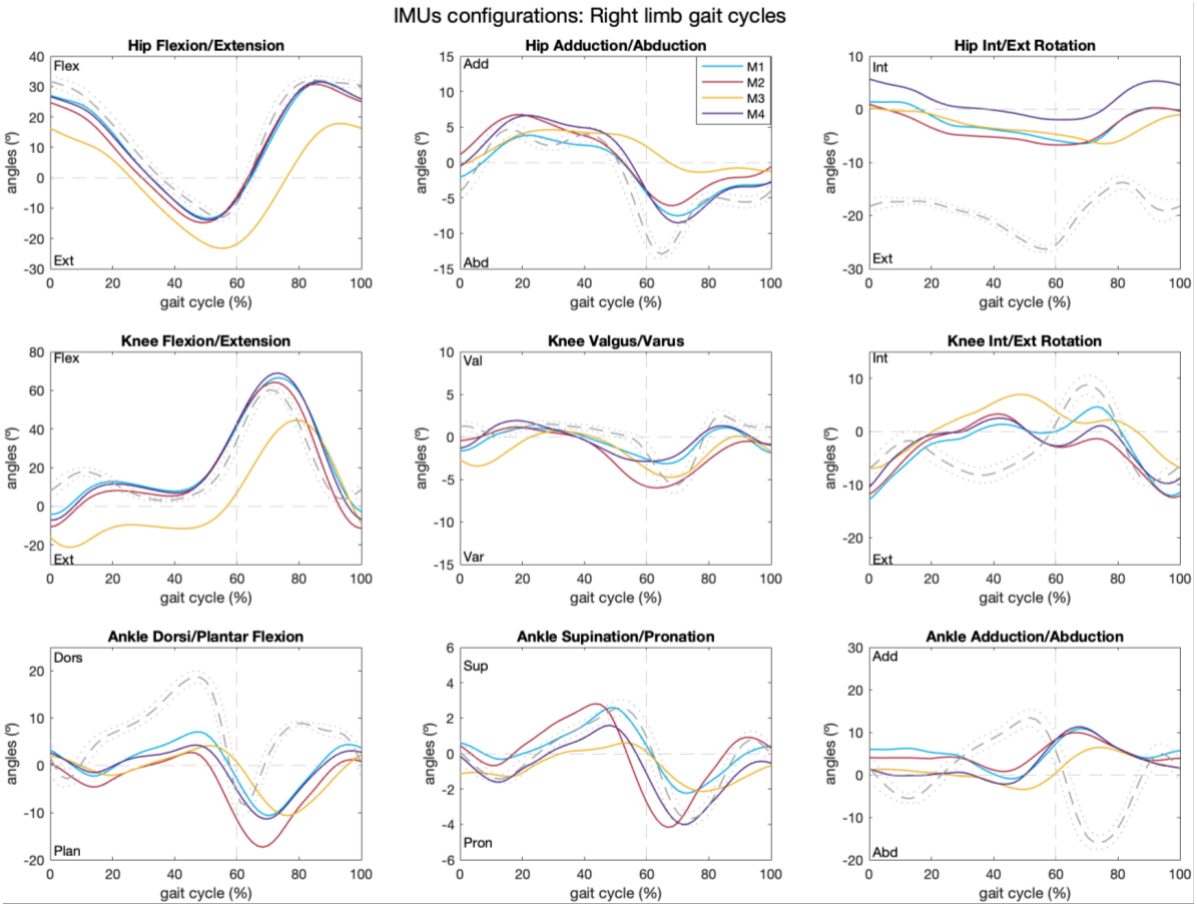


*Figure 36. Right limb mean gait cycle for each IMUs configuration plotted against Vicon normality (---: mean, ⋯ : ±std).*

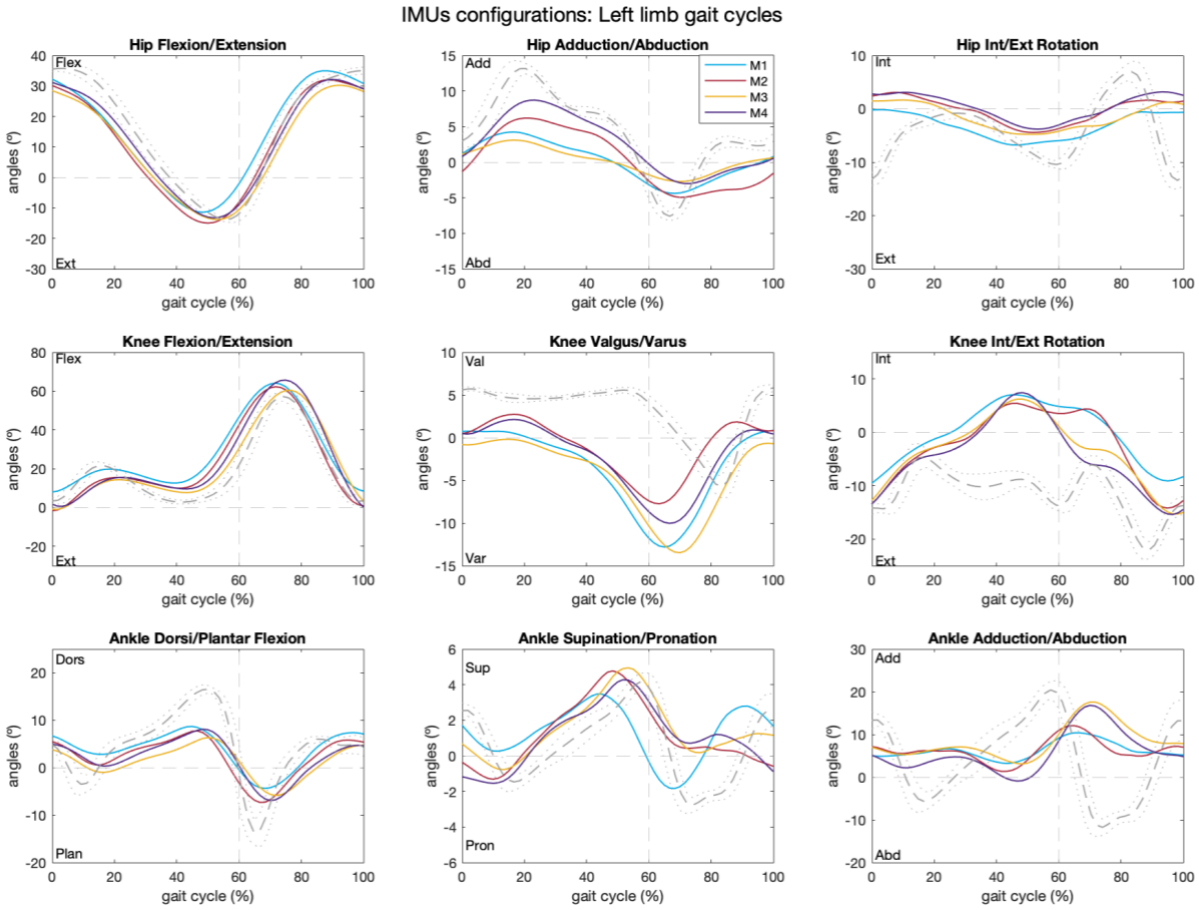


*Figure 37. Left limb mean gait cycle for each IMUs configuration plotted against Vicon normality (---: mean,⋯ : ±std).*

## 5.2. Part II. Validation of IMUs with Vicon: similarity assessment

### 5.2.1. Condition 1: walking test

In the following, the results of the parameters calculated for each pair of gait cycles [I(t), V(t)] in Part II Condition 1 are shown. Figures from 38 to 43 show the distributions of r, ΔROM, offset, RMSE, $CMC1_p$ and $CMC2_p$ for each joint angle of interest, over the measured joints (hips, knees, and ankles) considering all acquired gait cycles. Each plot shows two boxplots, one for each leg, with data from 11 pairs of gait cycles [I(t), V(t)] each. In total, each boxplot contains 11*9 = 99 values (9 joint angles). It is reminded that the data are displayed in boxplots because not all parameters follow a normal distribution. Additionally, the results of the normality study performed for each parameter with the Shapiro-Wilk test are shown in Appendix 1.

For the sagittal plane hip and knee angles of both limbs, the r values within the whiskers are ≥ 0.95, which means an excellent correlation. Thus, there is a positive direct relationship between the gait cycles of each couple [I(t), V(t)]; when one increases, the other increases in constant proportion [62]. While for ankle dorsi/plantar flexion, the median r values are 0.7 for both limbs, which describes a moderate correlation. For both ankles, the upper whiskers (UW) represent a good correlation, but the lower whiskers (LW) are weak. The value for the LW of the left ankle is 0.65, showing a moderate correlation, and the right ankle LW shows even a lower correlation of 0.55. For the frontal and transverse planes for each joint and leg, the r values decrease. None of the boxes and their whiskers fall completely within the ranges established in the methodology (lowest range, moderate: 0.65 - 0.75). Some even reach values of 0 or negative, as seen in Figure 38. When the values of r are 0, it means that there is no linear relationship between pairs of signals, however, it does not imply that they are independent. And if r is negative, it means that both variables have an opposite relationship, which means that the waveform of both signals is not equivalent, because when one increases the other decreases in constant proportion. Both mean that there is weak or no similarity between signals [62].

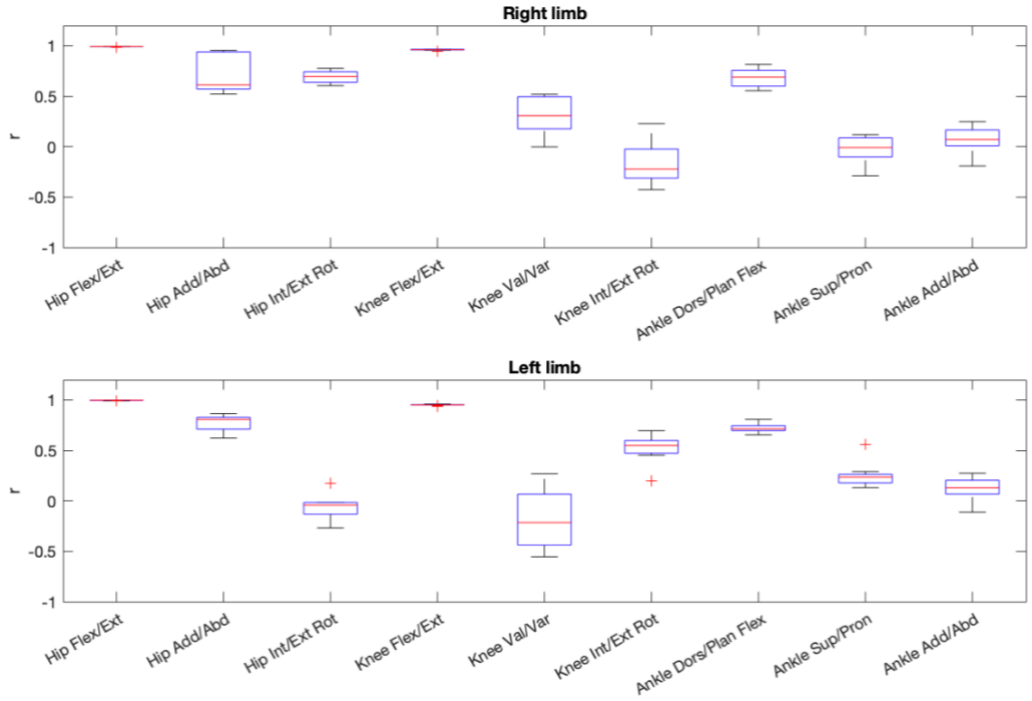


*Figure 38. Part II, condition 1: Box-and-whisker plot for r regarding the comparison IMUs vs VICON.*

Since the ΔROM is calculated according to the formula in (Eq. *8*, when the resulting value is negative, it means that the range measured by the IMUs is smaller than that measured by Vicon, while if it is positive, the opposite is true. In the sagittal plane, the median value of the ΔROM at the right hip joint is -3.63º and at the left hip -1.46º. In knee flexion-extension the median is around 1° for both legs, and in ankle dorsiflexion the variation increases to -13°. For all three joints in this plane, the whiskers have a low dispersion, varying between 1° and 2° above and below their median. In both hip and knee, in the frontal and transverse planes, the difference in the measured ranges is greater in the left limb than in the

right. For the hip, the ΔROM median in the right leg for frontal and transverse plane are around 0º whereas for the left limb it is near -10º. For the right knee, the angles measured by each system in frontal and transverse planes have a median difference of 2.7º and -1.7º respectively, while for the left knee these differences almost reach -6º. For the ankle, the ΔROM median value in both planes is similar for both legs, reaching > 10º for supination/pronation and < -25º for adduction/abduction (Figure 39).

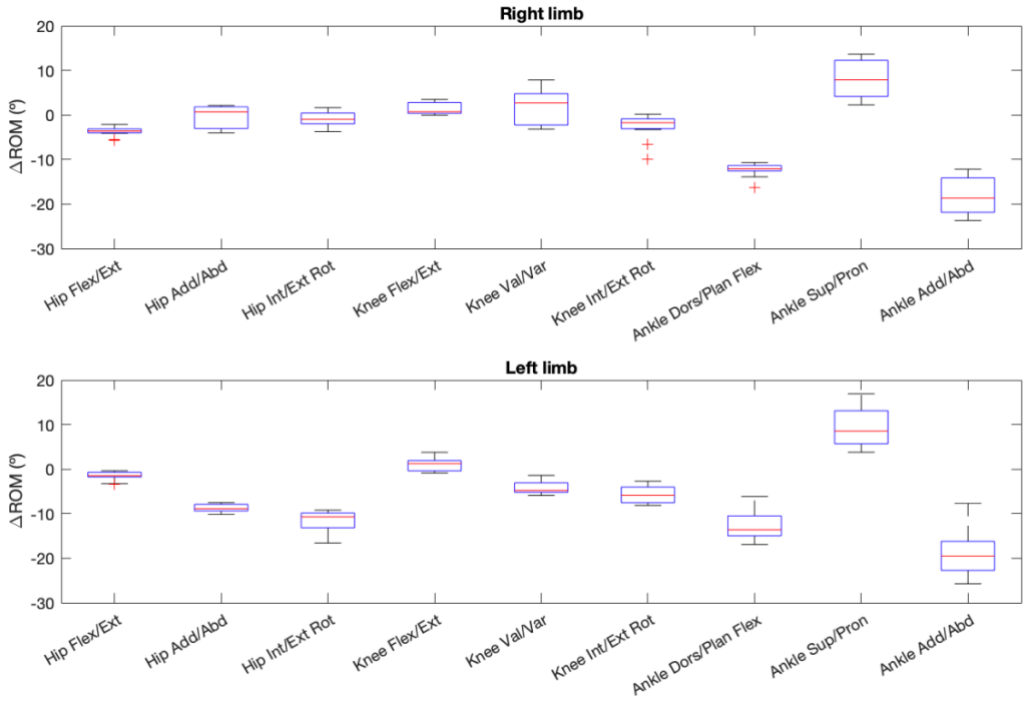


*Figure 39. Part II, condition 1: Box-and-whisker plot for ΔROM regarding the comparison IMUs vs VICON.*

According to the offset calculation (Eq. 8), when the resulting value is negative, it means that the IMUs measurement has a negative offset (lower values) with respect to Vicon, and if it is positive, the opposite happens. The median offset values for hips and knees flexion and extension are around -3º and -4º, and for the ankles dorsi/plantar flexion the medians are between -4º and -7º. The whiskers are around ±3º over/below the median for the right limb, however, for the left limb, the LWs are greater, reaching 7º beyond the median. It is confirmed that the frontal and transverse plane angles are the most affected by the displacement (offset), and the value for the same plane and the same joint varies too much between legs. Especially in the right hip rotation, the median offset value is 17.67º, and in the left hip rotation it is 2.93º (Figure 40).

In the sagittal plane, the RMSE values for the left leg show larger dispersion. The median RMSE at the hips, right and left, has a value of 4° and 5°, respectively. For both knees the median is 6.3º, for the right ankle 8.55° and for the left ankle 7.06°. For all joints, the median values in the frontal plane are between 4° and 7°. For the hip and knee the dispersion of the data is greater for the right leg, and the ankle for the left leg. In the transverse plane the RMSE values are higher (> 7°), mainly in the right hip rotation, which reaches 18º (Figure 41).

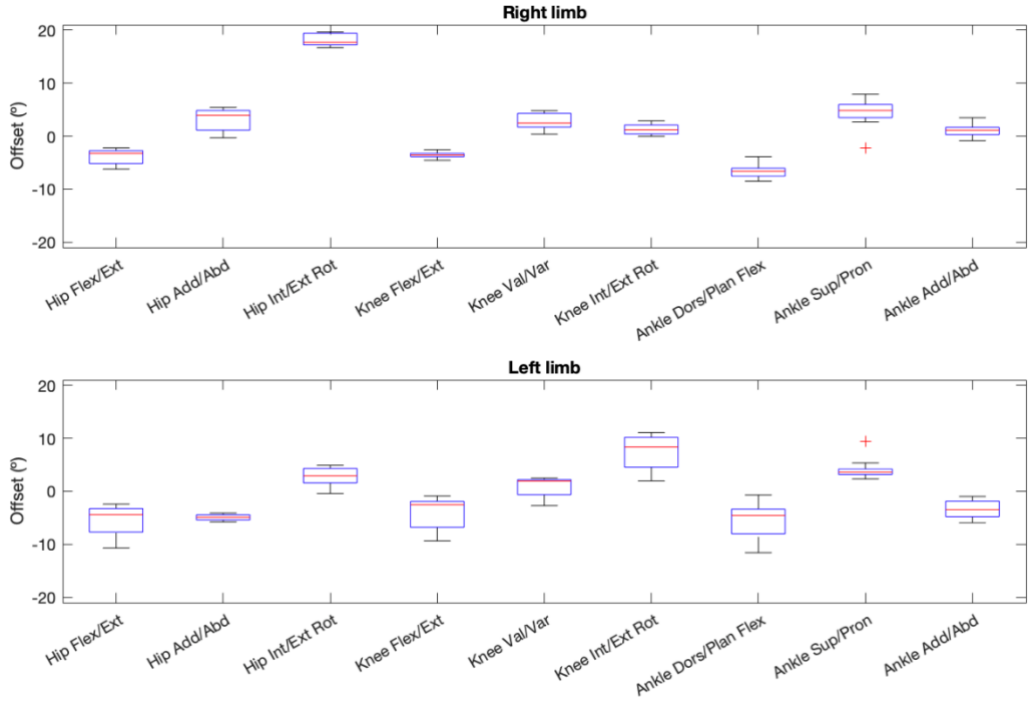


*Figure 40. Part II, condition 1: Box-and-whisker plot for off regarding the comparison IMUs vs VICON.*

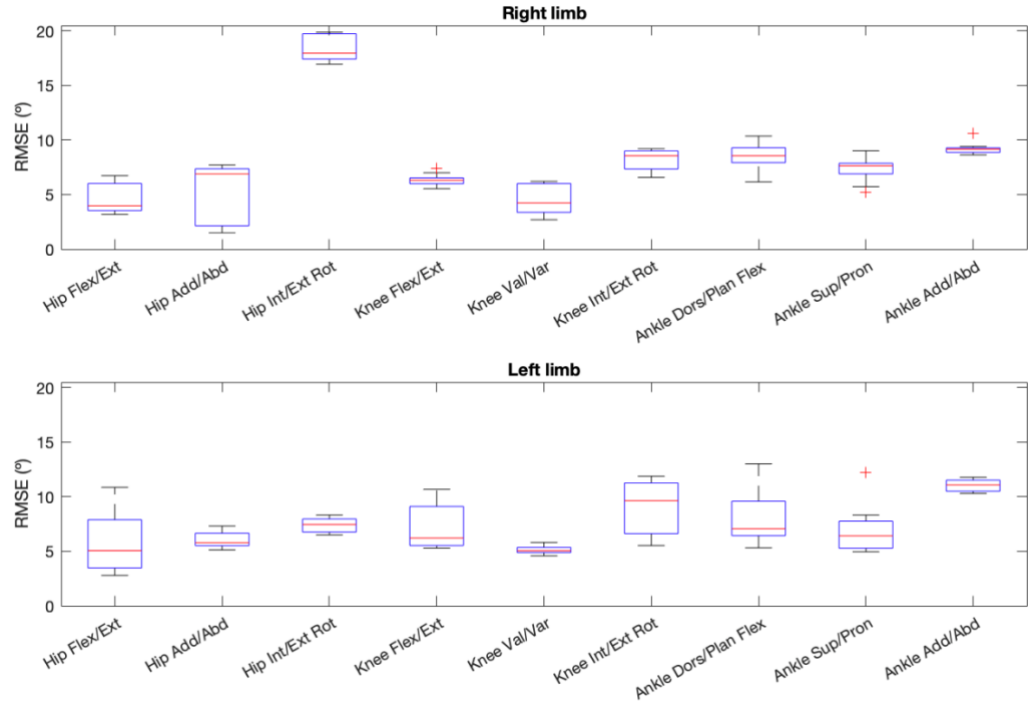


*Figure 41. Part II, condition 1: Box-and-whisker plot for RMSE regarding the comparison IMUs vs VICON.*

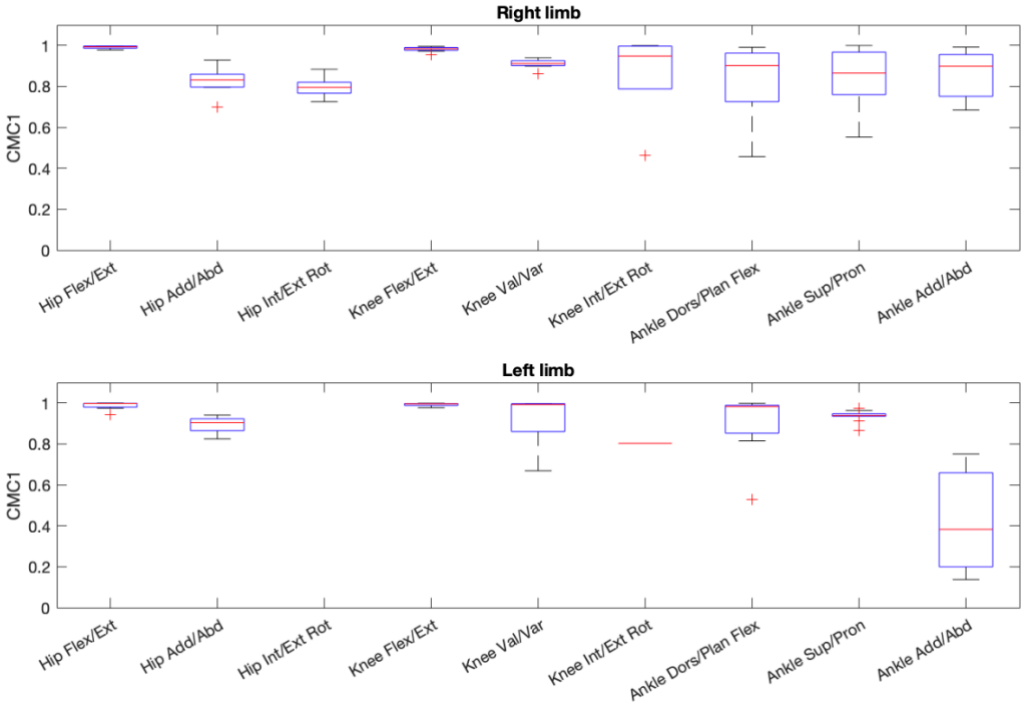


*Figure 42. Part II, condition 1: Box-and-whisker plot for CMC1 regarding the comparison IMUs vs VICON.*

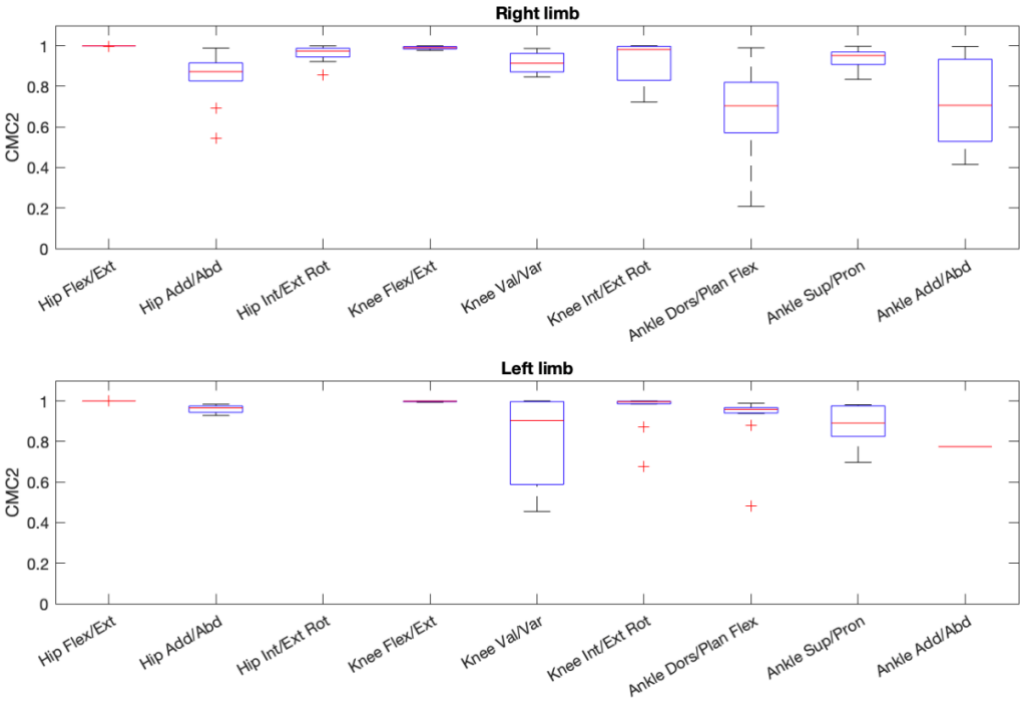


*Figure 43. Part II, condition 1: Box-and-whisker plot for CMC2 regarding the comparison IMUs vs VICON.*

In terms of the $CMC_p$ calculation (Eq. 9), as for $CMC_w$, for each gait cycle, if the variability of the P waveforms (P=2) around its mean waveform ($Y_{gpf} - \bar{Y}_{gf}$) is greater than the variance around its overall mean ($Y_{gpf} - \bar{Y}_g$), the $CMC_p$ tends to zero or becomes a complex number. This happens when the value of ROM is low or similar to the value of the existing offset [59, 62]. Boxplots are only reported for those join-angles in which 3 or less values are complex numbers. On $CMC1_p$, all joint angles reach a median > 0.8. Except for the left limb in the transverse plane, being a complex number for the hip and the knee, and 0.38 for the ankle. In the sagittal plane, all joints reach median and both whiskers values > 0.95, showing an excellent correlation, excluding the right ankle ($CMC1_p$ = 0.9, UW = 0.99, LW = 0.46) and the left ankle ($CMC1_p$ = 0.98, UW = 0.99, LW = 0.81) (Figure 42). The flexion/extension of hips and knees, both right and left, comply with Cond. 1.1 established in the methodology. Right knee adduction/abduction ($CMC1_p$ = 0.91, UW = 0.94, LW = 0.9) and left ankle supination/pronation ($CMC1_p$ = 0.94, UW = 0.96, LW = 0.94) meet Cond. 1.2.

Regarding the $CMC2_p$ (offset removed), all inter-protocol CMC median values increase for the right limb, which means that the offset affects the measurement negatively, except for ankle dorsi/plantar flexion and adduction/abduction, which decrease from 0.9 to 0.7. Regarding the left limb, ankle flexion ($CMC1_p$ = 0.98, $CMC2_p$ = 0.96) and supination/rotation ($CMC1_p$ = 0.94, $CMC2_p$ = 0.89) angles decrease, as well as knee valgus/varus ($CMC1_p$ = 0.99, $CMC2_p$ = NaN). In addition, there is no improvement in hip rotation and ankle adduction/abduction, remaining as complex numbers (Figure 43). If the conditions established in the methodology were based on $CMC2_p$, Cond. 1.1 would be met again by both hips and knees flexion/extension ($CMC2_p$ and whiskers > 0.95), and Cond. 1.2 would be met by the right knee adduction/abduction ($CMC2_p$ = 0.91, UW = 0.99, LW = 0.85), right hip rotation ($CMC2_p$ = 0.97, UW = 0.99, LW = 0.92), left hip adduction/abduction ($CMC2_p$ = 0.97, UW = 0.98, LW = 0.93) and left knee rotation ($CMC2_p$ = 0.99, UW = 0.99, LW = 0.98).

Finally, the results of the $CMC1_T$ and $CMC2_T$ calculation for all the extracted [I(t), V(t)] pairs for each limb are shown in Figure 44 and Figure 45, together with the gait cycles with the kinematic pattern recorded by each system. For both limbs, the knee and hip angles on sagittal plane present an excellent correlation ($\geq$ 0.95) between the gait cycles recorded by the IMUs and the ones captured by Vicon, corresponding with the median $CMC1_p$ and median $CMC2_p$ values obtained (Figure 42 and Figure 43). In this same plane, in the right ankle of the $CMC1_T$ value is 0.82, however, it decreases when the offset between cycles is eliminated ($CMC2_T$ = 0.21). While the left ankle shows an excellent correlation ($CMC1_T$ = 1, $CMC2_T$ = 0.96). The same behavior occurs with the median values of $CMC1_p$ and $CMC2_p$.

In the frontal plane, complex values, represented as NaN, are obtained for the right hip (this does not happen in boxplot values), while the left hip shows, without offset correction, a very good correlation ($CMC1_T$ = 0.84). The opposite happens in the transverse hip plane, corresponding with the boxplot median behavior. As for the knees, the frontal plane angles show high $CMC1_T$ values for both limbs (right: $CMC1_T$ = 0.91; left: $CMC1_T$ = 1), but when the offset is removed, the $CMC2_T$ increases on the right (0.99) and becomes a complex number on the left. In the transverse plane, the right knee shows an

excellent correlation ($CMC1_T$ = 1; $CMC2_T$ = 1), while the left knee only shows an excellent correlation when the offset is removed ($CMC1_T$ = NaN; $CMC2_T$ = 1). And lastly, both ankles show similar values in the frontal and transversal planes. In supination and pronation, the right ankle shows an excellent correlation ($CMC1_T$ = 0.98; $CMC2_T$ = 0.95), and the left ankle a very good correlation (excellent with offset correction) ($CMC1_T$ = 0.94; $CMC2_T$ = 0.98). Whereas both are complex values in the transverse plane. This is also true of the $CMC1_p$ and $CMC2_p$ data obtained above.

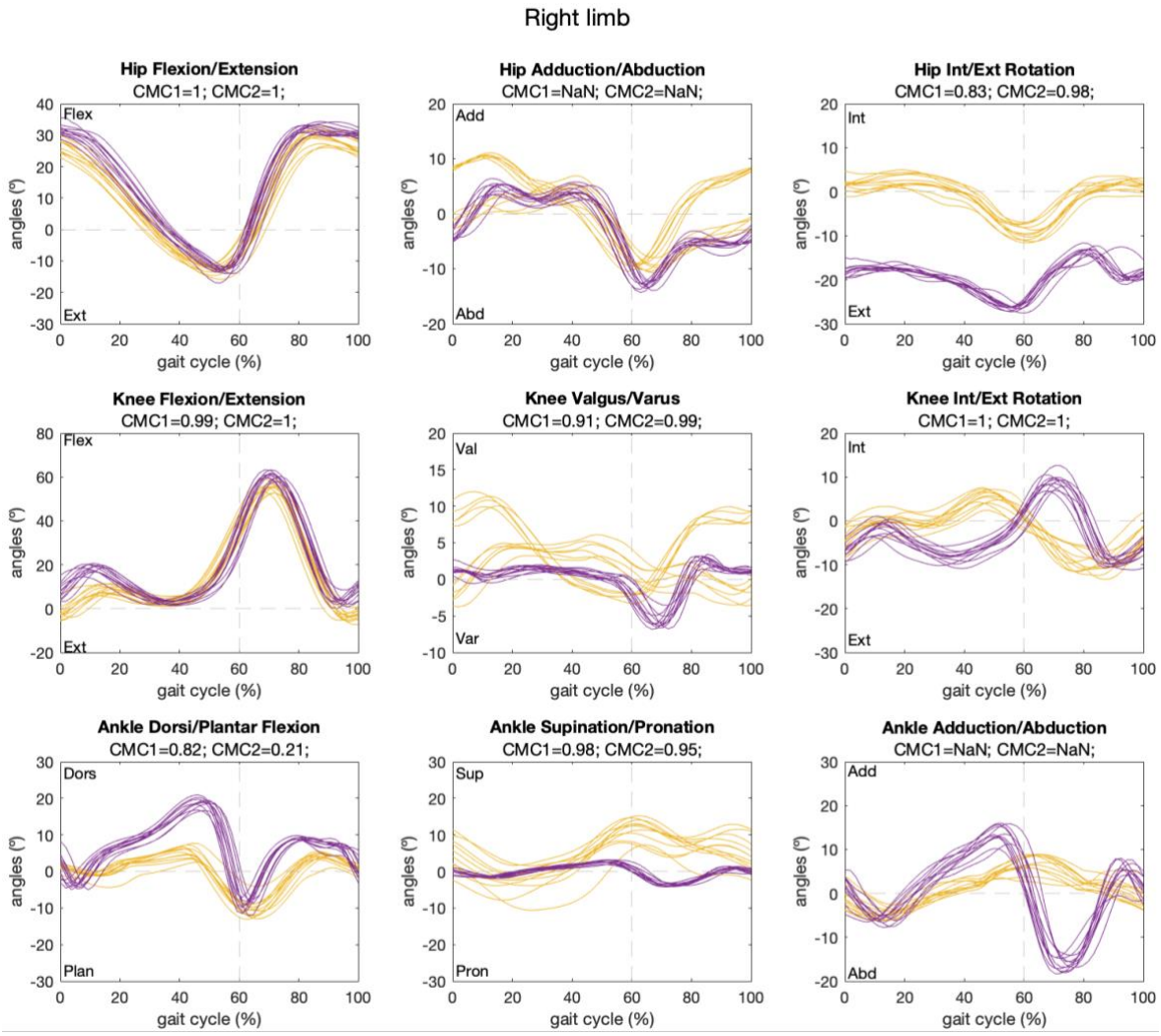


*Figure 44. Part II, condition 1: right limb CMC1 and CMC2 regarding the comparison IMUs (yellow) vs VICON (purple).*

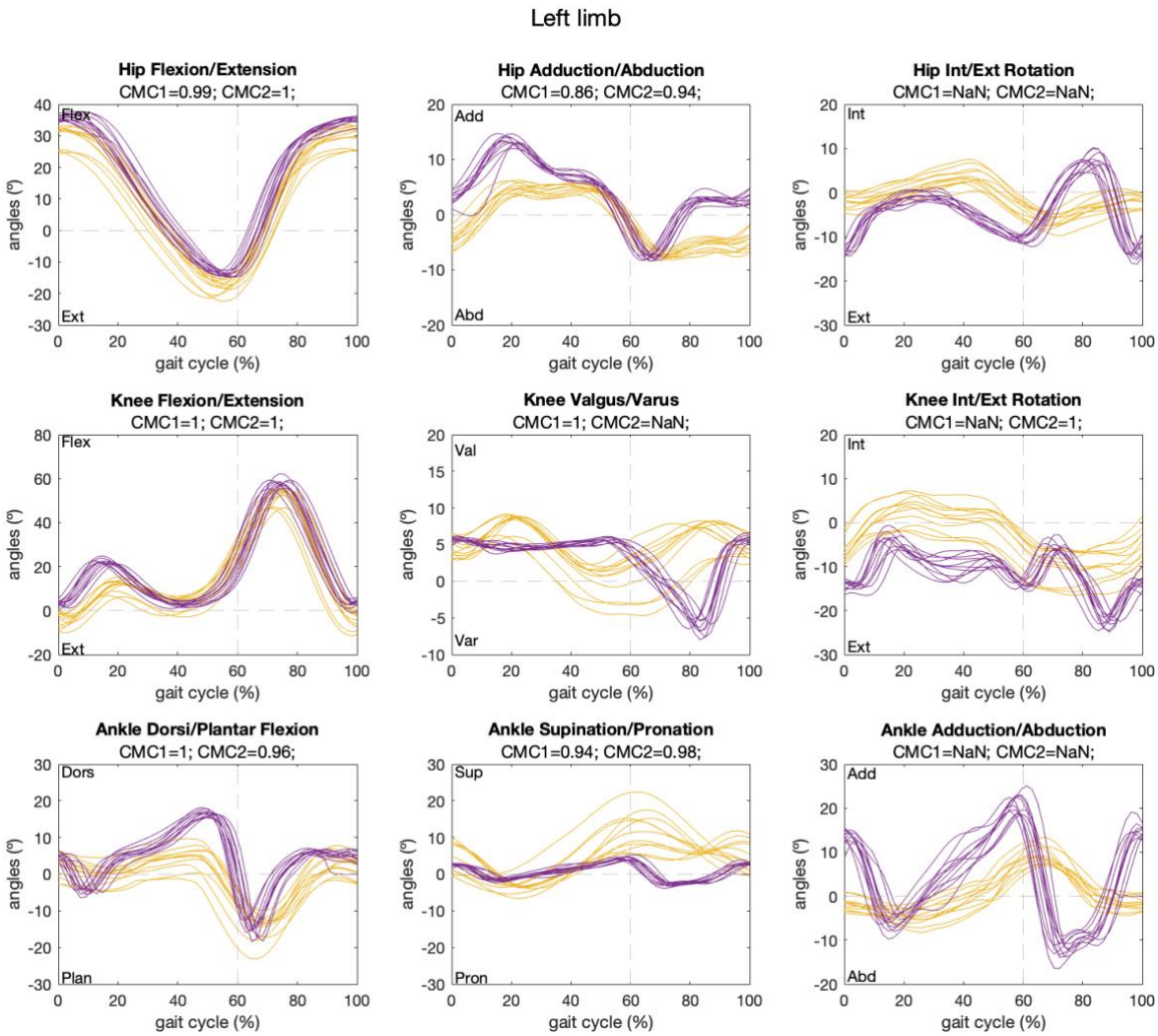


*Figure 45. Part II, condition 1: left limb CMC1 and CMC2 regarding the comparison IMUs (yellow) vs VICON (purple).*

### 5.2.2. Condition 2: exoskeleton-assisted walking test with Exo-H3

The distributions of r, ΔROM, off and RMSE are shown for each pair of cycles and joint angles in Part II Condition 2, in gait assisted with the Exo-H3 exoskeleton. In this case, after retrieving the captured data, it is only possible to obtain correct measurements for four gait cycles, therefore, each plot shows two boxplots, one for each leg, with data for four pairs of gait cycles [I(t), V(t)] each. Thus, each boxplot contains 36 values (9 joint angles). The results of the normality study performed for each parameter with the Shapiro-Wilk test are shown in Table 6, Appendix 1.

About the values of r in the sagittal plane, the medians and whiskers of the hips and knees show an excellent correlation (> 0.95). The left ankle has an excellent median and UW, but the LW drops to 0.83, showing a good correlation. While the right ankle has a median of 0.85 and an UW of 0.89, that is, a very good correlation, but the LW presents a moderate correlation (0.72). In the frontal and transverse

planes, the r values worsen considerably and show a greater dispersion, except for the values for adduction/abduction and rotation of the right hip, whose medians are 0.96 and the whiskers present a very good to excellent correlation, and 0.82 and ranges between moderate and excellent, respectively. For the knees the r presents very low values, on the right the medians of adduction/abduction and rotation are very close to 0, and on the left they reach values < -0.5. For both ankles the median values are close to 0 and the dispersion is very large (Figure 46).

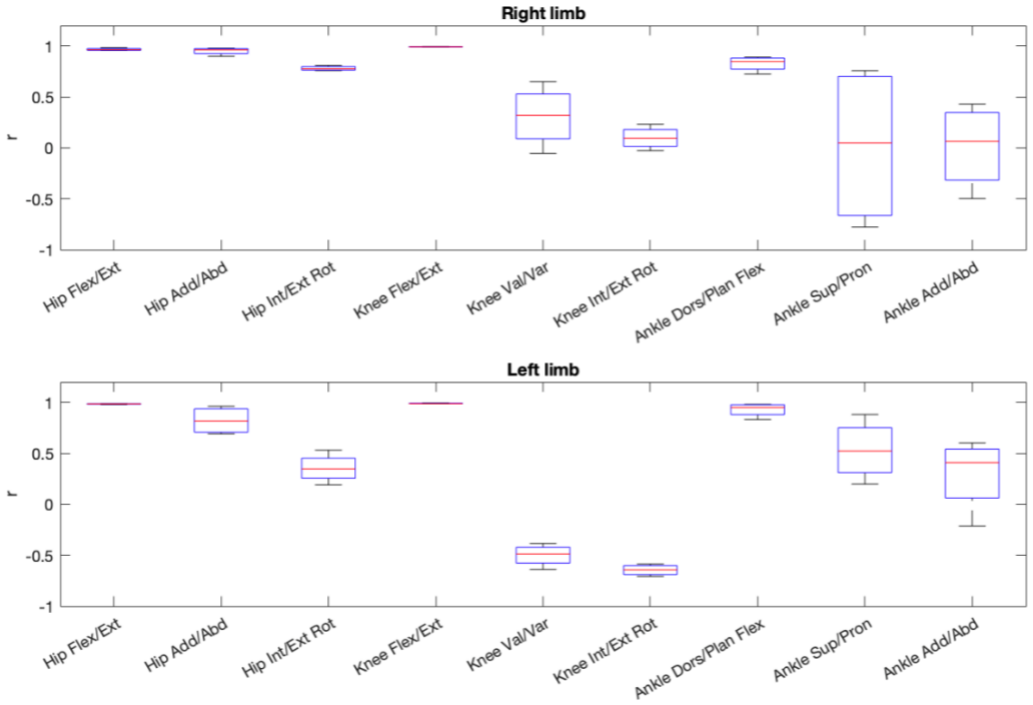


*Figure 46. Part II, condition 2: Box-and-whisker plot for r regarding the comparison IMUs vs VICON.*

In the hip, IMUs measure greater ROM than Vicon, the difference in right flexion-extension has a median of 8.54º, and the left of 4.26º, but in both cases the whiskers are $\pm 2$º above and below the medians. In the case of knee flexion/extension, the IMUs measure a lower range. The median for the right is -3.78° and -14.24° for the left. In addition, the dispersion of the data is greater, as can be seen in the dimensions of the boxes and whiskers. For the ankle in the sagittal plane, the median ROM difference for the right leg is 0.36º, while for the left leg it is 9.44º. For both cases the whiskers vary $\pm 2$º around the median. The ΔROM in the frontal plane of the right limb is negative for the hip and knee, with median values of -2.38º and -1.69º respectively. However, in the left leg, these values are positive, 1.59º and 3.86º. That means that in the right leg, the IMUs measure lower range than Vicon, while in the left leg the opposite is true. On the other hand, the differences of ROM increase for both ankles in every joint angle, reaching even -51.96º in adduction/abduction (Figure 47).

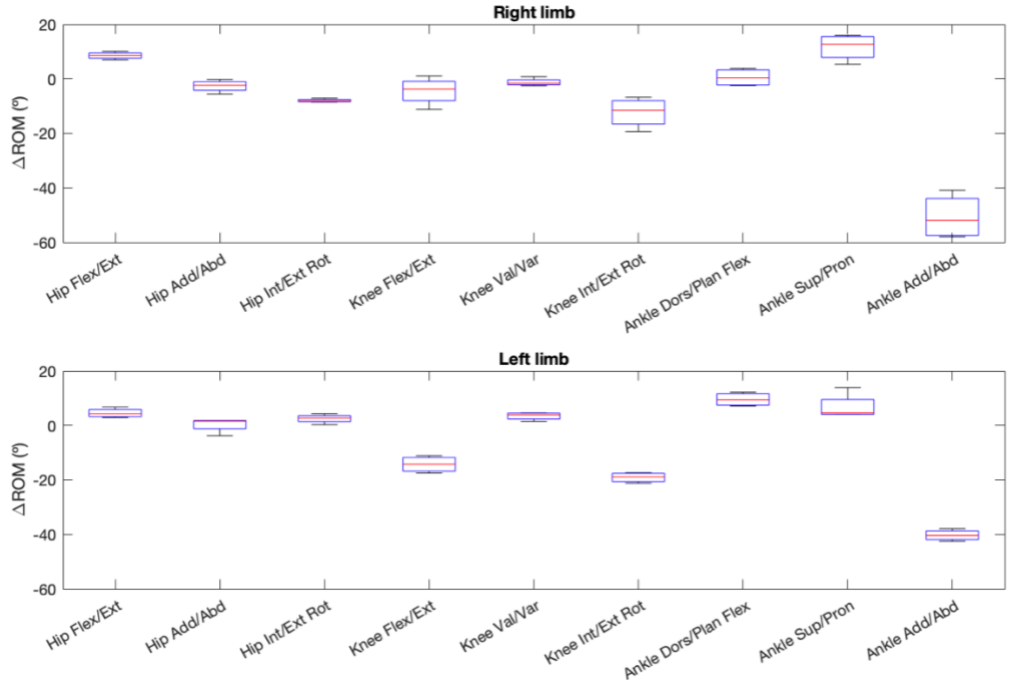


*Figure 47. Part II, condition 2: Box-and-whisker plot for ΔROM regarding the comparison IMUs vs VICON.*

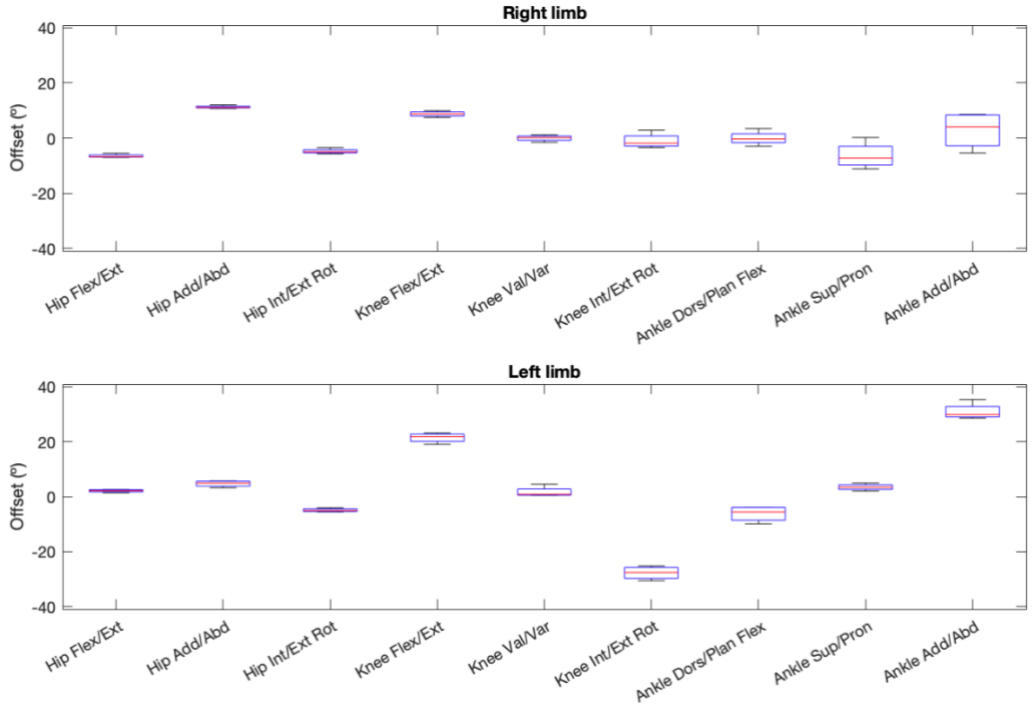


*Figure 48. Part II, condition 2: Box-and-whisker plot for off regarding the comparison IMUs vs VICON.*

In terms of the offset values obtained, in the sagittal plane, the right hip has a median of -6.76º and the left hip has a median of 2.21º. As for the knees, the offset of the right knee is 8.79º, while that of the left increases to 21.78º. The median for the ankles is -0.32º on the right and -5.58º on the left. In the frontal and transverse plane, the offset values increase in both limbs, reaching very extreme values in the left leg of -27.66º in knee rotation and 29.93º in ankle adduction/abduction, except for knee valgus/varus, whose medians are 0.15º on the right and 0.83º on the left. Moreover, excluding the ankle angles, the dispersion of the data is very small, not exceeding $\pm 4$º in the whiskers around the medians (Figure 48).

As expected, according to the r, off and ΔROM results, the joint angles with the highest RMSE are the left knee in the sagittal (22.53º) and transverse (30.71º) planes, and both ankles in the transverse plane (right: RMSE = 19.5º; left: RMSE = 33.76º). Regarding the sagittal plane, the hip has RMSE medians of 7.47º and 3.61º, right and left limbs respectively. The right knee has 9.2° of error, the left > 20º, and the ankles have 4.58º right, and 5.16º left. In the frontal plane, no error exceeds 9º, with the only exception of the right hip, which reaches 11.35º (Figure 49).

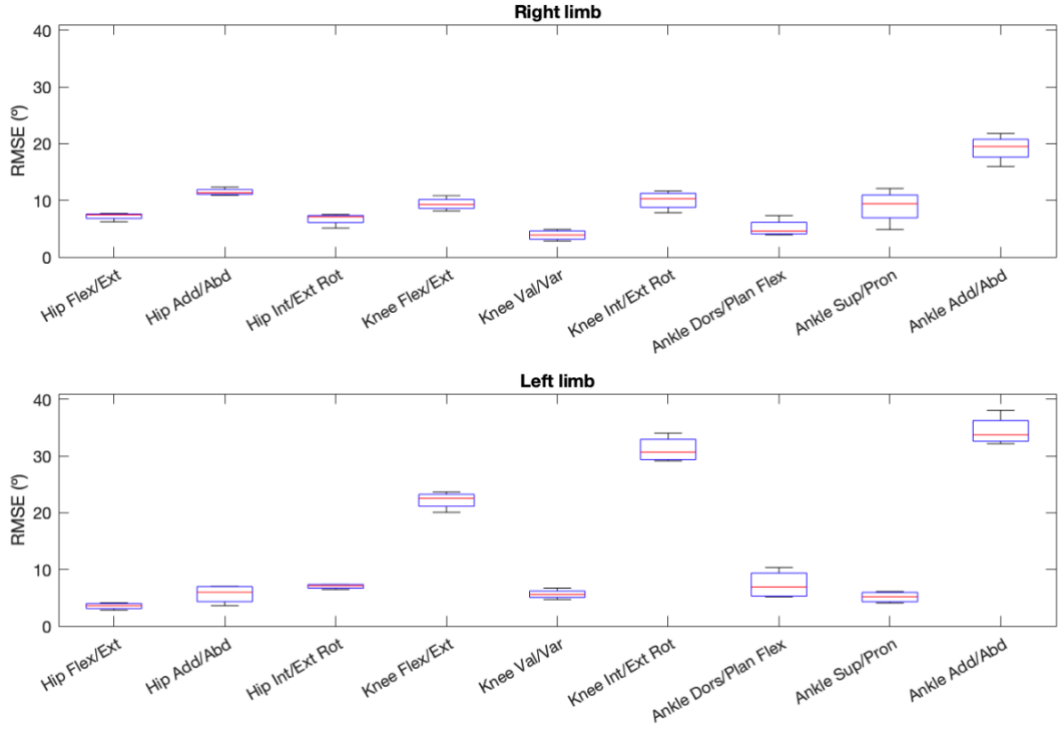


*Figure 49. Part II, condition 2: Box-and-whisker plot for RMSE regarding the comparison IMUs vs VICON.*

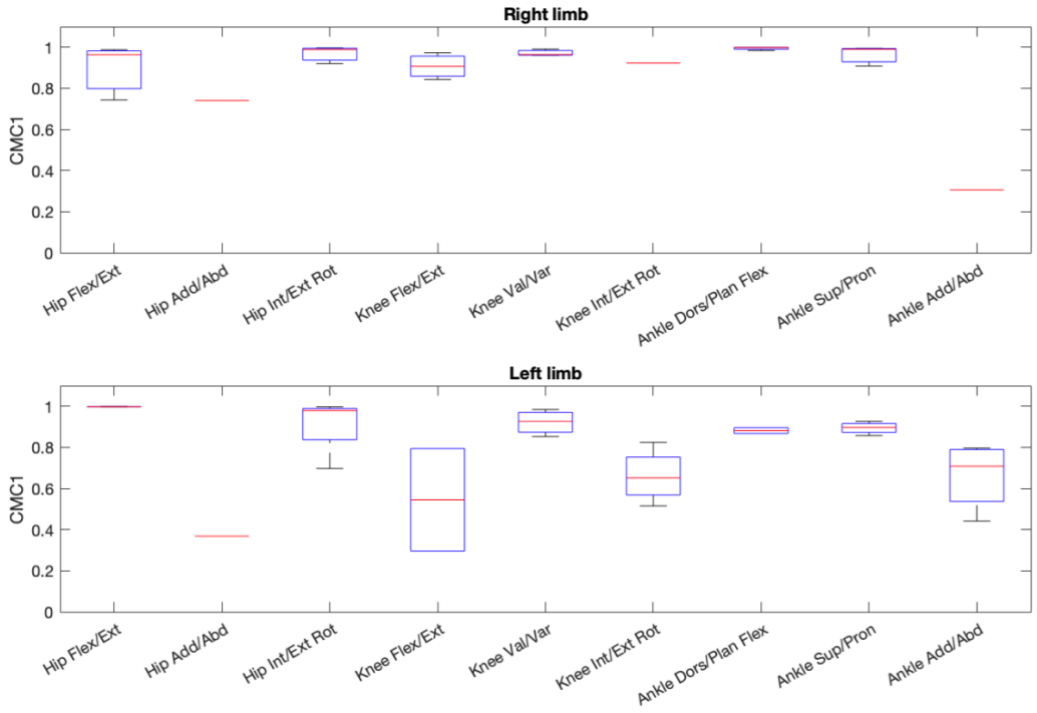


*Figure 50. Part II, condition 2: Box-and-whisker plot for CMC1 regarding the comparison IMUs vs VICON.*

For the $CMC1_p$ shown in Figure 50, in the sagittal plane of both extremities, median values are very good for the right knee (0.91) and left ankle (0.88), and excellent for both hips (right: 0.96; left: 1) and right ankle (0.99). All the LWs fall within the good to excellent correlation ranges. The exception is the left knee, whose median value is 0.54, being less than a moderate correlation. These data satisfy Cond. 2.1 for right ($CMC1_p$ = 0.96, UW = 0.99, LW = 0.75) and left ($CMC1_p$ = 0.99, UW = 0.99, LW = 0.99) hip, right ($CMC1_p$ = 0.99, UW = 0.99, LW = 0.98) and left ($CMC1_p$ = 0.88, UW = 0.89, LW = 0.87) ankle, and for right knee ($CMC1_p$ = 0.91, UW = 0.97, LW = 0.84).

As for the hip joints, the $CMC1_p$ value in the frontal plane is a complex number for both limbs, since all the values obtained for the pairs [I(t), V(t)] are complex numbers, except one (red line, right: 0.74; left: 0.34). However, in the transverse plane, the right hip has a median of 0.99, with its UW and LW being 0.99 and 0.92, thus presenting a very good to excellent correlation. For the left hip, the median is 0.98, its UW is 0.99, and the LW has more dispersion, varying from excellent to moderate correlation (LW = 0.7). Both right ($CMC1_p$ = 0.96, UW = 0.99, LW = 0.96) and left ($CMC1_p$ = 0.93, UW = 0.98, LW = 0.85) knees show very good to excellent correlation in the frontal plane, while in the transverse plane the correlation decreases, with mostly complex values for the right and a moderate correlation ($CMC1_p$ = 0.65) for the left. The same occurs with the ankles, in the frontal plane the $CMC1_p$ values are very good and excellent, being the median for the right 0.99 and for the left 0.89. While the values in adduction/abduction are complex for the right and 0.71 for the left, and with great dispersion in the whiskers. Therefore, the movements of adduction/abduction of both knees, supination/pronation of right ($CMC1_p$ = 0.99, UW = 0.99, LW = 0.91) and left ($CMC1_p$ = 0.93, UW = 0.89, LW = 0.86) ankles, and

rotation of the right hip ($CMC1_p$ = 0.99, UW = 0.99, LW = 0.92) comply Cond. 2.2.

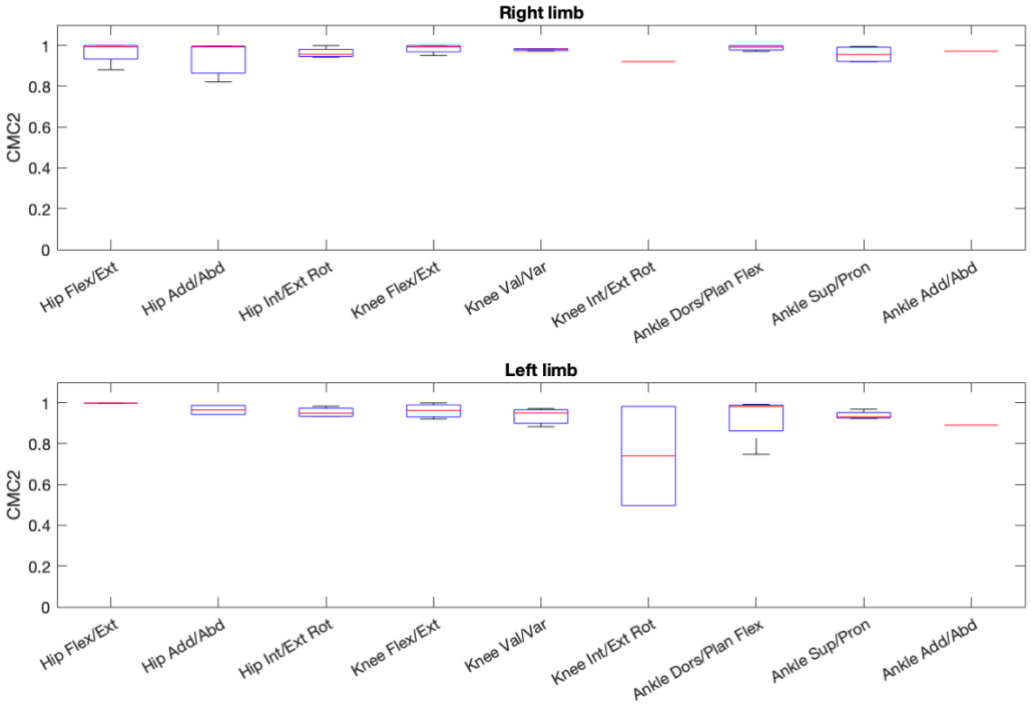


*Figure 51. Part II, condition 2: Box-and-whisker plot for CMC2 regarding the comparison IMUs vs VICON.*

After removing the offset between pairs of gait cycles, $CMC2_p$ values increase with respect to $CMC1_p$ (offset included) ((Figure 51). Values in the sagittal plane improve for the right hip, both knees and the left ankle, so that the new medians for all joints in this plane are > 0.95 and all their LWs present a very good correlation (> 0.85). Excluding the left ankle, whose LW value reaches 0.75. The correlation improves in the frontal plane for both hips and knees with medians > 0.95, and for the left ankle, whose median increases to 0.93 ($CMC2_p$ = 0.93, UW = 0.97, LW = 0.92). Finally, in the transverse plane, no notable improvements are observed. If the conditions established were based on the $CMC2_p$ values, Cond 2.1 and 2.2 would be met for all joints in the sagittal and frontal plane, and for both hips in the transverse plane.

At last, the results of the $CMC1_T$ and $CMC2_T$ calculation for all pairs [I(t), V(t)] extracted for each limb are shown in Figure 52 and Figure 53, along with the gait cycles with the kinematic pattern recorded by each system. For both limbs, the hip presents an excellent $CMC1_T$ (right: 0.98; left: 1) and $CMC2_T$ (right: 1 ; left: 1) correlation in the sagittal plane between the cycles recorded with IMUs and those of Vicon, as happens in the $CMC1_p$ box-and-whiskers plots of Figure 50. For the right knee flexion/extension, the value of $CMC1_T$ is 0.75, and for the left 0.81, which shows a good correlation between all the cycles of both extremities. However, when the offset is removed, $CMC2_T$ improves to an excellent correlation for the right leg (0.98) and becomes complex for the left. In this same plane, the right ankle has an excellent $CMC1_T$ = 1 and the left ankle has a complex $CMC1_T$, but when the offset is removed both are excellent ($CMC2_T$ = 0.98). Nevertheless, the medians computed from the $CMC1_p$ values of each pair of cycles

[I(t), V(t)] demonstrate an excellent correlation for the right knee and both ankles (Figure 50).

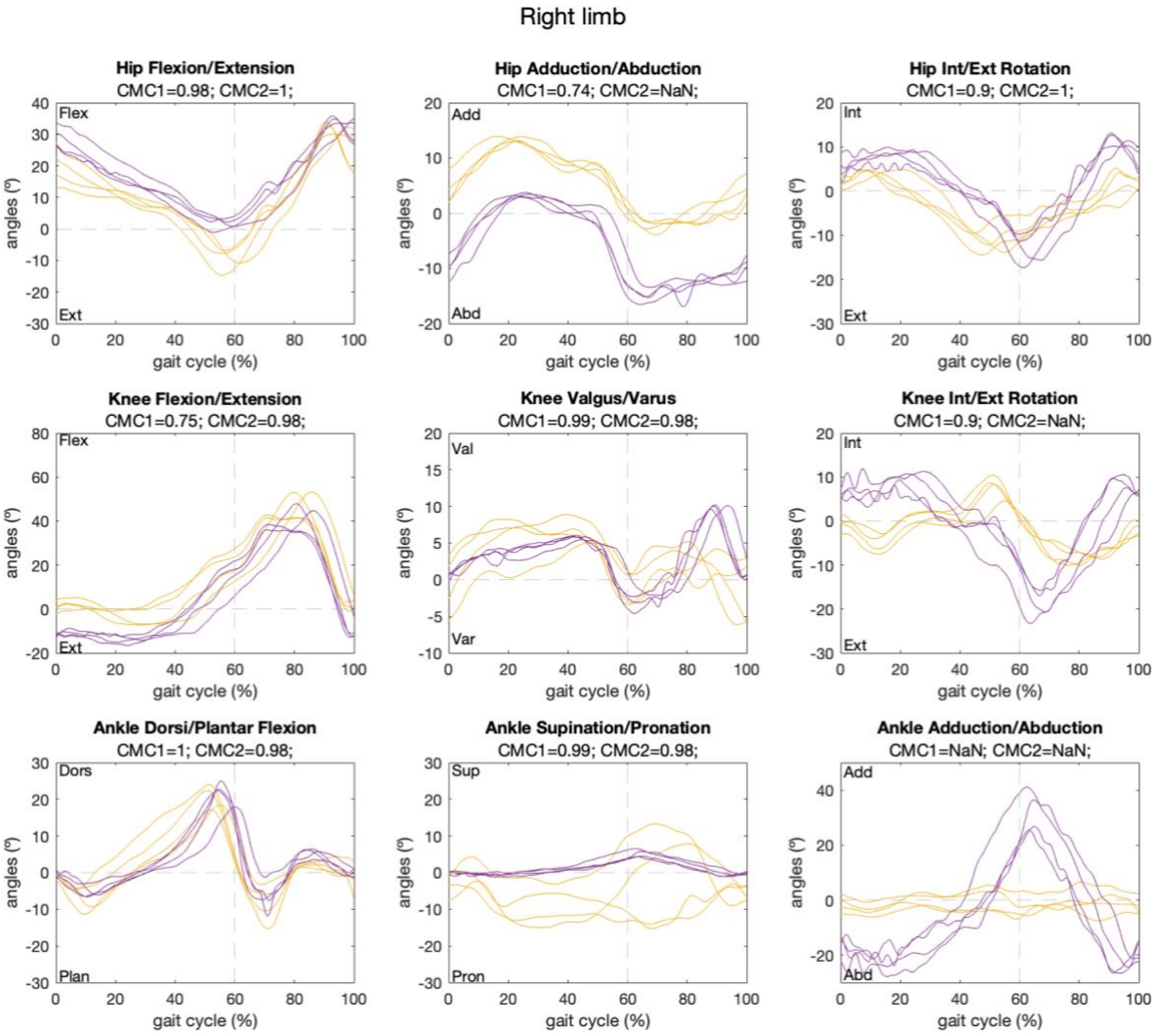


*Figure 52. Part II, condition 2: right limb CMC1 and CMC2 regarding the comparison IMUs (yellow) vs VICON (purple).*

In the frontal plane, the hips adduction/abduction values are complex, except for the $CMC1_T$ of the right hip (0.74). For this movement in the knee joints, the correlation is excellent ($CMC1_T$ and $CMC2_T$ >0.95) and for the ankles, from very good (left: $CMC1_T$ = 0.86 and $CMC2_T$ = 0.92) to excellent (right: $CMC1_T$ = 0.99 and $CMC2_T$ = 0.98). Both hips present a very good (right: $CMC1_T$ = 0.9 and $CMC2_T$ = 1) or excellent (left: $CMC1_T$ = 1 and $CMC2_T$ = 0.97) correlation in the rotation movement. For the knees however, the $CMC1_T$ value is 0.9 for the right and 0.54 for the left, but both become complex when recalculating $CMC2_T$ without offset. As for the ankles, for the right both values $CMC1_T$ and $CMC2_T$ are complex, and for the left, $CMC1_T$ = 0.54 and $CMC2_T$ = 0.8. A similar behavior is described for hips and ankles in frontal and transversal planes in the previous $CMC1_p$ medians computation in Figure 50.

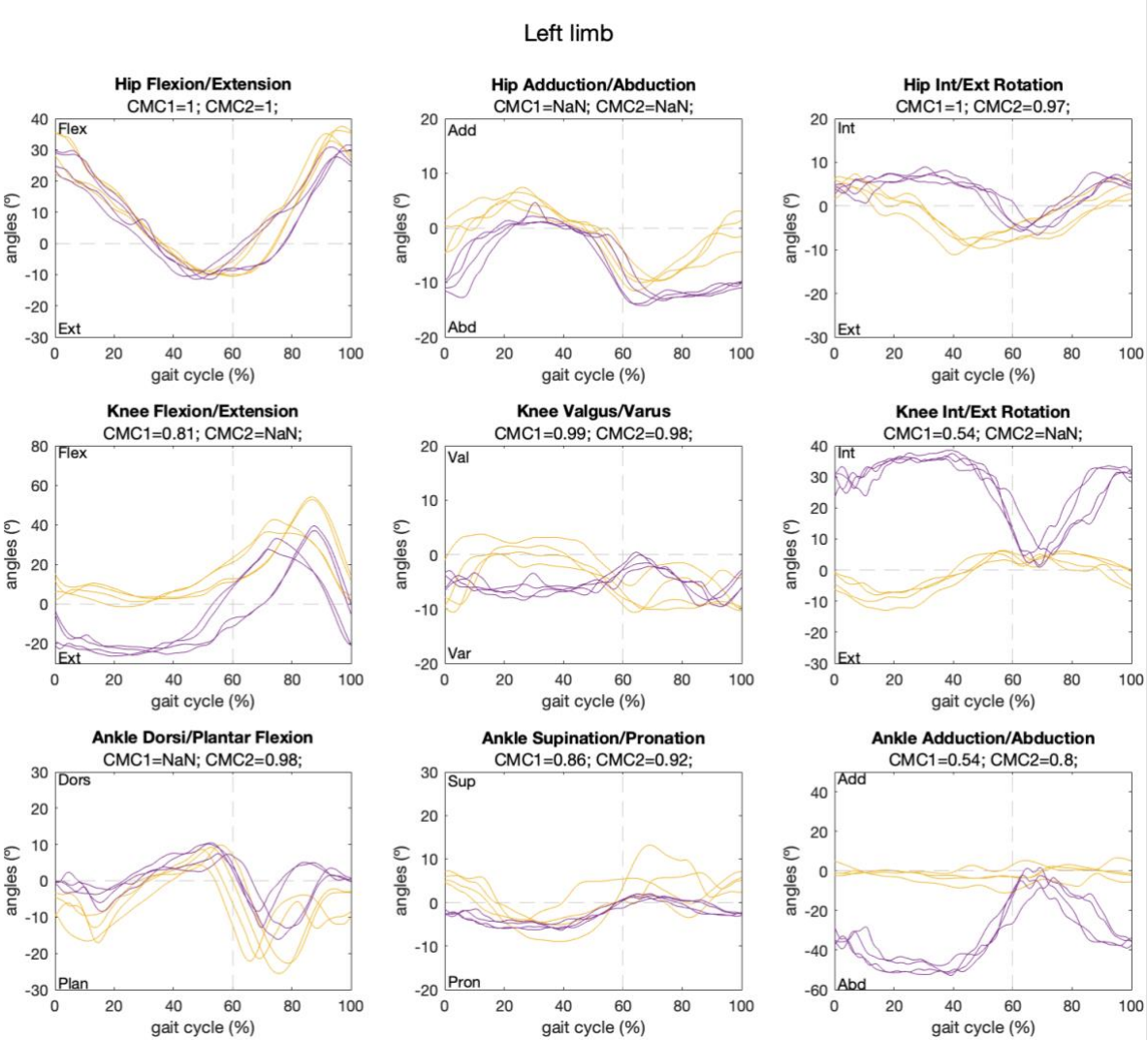


*Figure 53. Part II, condition 2: left limb CMC1 and CMC2 regarding the comparison IMUs (yellow) vs VICON (purple).*

# 6. Discussion

## 6.1. Part I. Exploring different configurations offered by the IMUs

It is worth reminding that this phase aims to understand how IMUs work and which factors influence them in order to reach the optimal configuration for evaluating gait rehabilitation therapy. To choose one of the IMUs configuration models to continue the project, the results obtained in this first part are discussed.

As mentioned above, there are studies that have evaluated the efficacy of CMC ($CMC_w$ and $CMC_p$) that show that lower ROM ranges result in lower CMC values or in the formula breakdown giving complex numbers [61]. When the ROM is limited, the variability of the waves studied around their mean waveform ($Y_{swf} - \bar{Y}_{sf}$) is greater than the variance around their overall mean ($Y_{swf} - \bar{Y}_{s}$), which leads to the root of a negative number, whose result is a complex value. The same happens when the offset between waveforms is large or the ROM value is similar to the offset. From a clinical perspective, obtaining real values is interpreted as a complete dissimilarity between waveforms [59, 62].

Figure 35 shows the $CMC_w$ results for each model. As mentioned above, despite analyzing all planes, the movement of the exoskeleton is only in the sagittal plane, thus, the analysis on this plane is essential. For this reason, the first condition to be able to consider an adequate model is that the within-day correlation has high values for all the joints in this plane. Model 3 is the only one for which the $CMC_w$ is a complex value for this plane in some joints, that is why it is discarded.

Looking at the same figure, moreover, it can be concluded that the joint whose values vary the most in all planes for all models is the ankle. This is associated with poor positioning of the IMUs in these joints, leading to offset and inconsistent kinematic recordings. Furthermore, the ROM of the ankle in all planes is limited, which, together with the offset and the low correlation between waveforms, affects the $CMC_w$ calculation, resulting in real numbers. Therefore, it is considered relevant to obtain information on the hip and knee joints in the three planes. It is observed that the only model that obtains $CMC_w$ values between recorded gait cycles greater than 0.6 for all hip and knee planes of both limbs, is Model 2. Besides, this configuration offers a very high $CMC_w$ for dorsal/plantar flexion of the right ankle (0.85) and adduction/abduction of the left ankle (> 0.9), in addition to providing some information on the frontal plane of the right (> 0.2), which means that it can obtain consistent ankle records if the factors that alter the measurement are controlled.

Regarding the variation of the ROM recorded by each model, the CV value for Model 2 is around 5% in sagittal planes of the hip and knee and does not exceed 15% in the ankle. This means that the ranges recorded in each cycle are consistent. Besides, for the rest of the planes, excluding the ankles, it is one

of the models with lower CV. Models 1 and 3 have higher CV, the dispersion of these data is caused by the drift accumulated during the records (Figure 34).

Finally, the RMSE values show that the error is much lower for Models 1 and 2 than for 3 and 4 (Table 2). Furthermore, in Figure 36 and Figure 37 displaying the kinematic data recorded by each model against normality, the differences and offsets between models can be visually observed. The average gait cycle of each configuration shows that Models 3 and 4 record less ROM in the frontal and transverse planes of both limbs, see for example hip adduction/abduction. In addition, the accumulated offset at all joints in the sagittal plane of the right leg is also observed for Model 3. It can also be deduced from these plots that the orientation of the axes does not interfere in the measurement.

During both recordings and data analysis, it is evident that models with 8 IMUs calibrate the subject better and avoid drift accumulation throughout the captures. Models 1 and 3, made up of 7 IMUs, do a wrong trunk calibration that leads to the introduction of bias into the measures registered by the following sensors. Because of these reasons, the configuration chose to continue with the project is Model 2.

## 6.2. Part II. Validation of IMUs with Vicon: similarity assessment

After presenting the statistical and kinematic results for both limbs, many irregularities have been observed in the measurements of the left leg. As human gait in healthy subjects has a high unilateral and bilateral repeatability in captures performed on the same day, and since the configuration of IMUs used is symmetrical and each sensor has always the same placement, the variability and inconsistency of the calculated parameters have allowed to detect the erroneous functioning of one of the sensors placed on the left limb [6, 58]. Therefore, from this point on, the discussion focuses only on the right leg.

### 6.2.1. Condition 1: walking test

The aim of this study is to create a new model based on IMUs to record and assess biomechanics in therapies involving multiple technologies. For this, it is necessary to validate the accuracy and consistency of the sensors, for which the similarity of the waveform recorded by this system with the data recorded by Vicon synchronously is evaluated. In this first test, similarity analysis is performed during barefoot gait.

Although the conditions established to consider both systems interchangeable are based on $CMC1_p$, because this parameter involves the effects of the other four variables, it is considered necessary to study individually the variability, trend, and dispersion of each of them to properly evaluate the accuracy of the synchronous pairwise measurements [I(t), V(t)]. Obviously, the worse the results for each joint angle in r, offset, ΔROM and RMSE, the worse the assessment in $CMC1_p$.

In this test, as seen in Figure 42, the $CMC1_p$ values for the right limb satisfy Cond.1.1 in the

flexion/extension movement of hip and knee ($CMC1_p$ and whiskers ≥ 0.95) and Cond1.2 in the adduction/abduction movement of the right knee ( $CMC1_p$ and whiskers ≥ 0.85). No articulation fulfils the specification in the transverse plane. It is shown that the frontal and transverse planes, which have lower ROM, obtain poorer r values and more offset, and therefore low or complex $CMC1_p$ values, which are interpreted as lack of similarity (Figure 38,Figure 40Figure 42). Thus, joint angles that meet Cond. 1.1 and Cond. 1.2 demonstrate that the kinematic measurements recorded by both IMUs and Vicon systems are equivalent, in other words, that both protocols and systems are interchangeable in these planes to assess biomechanics.

However, the right ankle does not satisfy Cond. 1.1 in the sagittal plane due to its large whiskers dispersion. This means that the measurements provided by the IMU are not sufficiently accurate to assess ankle movement. Even tough, their $CMC1_p$ median value is quite high, 0.9. None of the ankle movements in the frontal or transverse plane comply with Cond. 1.2 either. The results obtained for $CMC1_p$ for the ankle in the 3D of space are consistent since it is the joint with the greatest ΔROM (sagittal plane: ΔROM = -13º; frontal plane: ΔROM >10º; transverse plane: ΔROM < -25º) and the poorer correlation (sagittal plane: r = 0.7; frontal and transversal plane: r = 0). With the aim of improving every ankle parameter value, and because of Exo-H3 actuators located on the ankles, the IMUs 3 and 6 are repositioned frontally in the upper instep area of the feet, as shown in Figure 26.

On the other hand, when the offset is removed for every pair of cycles [I(t), V(t)], the $CMC2_p$ value increases for almost every joint angle. This problem can be observed on the right hip adduction/abduction and rotation kinematics of Figure 44. Thus, the highest RMSE value is obtained for hip rotation (18º). This demonstrates the existing offset between IMUs and Vicon signals, which is induced due to the not exact definition of the IMUs placement. As Vicon has a global coordinate system and reconstructs data by estimating the real joint centers starting at the markers position and the anthropometric measures of the subject, it enables to detect if a movement starts beyond 0º at any plane. Whereas the IMUs record the movement angles according to the relative positions between each other during calibration, which always determines the initial position as the origin, that is, their measures always start from 0º. All this influences the kinematics recorded by each system, adding technological limitations and differences between pairs of gait cycles reflected in the calculated parameters.

To calculate the $CMC1_T$ and $CMC2_T$ values, all pairs of gait cycles obtained for each joint angle are entered in (Eq. 9. However, these values do not always correspond to the median values of $CMC1_p$ and $CMC2_p$ obtained in the boxplots of Figure 42 and Figure 43. This is the case for hip adduction/abduction, whose values of $CMC1_T$ and $CMC2_T$ are complex numbers, while those of $CMC1_p$ and $CMC2_p$ are 0.83 and 0.87, respectively. It should be remembered that boxplots are not generated for those joints that had more than 3 complex CMC values. Therefore, as each pair of gait cycles is entered into the formula, the sum of all the gait cycles (G) magnifies the variability of the waves studied around their mean waveform with respect to the variance around their global mean, resulting again in the root of a negative component that breaks down the formula and leads to another real number. For all these reasons, the decisive conditions for the validation of the systems are based on the CMC results obtained by gait pairs [I(t),

V(t)], represented throughout all the boxplots.

Finally, there are also studies that determine that the CMC equation overestimates the similarity between waveforms when comparing these numeric values with the kinematics obtained [61]. In this case, despite satisfying Cond. 1.2, an overestimation can be observed when looking at the kinematics of right knee valgus-varus on Figure 44.

### 6.2.1. Condition 2: exoskeleton-assisted walking test with Exo-H3

Despite the reconstruction troubles caused by the occlusion of some markers and the need to manually adjust the segments and joint axis in the model of the subject in Nexus, four pairs of gait cycles for each limb are recovered. The results for the right leg are then discussed.

Because of this and of the bias caused by the exoskeleton, and thus considering the irregularities on gait cycles, the conditions are redefined, expanding the $CMC1_p$ acceptance ranges for the three planes. This gives rise to the specifications Cond. 2.1 and Cond. 2.2 described in methodology.

From the results obtained for this exoskeleton-assisted walking test, the $CMC1_p$ values that satisfy Cond. 2.1 are the ones of the right hip ($CMC1_p$ = 0.96, UW = 0.99, LW = 0.75), knee ($CMC1_p$ = 0.91, UW = 0.97, LW = 0.84) and ankle ($CMC1_p$ = 0.99, UW = 0.99, LW = 0.98) in the sagittal plane. Compared to the previous test, the ankle ΔROM is much lower (0.36º) and the r increases (0.85) in the sagittal plane, and therefore the $CMC1_p$ value is improved regarding the previous one, meaning that the measured kinematics are more accurate with the frontal location of the IMUs, what can also be seen in the kinematics in Figure 52. In addition, right knee and ankle frontal plane and right hip rotation $CMC1_p$ values fulfill Cond. 2.2, confirming the measures are equivalent ($CMC1_p \geq 0.96$) (Figure 50). Therefore, IMUs and Vicon recordings are equivalent for every joint in the sagittal plane, for knee and ankle in the frontal plane, and for the hip in transverse plane. In this second test, the equivalence of more joints in the frontal and transverse plane is achieved.

However, the knee flexion/extension $CMC1_p$ value decreases in comparison with the ones obtained for the walking test, even though it complies the requirements (Condition 1: $CMC1_p$ = 0.98, UW = 0.99, LW = 0.97; Condition 2: $CMC1_p$ = 0.91, UW = 0.97, LW = 0.84). A slight increase to 8.8º in the offset can be observed during these gait cycles, that means that the IMUs measure higher values than Vicon, which may be caused by the exoskeleton gait limitations, the motion perturbances and the placement of markers (Figure 48 and Figure 52). The $CMC2_p$ is higher when the offset is removed from the signals for the right knee flexion/extension ($CMC1_p$ = 0.91, $CMC2_p$ = 0.99).

Also, the offset problem can be appreciated on frontal plane for the right hip joint kinematics (11º), shown in Figure 52. The adduction/abduction hip movement only is interchangeable if the offset is removed ($CMC1_p$ = NaN, $CMC2_p$ = 0.99). For this joint angle, there is also difference between the values obtained for $CMC_p$ and $CMC_T$. In the total CMC calculation involving the four gait couples the values of $CMC1_T$ and $CMC2_T$ behave in the opposite way, being $CMC1_T$ = 0.74 and $CMC2_T$ a complex number

(NaN), which is inconsistent with what can be visually observed in the kinematics (Figure 52). For the ankle supination/pronation movement, it can be seen that the CMC values overestimate this movement with respect to the kinematics ($CMC1_p = 0.99$, $CMC2_p = 0.96$, $CMC1_T = 0.99$, $CMC2_T = 0.98$).

Finally, in the transversal plane, every $CMC_p$ and $CMC_T$ values for knee and ankle are complex numbers, which is consistent considering the low r between pairs of signals and the large differences in ΔROM and offset (Figure 46Figure 47Figure 48). Likewise, all this is consistent with the kinematics shown in Figure 52.

# 7. Conclusions, limitations, and future work

The objective of this project is to create a strategy to assess biomechanics during gait rehabilitation therapies assisted by different technologies. Specifically, in incomplete SCI gait rehabilitation assisted by an exoskeleton controlled by BCI and combined with tSCS. To be able to record biomechanics without interferences caused by the assistive technologies, IMUs are an alternative to the use of photogrammetry. To do so, it is necessary to validate their correct functioning by evaluating waveform similarity with respect to a reference system, Vicon.

To this end, it is needed to identify the optimal configuration of the IMUs to record kinematics as accurately as possible during exoskeleton-assisted walking. For this, in Part I it is concluded that adding an eighth sensor on the chest significantly improves the calibration of the system, that the orientation of the axes does not affect the registration, and that the best configuration for further registration in the project is Model 2. Additionally, the fixation of the IMUs must be guaranteed to prevent them from being affected by motion disturbances during gait.

In Part II, it is demonstrated that the data recorded by the adapted IMUs Model 2 (repositioned ankle sensors) are accurate and equivalent (interchangeable) with the ones obtained using Vicon, mainly in the sagittal plane for hip, knee, and ankle joints (Figure 26 and Figure 52). This enables the evaluation of gait kinematics in the most important plane on which the exoskeleton acts.

On the other hand, it is concluded that the frontal and transverse planes kinematics are more variable between protocols and systems. This is primarily caused by the offset introduced by the difference in the origin angles (that implies a technological limitation by the IMUs system) and by the susceptibility of the CMC ($CMC_w$ and $CMC_p$) formula to limited ROMs and great offsets. Even so, it has also been shown that knee and ankle angles in the frontal plane, and hip angles in the transverse plane, may also be interchangeable according to the similarity assessment executed with $CMC_p$. In any case, the reliability and utility of studying these planes still must be confirmed. To reach solid conclusions it is necessary to test more subjects, since the $CMC_p$ value varies between subjects and planes [61].

Finally, it is also worth mentioning the limitations caused by the damaged sensor in the left limb and by the problems with the rotation axes reconstruction performed in Vicon Nexus, which has strongly conditioned the number of analyzable cycles in the final part of the project.

As future work, further validation tests during exoskeleton-assisted walking with IMUs and Vicon with different healthy subjects are needed to adjust the IMUs configuration as much as possible, mainly to improve the frontal and transverse planes kinematics. It is also expected to fix or replace the damaged sensor that has disturbed the records of the left limb. In addition, it would be interesting to assess whether the offset detected in some joint angles is constant for each subject and, if so, to consider performing a brief test prior to rehabilitation therapy to estimate this variable for the subsequent correction of the IMUs measurements, as in the case of adduction/abduction hip motion during Condition 2 (Figure 52).

# 8. Project timeline, economic analysis, and environmental and social impact

## 8.1. Project timeline

The following figure shows the Gantt chart complied for this project, which describes the activities carried out and their duration. The estimated time for this project was 540 hours, which has been exceeded during these 18 weeks of work.

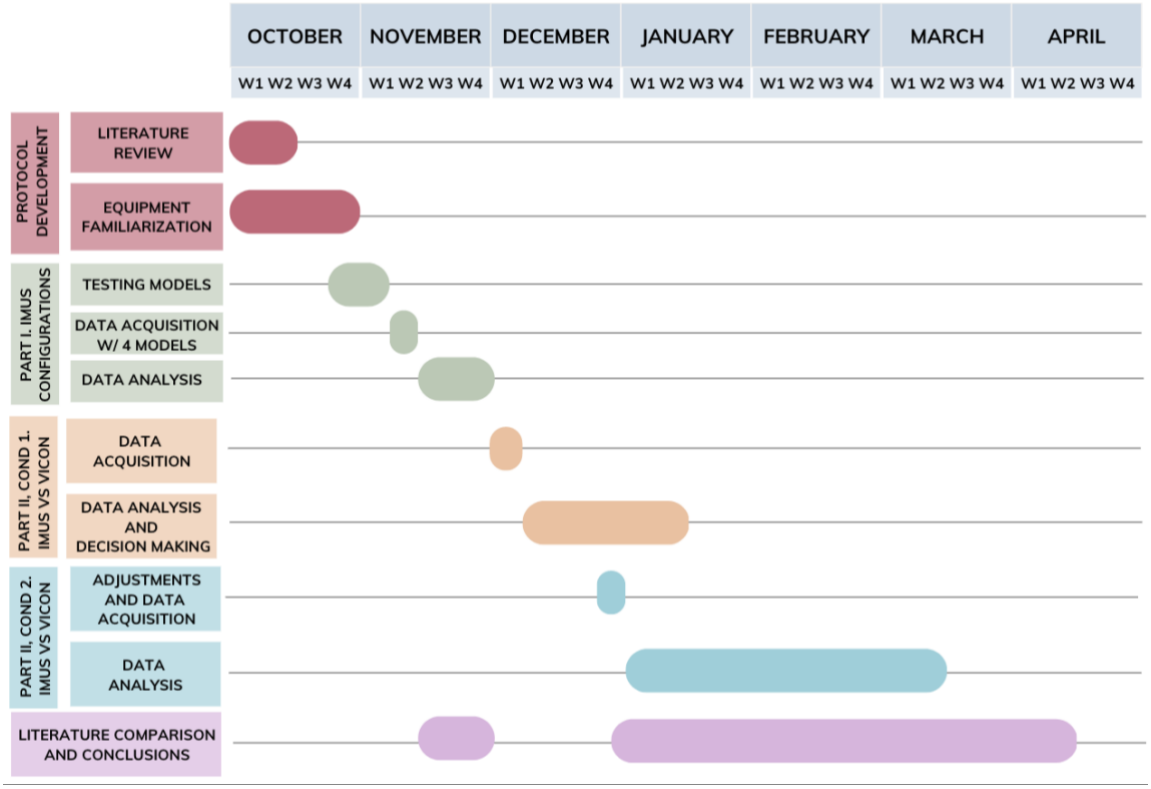


*Figure 54. Gantt chart.*

## 8.2. Economic analysis

To quantify the economic budget of this project, an analysis of equipment and personnel costs is carried out.

Table 3 includes the cost of the hardware and software used during the development of this project. However, all the material was already part of the laboratory equipment, either because it was acquired for other projects or because it is part of the clinical tests of the unit, so no additional equipment was

ordered for this project. Therefore, the actual cost of equipment to carry out this work was 0 €.

*Table 3. Equipment costs.*

| **Hardware and Software** | **Cost** |
|---|---|
| Tech-MCS Mocap System and Software | 5000.93 € (IVA excluded) |
| Vicon Mocap System and Softwares | 50000 € |
| PC DELL Precision 3640 Tower i7 | 2555.71 € |
| Display DELL SE2417HGX | 300 € |
| PC HP 290 G2 MT Business Tower i5 | 696 € |
| Display HP N240 | 183.33 € |
| Exoskeleton Exo-H3 | 70000 € |
| Lenovo TAB2 A10-30 | 150 € |
| MATLAB 2021b* | Free (Student version) |
| Office 365* | Free (Student version) |
| Laptop MacBook Pro 2019 | 1600 € |
| **TOTAL** | **130485.97 €** |

The personnel costs include the hiring of a junior engineer on internship for the duration of the project, a total of 540 hours. However, as the HNP is a public institution, the agreement provides for non-remunerated curricular internships. It also requires the hiring of a postdoctoral engineer for the same period, whose average hourly rate is considered to be 25 €. The cost in personnel is therefore 13500 €, which also corresponds to the final cost of the project.

*Table 4. Total cost of the project.*

| **Concept** | **Cost** |
|---|---|
| Hardware and Software | 0 € |
| Personnel | 13500 € |
| **TOTAL** | **13500 €** |

## 8.3. Environmental and social impact

As for the environmental impact caused by the development of this project, it can be considered low since the only impact is the electrical consumption of the equipment necessary to carry out the assessment.

On the other hand, the social impact of this project is very high, especially in the SCI population, since this work is essential to achieve the ultimate goal of the ReGAIT project: to create a new rehabilitation therapy to promote neuroplasticity and improve the quality of life of these patients.

# Acknowledgments

I would like to thank, first, my parents and my sister for always supporting me in my professional ambitions and for being a fundamental base in my life.

I also thank and dedicate this work to my grandmother, who every day makes me feel fortunate to have the opportunity to study and work in what motivates me and what I am passionate about.

Finally, thanks to the friendships forged over these years, and to the Biomechanics and Technical Aids Unit of the HNP, especially to Ángel Gil, for giving me the opportunity to enter this area of research in SCI rehabilitation.

This master's thesis is part of the R&D project PID2021-124111OB-C31 funded by MCIN/AEI/ 10.13039/501100011033 and by "ERDF A way of making Europe".

Project PID2021-124111OB-C31 funded by MCIN/AEI/ 10.13039/501100011033 funded by:

# Bibliography

## References

[1] M. E. L. Van Den Berg, J. M. Castellote, I. Mahillo-Fernandez, and J. De Pedro-Cuesta, "Incidence of spinal cord injury worldwide: a systematic review," *Neuroepidemiology*, vol. 34, no. 3, pp. 184–192, 2010, doi: 10.1159/000279335.

[2] C. Lo, Y. Tran, K. Anderson, A. Craig, and J. Middleton, "Functional Priorities in Persons with Spinal Cord Injury: Using Discrete Choice Experiments To Determine Preferences," *J. Neurotrauma*, vol. 33, no. 21, pp. 1958–1968, Nov. 2016, doi: 10.1089/NEU.2016.4423.

[3] L. A. Simpson, J. J. Eng, J. T. C. Hsieh, and D. L. Wolfe, "The health and life priorities of individuals with spinal cord injury: a systematic review," *J. Neurotrauma*, vol. 29, no. 8, pp. 1548–1555, May 2012, doi: 10.1089/NEU.2011.2226.

[4] B. H. Dobkin and P. W. Duncan, "Should body weight-supported treadmill training and robotic-assistive steppers for locomotor training trot back to the starting gate?," *Neurorehabil. Neural Repair*, vol. 26, no. 4, pp. 308–317, May 2012, doi: 10.1177/1545968312439687.

[5] A. Esquenazi, M. Talaty, and A. Jayaraman, "Powered Exoskeletons for Walking Assistance in Persons with Central Nervous System Injuries: A Narrative Review," *PM R*, vol. 9, no. 1, pp. 46–62, Jan. 2017, doi: 10.1016/J.PMRJ.2016.07.534.

[6] E. Growney, D. Meglan, M. Johnson, T. Cahalan, and K.-N. An, "Repeated measures of adult normal walking using a video tracking system 1," *Gait Posture*, vol. 6, pp. 147–162, 1997.

[7] G. Yavuzer, O. ¨ Znur O ¨ Ken, A. Elhan, and H. J. Stam, "Repeatability of lower limb three-dimensional kinematics in patients with stroke," doi: 10.1016/j.gaitpost.2006.12.016.

[8] "Motion Capture System | Technaid - Inertial Motion Capture." https://www.technaid.com/products/motion-capture-system-tech-mcs-hub-imu/ (accessed Mar. 14, 2023).

[9] A. Hammer and B. Lindmark, "Test-retest intra-rater reliability of grip force in patients with stroke," *J. Rehabil. Med.*, vol. 35, no. 4, pp. 189–194, 2003, doi: 10.1080/16501970306132.

[10] S. Kim and M. A. Nussbaum, "Performance evaluation of a wearable inertial motion capture system for capturing physical exposures during manual material handling tasks," *http://dx.doi.org/10.1080/00140139.2012.742932*, vol. 56, no. 2, pp. 314–326, Feb. 2013, doi: 10.1080/00140139.2012.742932.

[11] C. Schiefer *et al.*, "Optimization of inertial sensor-based motion capturing for magnetically distorted field applications," *J. Biomech. Eng.*, vol. 136, no. 12, Dec. 2014, doi: 10.1115/1.4028822.

[12] A. Ferrari *et al.*, "First in vivo assessment of "'Outwalk"': a novel protocol for clinical gait analysis based on inertial and magnetic sensors," doi: 10.1007/s11517-009-0544-y.

[13] J. T. Zhang, A. C. Novak, B. Brouwer, and Q. Li, "Concurrent validation of Xsens MVN measurement of lower limb joint angular kinematics," *Physiol. Meas.*, vol. 34, no. 8, 2013, doi: 10.1088/0967-3334/34/8/N63.

[14] "Devices | All The Hardware For Your Motion Capture Project | Vicon." https://www.vicon.com/hardware/devices/ (accessed Mar. 13, 2023).

[15] M. van der Linden, "Gait Analysis, Normal and Pathological Function, 2nd ed. J. Perry, J.M. Burnfield, Slack Inc., 576 pages, ISBN 978-1-55642r-r766-4," *Physiotherapy*, vol. 97, no. 2, p. 180, Jun. 2011, doi: 10.1016/J.PHYSIO.2010.05.007.

[16] F. Molina Rueda, *La marcha humana : biomecánica, evaluación y patología*. 2020.

[17] K. Takakusaki, "Functional Neuroanatomy for Posture and Gait Control," *J. Mov. Disord.*, vol. 10, no. 1, p. 1, Jan. 2017, doi: 10.14802/JMD.16062.

[18] K. Takakusaki, "Forebrain control of locomotor behaviors," 2007, doi: 10.1016/j.brainresrev.2007.06.024.

[19] P. S. Katz, "Neurons, networks, and motor behavior," *Neuron*, vol. 16, no. 2, pp. 245–253, 1996, doi: 10.1016/S0896-6273(00)80043-4.

[20] K. Takakusaki, N. Tomita, and M. Yano, "Substrates for normal gait and pathophysiology of gait disturbances with respect to the basal ganglia dysfunction," *J. Neurol.*, vol. 255, no. SUPPL. 4, pp. 19–29, Aug. 2008, doi: 10.1007/S00415-008-4004-7/METRICS.

[21] J. M. Hausdorff, "Gait variability: methods, modeling and meaning," 2005, doi: 10.1186/1743.

[22] T. Yuan *et al.*, "The mental representation of the human gait in young and older adults," 2015, doi: 10.3389/fpsyg.2015.00943.

[23] A. Shumway-Cook, J. Rachwani, M. H. Woollacott, and V. Santamaria, "Motor control : translating research into clinical practice," p. 718.

[24] Los Amigos Research & Education Center, "Observational Gait Assessment," 2001, Accessed: Mar. 21, 2023. [Online]. Available: https://books.google.com/books/about/Observational_Gait_Analysis.html?hl=es&id=sZdMPgAACAAJ.

[25] C. H. Barnett, "The phases of human gait," *Lancet (London, England)*, vol. 271, no. 6943, pp. 617–621, Sep. 1956, doi: 10.1016/S0140-6736(56)92309-1.

[26] L. N. Veilleux, M. Raison, F. Rauch, M. Robert, and L. Ballaz, "Agreement of spatio-temporal gait parameters between a vertical ground reaction force decomposition algorithm and a motion capture system," *Gait Posture*, vol. 43, pp. 257–264, Jan. 2016, doi: 10.1016/J.GAITPOST.2015.10.007.

[27] C. Kirtley, *Clinical gait analysis: Theory and practice*. Elsevier, 2006.

[28] M. W. Whittle, "Gait Analysis," *Gait Anal.*, 2007, doi: 10.1016/B978-0-7506-8883-3.X5001-6.

[29] M. Duarte, C. A. Fukuchi, and R. K. Fukuchi, "A public dataset of overground and treadmill walking kinematics and kinetics in healthy individuals," doi: 10.7717/peerj.4640.

[30] B. Pietraszewski, S. Winiarski, and S. Jaroszczuk, "Three-dimensional human gait pattern-reference data for normal men," *Acta Bioeng. Biomech. Orig. Pap.*, vol. 14, no. 3, 2012, doi: 10.5277/abb120302.

[31] Y. Lucero, "Kapandji Fisiologia Articular 5ed. 1998 (Tomo 2)," *Fisiol. Articul.*, Jan. 1998, Accessed: Mar. 24, 2023. [Online]. Available: https://www.academia.edu/39143712/Kapandji_Fisiologia_Articular_5ed_1998_Tomo_2_.

[32] A. Viladot Voegeli, "Anatomía funcional y biomecánica del tobillo y el pie," *Rev. Española Reumatol.*, vol. 30, no. 9, pp. 469–477, Nov. 2003, Accessed: Mar. 23, 2023. [Online]. Available: https://www.elsevier.es/es-revista-revista-espanola-reumatologia-29-articulo-anatomia-funcional-biomecanica-del-tobillo-13055077.

[33] L. H. Ting *et al.*, "Neuromechanical principles underlying movement modularity and their implications for rehabilitation," *Neuron*, vol. 86, no. 1, pp. 38–54, Apr. 2015, doi: 10.1016/J.NEURON.2015.02.042.

[34] E. Y. Y. Cheung, T. K. W. Ng, K. K. K. Yu, R. L. C. Kwan, and G. L. Y. Cheing, "Robot-Assisted Training for People With Spinal Cord Injury: A Meta-Analysis," *Arch. Phys. Med. Rehabil.*, vol. 98, no. 11, pp. 2320-2331.e12, Nov. 2017, doi: 10.1016/J.APMR.2017.05.015.

[35] A. Rodríguez-Fernández, J. Lobo-Prat, and J. M. Font-Llagunes, "Systematic review on

wearable lower-limb exoskeletons for gait training in neuromuscular impairments," *J. NeuroEngineering Rehabil. 2021 181*, vol. 18, no. 1, pp. 1–21, Feb. 2021, doi: 10.1186/S12984-021-00815-5.

[36] X. Xue *et al.*, "The improvement of the lower limb exoskeletons on the gait of patients with spinal cord injury A protocol for systematic review and meta-analysis The improvement of the lower limb exoskeletons on the gait of patients with spinal cord injury: a protocol for systematic review and meta-analysis Study Protocol Systematic Review Medicine ® OPEN 1," *Medicine (Baltimore).*, vol. 101, p. 4, 2022, doi: 10.1097/MD.0000000000028709.

[37] S. De Bock *et al.*, "Benchmarking occupational exoskeletons: An evidence mapping systematic review," *Appl. Ergon.*, vol. 98, Jan. 2022, doi: 10.1016/J.APERGO.2021.103582.

[38] R. W. Bohannon and R. Crouch, "1-Minute Sit-to-Stand Test: SYSTEMATIC REVIEW OF PROCEDURES, PERFORMANCE, AND CLINIMETRIC PROPERTIES," *J. Cardiopulm. Rehabil. Prev.*, vol. 39, no. 1, pp. 2–8, Jan. 2019, doi: 10.1097/HCR.0000000000000336.

[39] C. Y. Fang, J. L. Tsai, G. S. Li, A. S. Y. Lien, and Y. J. Chang, "Effects of Robot-Assisted Gait Training in Individuals with Spinal Cord Injury: A Meta-analysis," *Biomed Res. Int.*, vol. 2020, 2020, doi: 10.1155/2020/2102785.

[40] C.-H. Wu, H.-F. Mao, J.-S. Hu, T.-Y. Wang, Y.-J. Tsai, and W.-L. Hsu, "The effects of gait training using powered lower limb exoskeleton robot on individuals with complete spinal cord injury," doi: 10.1186/s12984-018-0355-1.

[41] C. Sanchez, L. Blanco, C. del Río, E. Urendes, V. Costa, and R. Raya, "A 3D-printed passive exoskeleton for upper limb assistance in children with motor disorders: proof of concept through an electromyography-based assessment," *PeerJ*, vol. 11, p. e15095, Mar. 2023, doi: 10.7717/PEERJ.15095.

[42] A. Blanco, J. M. Catalán, J. A. Díez, J. V. García, E. Lobato, and N. García-Aril, "Electromyography assessment of the assistance provided by an upper-limb exoskeleton in maintenance tasks," *Sensors (Switzerland)*, vol. 19, no. 15, Aug. 2019, doi: 10.3390/s19153391.

[43] A. Cisnal, P. Gordaliza, J. Pérez Turiel, and J. C. Fraile, "Interaction with a Hand Rehabilitation Exoskeleton in EMG-Driven Bilateral Therapy: Influence of Visual Biofeedback on the Users' Performance," *Sensors*, vol. 23, no. 4, 2023, doi: 10.3390/s23042048.

[44] T. E. Lockhart, "Biomechanics of Human Gait - Slip and Fall Analysis," *Encycl. Forensic Sci. Second Ed.*, pp. 466–476, 2013, doi: 10.1016/B978-0-12-382165-2.00151-3.

[45] V. Fanti, V. Sanguineti, D. G. Caldwell, J. Ortiz, and C. Di Natali, "Assessment methodology for human-exoskeleton interactions: Kinetic analysis based on muscle activation," *Front.*

*Neurorobot.*, vol. 16, 2022, doi: 10.3389/fnbot.2022.982950.

[46] "What is Motion Capture? | What Can I Use Motion Capture For?" https://www.vicon.com/about-us/what-is-motion-capture/ (accessed Mar. 20, 2023).

[47] J. Figueiredo, S. P. Carvalho, J. Paulo Vilas-Boas, L. M. Gonçalves, J. C. Moreno, and C. P. Santos, "Wearable Inertial Sensor System towards Daily Human Kinematic Gait Analysis: Benchmarking Analysis to MVN BIOMECH," doi: 10.3390/s20082185.

[48] M. Goffredo *et al.*, "Kinematic Analysis of Exoskeleton-Assisted Community Ambulation: An Observational Study in Outdoor Real-Life Scenarios," *Sensors*, vol. 22, no. 12. 2022, doi: 10.3390/s22124533.

[49] S. Gonzalez, P. Stegall, S. M. Cain, H. C. Siu, and L. Stirling, "Assessment of a powered ankle exoskeleton on human stability and balance," *Appl. Ergon.*, vol. 103, p. 103768, Sep. 2022, doi: 10.1016/J.APERGO.2022.103768.

[50] X. Robert-Lachaine, H. Mecheri, C. Larue, and A. Plamondon, "Validation of inertial measurement units with an optoelectronic system for whole-body motion analysis," *Med. Biol. Eng. Comput.*, vol. 55, no. 4, pp. 609–619, Apr. 2017, doi: 10.1007/S11517-016-1537-2/METRICS.

[51] W. H. K. de Vries, H. E. J. Veeger, C. T. M. Baten, and F. C. T. van der Helm, "Magnetic distortion in motion labs, implications for validating inertial magnetic sensors," *Gait Posture*, vol. 29, no. 4, pp. 535–541, Jun. 2009, doi: 10.1016/J.GAITPOST.2008.12.004.

[52] "About the Plug-in Gait model - Nexus 2.13 Documentation - Vicon Documentation." https://docs.vicon.com/display/Nexus213/About+the+Plug-in+Gait+model#AboutthePluginGaitmodel-PiGRefs (accessed Mar. 20, 2023).

[53] R. B. Davis, S. Õunpuu, D. Tyburski, and J. R. Gage, "A gait analysis data collection and reduction technique," *Hum. Mov. Sci.*, vol. 10, no. 5, pp. 575–587, 1991, doi: 10.1016/0167-9457(91)90046-Z.

[54] M. P. Kadaba, H. K. Ramakrishnan, and M. E. Wootten, "Measurement of lower extremity kinematics during level walking," *J. Orthop. Res.*, vol. 8, no. 3, pp. 383–392, 1990, doi: 10.1002/JOR.1100080310.

[55] "Plug-in Gait Reference Guide - Nexus 2.12 Documentation - Vicon Documentation." https://docs.vicon.com/display/Nexus212/Plug-in+Gait+Reference+Guide (accessed Mar. 20, 2023).

[56] "Lower body kinematics - Nexus 2.12 Documentation - Vicon Documentation." https://docs.vicon.com/display/Nexus212/Lower+body+kinematics (accessed Mar. 20, 2023).

[57] "Exoesqueleto Robótico - Exo-H3 | Technaid - Leading Motion." https://www.technaid.com/es/productos/robotic-exoskeleton-exo-h3/ (accessed Mar. 17, 2023).

[58] M. P. Kadaba, H. K. Ramakrishnan, M. E. Wootten, J. Gainey, G. Gorton, and G. V. B. Cochran, "Repeatability of kinematic, kinetic, and electromyographic data in normal adult gait," *J. Orthop. Res.*, vol. 7, no. 6, pp. 849–860, Nov. 1989, doi: 10.1002/JOR.1100070611.

[59] A. Ferrari, A. G. Cutti, and A. Cappello, "A new formulation of the coefficient of multiple correlation to assess the similarity of waveforms measured synchronously by different motion analysis protocols," *Gait Posture*, vol. 31, pp. 540–542, doi: 10.1016/j.gaitpost.2010.02.009.

[60] J. L. Mcginley, R. Baker, R. Wolfe, and M. E. Morris, "The reliability of three-dimensional kinematic gait measurements: A systematic review," doi: 10.1016/j.gaitpost.2008.09.003.

[61] J. Røislien, Skare, A. Opheim, and L. Rennie, "Evaluating the properties of the coefficient of multiple correlation (CMC) for kinematic gait data," *J. Biomech.*, vol. 45, no. 11, pp. 2014–2018, 2012, doi: 10.1016/j.jbiomech.2012.05.014.

[62] V. Kotu and B. Deshpande, "Data Science : Concepts and Practice," *Data Sci.*, p. 650, 2019.

# Appendix 1

The results of the Shapiro-Wilk test for normality of each parameter computed for Condition 1 are shown in Table 5, and for those of Condition 2 the results are shown in Table 6. To conclude that the samples are from a normally distributed population, the p-value obtained with this test must be above the 5% significance level. As can be seen in the table, not all p-values are greater than 0.05, so not all parameters are normally distributed.

*Table 5. Part II, condition 1: Shapiro-Wilk normality test.*

| | **r p-value** | | **ROM p-value** | | **off p-value** | | **RMSE p-value** | | **CMC1 p-value** | | **CMC2 p-value** | |
|---|---|---|---|---|---|---|---|---|---|---|---|---|
| | R | L | R | L | R | L | R | L | R | L | R | L |
| **Hip Flex/Ext** | 6.54e-04 | 0.01 | 0.24 | 0.08 | 0.007 | 0.02 | 0.01 | 0.04 | 0.06 | 2.08e-04 | 4.44e-05 | 9.79e-07 |
| **Hip Add/Abd** | 0.002 | 0.04 | 0.01 | 0.58 | 0.07 | 0.40 | 0.002 | 0.21 | 8.16e-06 | 0.63 | 5.52e-04 | 0.35 |
| **Hip Int/Ext Rot** | 0.59 | 0.23 | 0.82 | 0.11 | 0.04 | 0.29 | 0.03 | 0.42 | 0.94 | NaN | 0.03 | NaN |
| **Knee Flex/Ext** | 0.07 | 0.42 | 0.02 | 0.61 | 0.95 | 0.005 | 0.78 | 0.005 | 0.22 | 0.006 | 0.56 | 0.09 |
| **Knee Val/Var** | 0.23 | 0.15 | 0.22 | 0.19 | 0.23 | 0.003 | 0.03 | 0.54 | 0.34 | 2.73e-04 | 0.17 | 0.03 |
| **Knee Int/Ext Rot** | 0.29 | 0.10 | 0.01 | 0.43 | 0.44 | 0.15 | 0.05 | 0.11 | 0.003 | 2.24e-08 | 1.87e-04 | 2.87e-06 |
| **Ankle Dors/Plant Flexion** | 0.63 | 0.67 | 0.03 | 0.49 | 0.79 | 0.79 | 0.87 | 0.09 | 0.003 | 0.002 | 0.002 | 1.74e-06 |
| **Ankle Sup/Pron** | 0.05 | 0.003 | 0.16 | 0.42 | 0.12 | 7.17e-04 | 0.47 | 0.02 | 0.001 | 2.25e-07 | 0.34 | 0.05 |
| **Ankle Add/Abd** | 0.74 | 0.61 | 0.39 | 0.54 | 0.94 | 0.51 | 0.006 | 0.44 | 0.002 | 1.24e-05 | 0.15 | 2.24e-08 |

*Table 6. Part II, condition 2: Shapiro-Wilk normality test.*

| | **r p-value** | | **ROM p-value** | | **off p-value** | | **RMSE p-value** | | **CMC1 p-value** | | **CMC2 p-value** | |
|---|---|---|---|---|---|---|---|---|---|---|---|---|
| | R | L | R | L | R | L | R | L | R | L | R | L |
| **Hip Flex/Ext** | 0.55 | 0.74 | 0.99 | 0.73 | 0.09 | 0.64 | 0.06 | 0.81 | 0.09 | 0.85 | 0.02 | 0.56 |
| **Hip Add/Abd** | 0.29 | 0.28 | 0.90 | 0.009 | 0.27 | 0.47 | 0.56 | 0.34 | 0.001 | 0.001 | 0.04 | 0.04 |
| **Hip Int/Ext Rot** | 0.74 | 0.95 | 0.25 | 0.76 | 0.42 | 0.69 | 0.08 | 0.42 | 0.008 | 0.007 | 0.32 | 0.29 |
| **Knee Flex/Ext** | 0.95 | 0.25 | 0.85 | 0.54 | 0.99 | 0.74 | 0.92 | 0.63 | 0.03 | 0.19 | 0.13 | 0.009 |
| **Knee Val/Var** | 0.99 | 0.91 | 0.32 | 0.34 | 0.76 | 0.03 | 0.76 | 0.89 | 0.003 | 0.75 | 0.001 | 0.01 |
| **Knee Int/Ext Rot** | 0.98 | 0.80 | 0.79 | 0.45 | 0.38 | 0.72 | 0.82 | 0.49 | 0.001 | 0.96 | 0.001 | 0.27 |
| **Ankle Dors/Plant Flexion** | 0.46 | 0.29 | 0.19 | 0.36 | 0.61 | 0.29 | 0.20 | 0.36 | 0.06 | 0.03 | 0.29 | 0.006 |
| **Ankle Sup/Pron** | 0.17 | 0.99 | 0.49 | 0.02 | 0.74 | 0.96 | 0.73 | 0.39 | 0.009 | 0.96 | 0.08 | 0.16 |
| **Ankle Add/Abd** | 0.74 | 0.33 | 0.36 | 0.91 | 0.29 | 0.19 | 0.74 | 0.47 | 0.001 | 0.34 | 0.001 | 0.001 |